Carbon Dots as Targeted Drug Delivery System for Treatment of Cancer Cells

（癌細胞の治療に向けたドラッグデリバリーとしてのカーボンドット）

ASHMI BHUPENDRA MEWADA

Nagoya Institute of Technology

Japan

2016

Carbon Dots as Targeted Drug Delivery System for Treatment of Cancer Cells

by

ASHMI BHUPENDRA MEWADA

A thesis submitted in partial fulfilment of the requirements for the degree of

DOCTOR OF ENGINEERING

Department of Frontier Materials

Graduate School of Engineering

Nagoya Institute of Technology

Supervised by:

Prof. Dr. Tetsuo Soga

Guided by:

Dr. Madhuri Sharon

(Walchand Centre of Research in Nanotechnology and Bio-nanotechnology, Solapur, India)

CONTENTS

ABSTRACT

Ever since the debut of C-dots in Carbon nano world, they have been in extreme lime light due to their exceptional optical and physical properties. These illuminating dots under UV-light falls in size range of 1-10nm and share the properties like semiconductor quantum dots and exhibit excitation dependent emission spectra. The exact reason for commencement of fluorescence in C-dots is still remained obscure. However, energy emissive traps, oxygen containing functional groups, surface passivation and quantum confinement effect, turbostratic nature of Carbon or edge defects may result in initiation of photoluminescence of C-dots.

C-dots are found to be stable in fluorescence emission for long hours without alteration in their PL spectra. C-dots have drawn great attention in the field of research due to their excellent tuneable optical properties. Last but not the least, the most celebrated properties of C-dots is its biocompatibility and water solubility. C-dot being inert does not cause any toxic effects, unlike semiconductor quantum dots. For application like drug delivery and Bio-imaging, water soluble C-dots hold an added advantage over conventional Quantum dots. It allows easy harvesting and functionalisation of C-dots with drugs and other vital molecules.

In present work, various natural precursors (water chestnut peel, Neem gum, Sugarcane juice, Gum Arabic) and chemical precursors (Sorbitol and Phenylalanine) have been exploited on the basis of their high carbon content and the ratio of C, H and O in their sugar moieties. Among different synthesis methods, three methods namely refluxing at high temperature (Water chestnut peel), microwave assisted heating (Gum arabic, Sorbitol & Phenylalanine) and synthesis at room temperature (Neem gum & Sugarcane juice) was employed for different precursors. Conventional dialysis method was proven most promising for separation and purification of C- dots. Rice Husk (RH) being rich in silica and carbon content, an attempt for synthesis of mesoporous silica oxide micro-particles (MesoSiO_2/ C-dots) complex for biological imaging by hot injection method generally used for semiconductor quantum dots. This complex demonstrated fluorescence property and NIR absorbance which can be explored for photo-thermal therapy and thus can serve as a potential candidate for theranaustic application of simultaneous cellular imaging and drug delivery. Gold Nanorods (GNR) are metal nanoparticles explored for a broad spectrum of bio-medical applications

such as drug/gene delivery, computational tomography, optical imaging etc. GNRs with suitable aspect ratios can absorb and scatter electromagnetic radiation intensely in the NIR region, which can be used for improved optical imaging and photothermal cancer therapy but are restricted in use due to the cytotoxic effects of CTAB used in synthesis. To eliminate detrimental effects of CTAB, we created a modified protocol for the attachment of exceptionally biocompatible C-dots on the surface of GNRs via weak interactions.

In contrast to all other precursors derived C-dots, Sorbitol derived C-dots were found to be most stable and did not show any signs of agglomeration or contamination till a period of 3 months. On the other hand, C-dots synthesized from natural precursors showed signs of clustering and increase in turbidity possibly due to the natural moieties present on their surfaces. C-dots have been used as a drug delivery vehicle to ferry Doxorubicin, a potent anti-cancer drug to target and kill tumor cells.

Crystals are fascinating matters which have been grown since long ago but getting a biocompatible fluorescent crystals is a challenging job. We have reported the growth of fluorescent crystals using C-dot solution using hydrothermal process. Growth temperature and pressure was maintained at 60^{o}C and 200 mmHg respectively for crystal growth. A green fluorescence was observed when crystals were irradiated with ultra violet radiation. The speculated mechanism for the formation of Crystals is explained by Classical Nucleation theory.

One of the pivotal biological applications of C-dots is in drug delivery of anticancer drugs. The effectiveness of a cancer therapeutic device is measured by its ability to reduce and eliminate tumors without damaging the surrounding (healthy tissues) which is not possible with conventional chemotherapy. In case of C-dots as a chemotherapeutic agent, it can act as dual functional nano-carriers for delivering therapeutic payloads to targeted sites as well as used in biological imaging. The particle size and surface properties of C-dots can be manipulated to circumvent rapid clearance by phagocytic cells, allowing both passive and active drug target. For this purpose, we have explored the drug carrying capacity of highly fluorescent Sorbitol derived C-dots for targeted delivery of Doxorubicin (DOX). We have used Folic Acid (FA) as navigational molecule due to its high expression in most of the cancer cells. Before attachment of the DOX, the surfaces of C-dots were protected with Bovine Serum Albumin (BSA) to make them more biocompatible and hold high amount

of drugs. Release profile of DOX was studied using standard statistical models and confirmed to be First order at pH 7.2. Cellular imaging was performed using epifluorescence microscopy which showed bright green coloured fluorescence due to internalization of C-dots specifically targeted with FA in HeLa cells.

LIST OF FIGURES

Chapter III:
Characterisation of C-dots and Meso-SiO_2/C-dots

Chapter IV:
Formation of Fluorescent Dendrites using C-dots

LIST OF TABLES

CHAPTER I

Introduction

1.1 INTRODUCTION TO C-DOTS AND CANCERTHERAPEUTICS

"If we can reduce the cost and improve the quality of medical technology through advances in Nanotechnology, we can more widely address the medical conditions that are prevalent and reduce the level of Human suffering"

- Ralph Merkle

1.1.1 Discovery of fluorescent Carbon Dots (C-dots)

Ever since the discovery of Fullerenes in 1985**[1]**, it has been studied widely for its unique and novel properties followed by Carbon Nanotubes (CNT) **[2]**which opened a wide field in the area of Carbon nanomaterial research all around the world. Apart from the various types of nanoforms of Carbon; Graphene, Graphene Oxide (GO) and fluorescent carbon nanomaterials have recently found a new place in the family of Carbon nanoparticles. An era of Fluorescent Carbon nanoparticles began with its accidental discovery during electrophoretic purification of Single Walled Carbon Nano Tube (SWCNT) obtained from arc discharge soot in 2004 by Xu et al **[3]**. This breakthrough is the highlight of nanoworld in terms of excellent properties and potential applications of these luminescent carbonaceous material also called as "*Carbon dots*" since they fall in the size range of 1-10 nm and share properties with the semiconductor quantum dots.

1.1.2 Synthesis of C-dots

A variety of techniques have been used for the synthesis of C-dots which include laser ablation of graphite, electrochemical oxidation of graphite, electrochemical soaking of CNT, thermal oxidation of suitable molecular precursors, vapor deposition of soot, proton-beam irradiation ofnano-diamonds, microwave assisted synthesis and bottom-up methods**[4-10].** Schematic of various methods used so far have been given in Chapter 2.

1.1.3 Properties and Applications of C-dots

Semi-conductor quantum dots like CdTe, CdS, CdSe, etc have been vastly used in bio-imaging and as biological sensors due to their distinct optical properties and small size **[11, 12].** However, the Cytotoxicity caused due to the heavy metals restricts them in practical application in the biological field. The properties of the C-dots can be exploited to replace

such metal containing semiconductor quantum dots which also involve use of extremely inimical precursors **[9, 13]**as well as high temperatures for their synthesis**[3, 9]**.

Photoluminescence (PL): C-dots show absorption in the UV region and exhibit a typical feature of excitation dependent emission spectra. Photoluminescence (PL) is one of the most important properties of C-dots from the fundamental and application point of view. There has been a lot of speculations and debate on the origin of fluorescence in C-dots. Hu et al **[4]** and Li et al **[14]** have claimed that the carboxylate groups present on the surface of C-dots are responsible for PL. On the other hand, Zhao et al **[15]** and Sun et al **[16]** speculated the presence of surface energy traps arising due to the defects to be the reason for PL. This was explained by the quantum confinement effect of nanoparticles which was also observed in Si nanocrystals **[17].** Kang et al **[18]** presented through their work that oxygen containing functional groups were responsible for the phenomena. The multi color PL observed may also arise due to the different size of C-dots as well as the distribution of the surface traps **[7].** Surface passivation can enhance or alter the PL of C-dots and can be used to modify their surface as per a particular application.From the above mentioned work by different groups, we can say that the inception of fluorescence has been tentatively suggested to arise from emissive traps, oxygen containing functional groups, surface passivation, quantum confinement effect, turbostratic nature of Carbon or edge defects. However, the exact mechanism of origin of PL in C-dots still remains unresolved and needs more detailed clarity. C-dots show extended fluorescence with less blinking effect and can be used instead of conventional dyes for bio-imaging. Multi-color C-dots can be simultaneously employed for determining heterogeneity amongst cancer cells.

Quantum Yield (QY): of C-dots differs with different protocols used for the synthesis of C-dots and reported to be dependent on surface passivation**.** Literature has shown that C-dots associated with metal coating shows high QY **[19].** C-dots have proven to display excellent photostability**[16].** The PL properties of C-dots remain unaltered for a long time (even as long as 1 year). Even after continuous exposure to excitation, C-dots do not record any decrease in PL as well as are resistant to blinking unlike semi-conductor Quantum dots **[20]**.

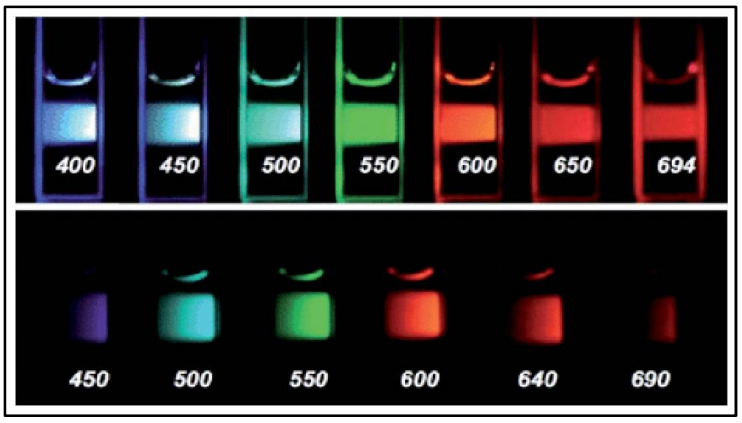

Figure 1.1: Aqueous solutions of the as-synthesized C-dots excited at the indicated wavelengths in nm and photographed directly (top panel), and excited at 400 nm and photographed through band-pass filters of different wavelengths as indicated (bottom panel) (Adapted from Ref no.16)

Biocompatibility of C-dots: Another important property is the biocompatibility of C-dots. Carbon being an inert material does not cause any toxic effects on cells **[21-24]** and can be used for in-vivo biological analysis. Also, the synthesis procedure involves use of eco-friendly precursors instead of heavy metal compounds used in inorganic quantum dots. The protocol used for synthesis of C-dots is also quite simple and non-laborious.

Tuneable optical properties: C-dots have drawn great attention in the field of research due to their excellent tuneable optical properties **[25].** It is a characteristic of nanoparticles in contrast to bulk materials which allows for designing size dependent photophysical properties as per the desirable application.

Solubility in water: For application like drug delivery and Bio-imaging, water soluble C-dots hold an added advantage over conventional Quantum dots **[26]**. It allows easy harvesting and functionalisation of C-dots with drugs and other vital moleculesand also reduces toxicity caused by other inorganic solvents. Moreover, synthesis, purification and storage also become simple.

Resistance to photobleaching:There have been many reports on the studies of fluorescence emission of C-dots which states that they are comparatively resistance to photobleaching which is generally observed trait of quantum dots which consequently leads to blinking nature and hinder in accurate detection for sensor purpose due to weak signals **[20].** On the

other hand C-dots are found to be stable in fluorescence emission for long hours without alteration in their PL spectra.

All the above properties of C-dots have led to its entry in various potential applications like photocatalysis, optoelectronics, Surface Enhanced Raman Scattering (SERS) **[20]**, Fluorescence Resonance Energy Transfer (FRET) **[27]**, biological imaging**[28],** biosensors/nanoprobes**[29]** and the most recent in drug delivery**[30]**.

1.1.4 C-dots and Cancer therapeutics

A commonly used scientific definition of "CANCER" classifies it as a number of diseases in which a healthy cell of the human body gets modified due to genetic defects and starts to grow in an uncontrolled way, invading the adjacent tissues and spreading throughout the whole body as metastasis. The defects in cells may be caused by chemicals – carcinogens – or mayrandomly occur due to errors in DNA replication, repair and recombination processes. The Figure 1.2 displays the 6 major hallmarks of Cancer **[31].**

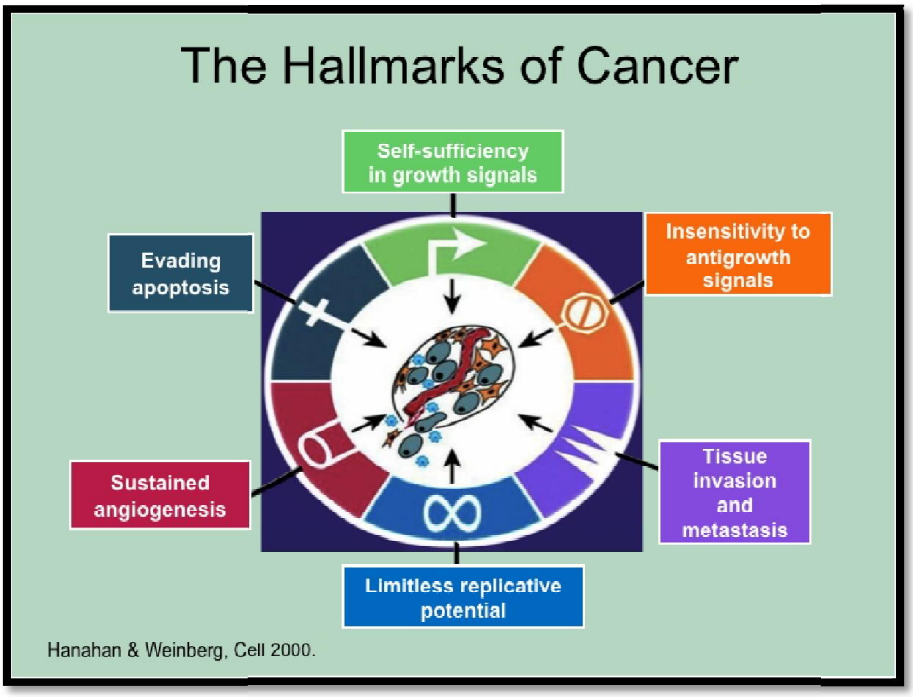

Figure 1.2: Six hallmarks of cancer (Adapted from Ref no. 31)

The effectiveness of a cancer therapeutic device is measured by itsability to reduce and eliminate tumors without damaging the surrounding (healthy tissues). Therefore, targeting of tumors becomes essential for efficient working of the therapeutic device. An increased site specificity andinternalization can improve the efficacy of treatment and decrease

thepossibility of the serious side effects that cancer patients oftenexperience in conventional therapy protocols (eg. chemotherapy).

As compared to Conventional drug delivery, controlled drug delivery strategies have made an impressive impact on medicine. Controlled drug release can be achieved by a combination of transport material and active agents. Apart from the maintenance of optimum therapeutic drug concentration in blood or in a cell, the advantages of controlled delivery systems include predictable and reproducible release for extended periods of time, enhancement of activity duration for short half-life drugs, reduction of side effects, reduce frequent dosage and consequent wastage of drug and increase convenience of the patient.

Nanoparticlesystems offer major improvements in therapeutics through sitespecificity, their ability to escape from multi-drug resistance, andthe efficient delivery of an agent. This approach to drug delivery is known as targeted drug delivery**[32, 33]**. Targeted delivery aims to achieve perfection by delivering the right amount at only the site of disease or injury. One of the prime aspects of a competent targeted-drug delivery system is the selection of an appropriate delivery profile. The delivery profile is usually a plot of the concentration of drug delivered from the vehicle with respect to time. The drug delivery profile is a trait for a specific type of drug, the drug delivery vehicle and the physiological factors at the delivery site i.e the tumor micro-environment. For instance, pore size, thickness, geometry, drug loading, temperature, surface roughness, bio-degradation, etc. of the drug vehicle determine the amount of drug that is released, thus controlling the profile of delivery**[34-36]**.

So far, various metallic and non- metallic nanoparticles like Gold nanoparticles **[37]**, gold Nanorods **[38]**, CNTs**[39]** and polymeric nanoparticles **[40, 41]** have been explored as drug delivery vehicle for cancer therapy.

C-dots have recently entered in the field of drug delivery; moreover, it can be speculated that C-dots can act as excellent dual functional nano-carriers for delivering therapeutic payloads to targeted sites as well as used in biological imaging due to the following properties-

- The particle size and surface properties of C-dots can be manipulated to circumvent rapid clearance by phagocytic cells, allowing both passive and active drug targeting.
- Drug loading capacity can be enhanced due to the porous nature of C-dots and can be achieved without harsh chemical reactions thus maintaining the activity of the drug.

- As stated in the above section, C-dots itself do not show any inherent cytotoxicity unlike other metal nanoparticles.
- The drug release profile can be altered and adjusted using polymer coatings and pH responsive linkers.
- Potential for administration through various routes, including oral, pulmonary, nasal, parental, intra-ocular etc.

The work done so far using C-dots as drug delivery vehicle and bio-imaging agent for cancer is discussed in the next section of this chapter.

1.2 REVIEW OF LITERATURE

Carbon dots are new class of carbon nanomaterials in nanotechnology field, with size of less than 10nm. Carbon is commonly known as black matrial, nobody imagine that it will show high fluorescence and soluble in water. Because of its nanosized carbon structured can synthesize and their properties are drastically changed from bulk materials. The reason why carbon dots are attracted by many researchers is because of their strong fluorescence.

These fluorescent carbon nanoparticles or Carbon Quantum dots or Carbon-dots (C-dots), since their discovery in 2004 **[3]**, are now a prime area of focus for its excellent properties mainly optical fluorescent property which has explored many potential uses in bioimaging and therapeutics in cancer nanotechnology.The work carried out by different Research groups so far in apllication of C-dots as drug delivery vehicle and for Bio-imaging are summarised in table 1.1.

Table 1.1: Shows major research highlighting C-dots as drug delivery vehicle for cancer therapy

No.	List of applications in cancer Nanomedicine	Remarks	Reference
1.	Manipulation of C-dots on various sites- core and the surface to enhance bioimaging potential.	Wang et al. demonstrated the overcooked barbeque could be the source of C-dots whereas Dong et al. showed how surface doping with N or S, might give higher fluorescence intensity.	42-54
2.	Cellular imaging, specific (active) tissue targeting using C-dots.	Zhang et al. and Yan et al. demonstrated polydopamine and cellulose derived C-dots for cellular imaging. Similarly, Wei et al. used paper ash C-dots synthesis and cellular localization of L02 hepatic cells. Chen et al. modified sucrose derived C-dots with oil for imaging 16HBE cells whereas Zhang et al. used BSA and TTDDA for viewing colorectal cancer cells. Saxena et al. showed bread derived C-dots for viewing human RBCs.	55-62
3.	*In vivo* imaging using fluorescent C-dots	Wu et al. used honey derived C-dots for imaging lymph nodes in mouse models. Huang et al. conjugated C-dots with fluorescent dye which absorbs in NIR to studyits in vivo biodistributionby conjugating with dye Ce6 they could suppress tumor growth using photodynamic therapy.	63-67
4.	C-dots in therapeutics.	Wang et al. prepared hollow C-dots whereas Lai et al. used C-dots conjugated mesoporous silica for therapeutics.	68-73
5.	Cytoplasm localization of fluorescent multi-color C-dots.	Wang et al., Zhang et al. and Mewada et al. showed cellular entry of C-dots in cell lines.	26, 42, 55, 56
6.	Cell membrane adsorption of florescent C-dots.	Zhang et al. and Chen et al. showed imaging using cell membrane adsorption.	45 & 52
7.	Simple eco-friendly precursors for C-dots synthesis &application in cellular imaging.	Saxena et al. showed synthesis of C-dots from wood wool and **Mewada et al**. showed economical use of *Trapabispinosa* peel for C-dots synthesis.	10, 16, 26, 47 & 51
8.	Specific targeting potential of C-dots using antibodies and/or targeting ligands in cancer.	**Mewada et al** showed folic acid targeting potential for C-dots drug delivery.	26, 49, 54, 61 & 74
9.	Theranaustics potential of C-dots.	Lai et al. achieved simultaneous imaging and drug release by conjugating C-dots with mesoporous silica. Mitra et al. showed both anti-bacterial and bioimaging using Zinc oxide conjugated C-dots.**Pandey and co-workers** could do simultaneous drug delivery of doxorubicin, bioimaging and photothermal therapy by using C-dots conjugated with gold nanorods.	68, 70, 73 & 74
10.	Drug delivery using multi-color C-dots.	Shen et al. haveused pH-sensitive C-dots for drug delivery.	62, 70, 75
11.	*In vivo* bio-distribution and near-infrared imaging using C-dots.	Li et al. sliced organs of C-dots treated mice and found fluorescence in organs such as heart, liver, spleen (maximum), kidney, brain and intestine. Srivastava et al. prepared iron-oxide conjugated carbon nanoparticle and when injected in rats they found fluorescence in spleen samples.	66, 76 & 77

1.3 AIMS AND OBJECTIVES

After streaming through the literature of Drug delivery using C-dots, the main aim of this work is to "Design an efficient drug delivery vehicle using C-dots for active targeting of Doxorubicin to Cancer cells"

To achieve the above aim, following will be my objectives-

- Screen novel biological as well as chemical precursors for the synthesis of C-dots using different parameters
- Purification of the synthesized crude C-dots solution by different techniques (eg. Sucrose Density Gradient Centrifugation, Centrifugation and Dialysis) to get pure fluorescent C-dots
- Characterization of C-dots using UV-Visible spectrophotometry, Fluorescence spectroscopy, Field Gun Scanning Electron Microscopy (FE-SEM), Transmission Electron Microscopy (TEM), Raman & Fourier Transform Infra-Red (FTIR) spectroscopy and X-Ray Diffraction (XRD)
- Surface functionalisation of purified C-dots with linker and targeting molecule
- Loading of anti-cancer drug Doxorubicin to surface modified C-dots
- Study the in-vitro drug release behaviour from the final conjugate in physiological conditions
- Statistical analysis of release kinetics using various standard mathematical models
- Study the Cytotoxic effects of Drug and C-dot-drug complex on normal and cancerous cell lines

1.4 REFERENCES

1. H. W. Kroto, J. R. Heath, S. C. O'Brien, R. F. Curl and R. E. Smalley, Nature, 1985, 318, 162.
2. S. Iijima, Nature, 1991, 354. 56.
3. X. Xu, R. Ray, Y. Gu, H. J. Ploehn, L. Gearheart, K. Raker and W. Scrivens, J. Am. Chem. Soc., 2004, 126, 12736.
4. S. L. Hu, K. Y. Niu, J. Sun, J. Yang, N. Q. Zhao, X. W. Du, J. Mater. Chem., 2009, 19, 484.
5. A. B. Bourlinos, A. Stassinopoulos, D. Anglos, R. Zboril, M. Karakassides and E. P. Giannelis, Small, 2008, 4, 455.
6. L. Y. Zheng, Y. W. Chi, Y. Q. Dong, J. P. Lin, B. B. Wang, J. Am. Chem. Soc., 2009, 131, 4564.
7. R. Liu, D. Wu, S. Liu, K. Koynov, W. Knoll, Q. Li, Angew. Chem., 2009, 121, 4668.
8. M. Bottini, C. Balasubramanian, M. I. Dawson, A. Bergama-schi, S. Belluci, T. Mustelin, J. Phys. Chem. B 2006, 110, 831.
9. A. B. Bourlinos, A. Stassinopoulos, D. Anglos, R. Zboril, V. Georga-kilas, E. P. Giannelis, Chem. Mater. 2008, 20, 4539.
10. J. Lu, J. X. Yang, J. Z. Wang, A. Lim, S. Wang, K. P. Loh, ACS Nano 2009, 3 , 2367.
11. P. Alivisatos, Nat Biotechnol, 2004, 22 (1), 47.
12. I. L. Medintz, H. T. Uyeda, E. R. Goldman, H. Mattoussi, Nat Mater., 2005, 4 (6), 435.
13. S. C. Ray, A. Saha, N. R. Jana and R. Sarkar, J. Phys. Chem. C, 2009, 113, 18546.
14. X. Y. Li, H. Q. Wang, Y. Shimizu, A. Pyatenko, K. Kawaguchi and N. Koshizaki, Chem. Commun., 2011, 47, 932.
15. Q. L. Zhao, Z. L. Zhang, B. H. Huang, J. Peng, M. Zhang and D. W. Pang, Chem. Commun., 2008, 5116.
16. Y. P. Sun, B. Zhou, Y. Lin, W. Wang, K. A. S. Fernando, P. Pathak, M. J. Meziani, B. A. Harruff, X. Wang, H. F. Wang, P. J. G. Luo, H. Yang, M. E. Kose, B. L. Chen, L. M. Veca and S. Y. Xie, J. Am. Chem. Soc., 2006, 128, 7756.

17. W. L. Wilson, P. F. Szajowski and L. E. Brus, Science, 1993, 262, 1242.
18. H. T. Li, X. D. He, Z. H. Kang, H. Huang, Y. Liu, J. L. Liu, S. Y. Lian, C. H. A. Tsang, X. B. Yang and S. T. Lee, Angew. Chem., Int. Ed., 2010, 49, 4430.
19. H. Peng and J. Travas-Sejdic, Chem. Mater., 2009, 21, 5563.
20. L. Haitao, K. Zhenhui, L. Yang and L. Shuit-Tong, J. Mater. Chem., 2012, 22, 24175.
21. X. L. Kong, L. C. L. Huang, C. M. Hsu, W. H. Chen, C. C. Han, H. C. Chang, Anal. Chem., 2005, 77, 259.
22. L. C. L. Huang, H. C. Chang, Langmuir, 2004, 20, 5879.
23. M. D. Cahalan, I. Parker, S. H. Wei, M. J. Miller, Nat. Rev. Immunol., 2002, 2, 872.
24. S. N. Baker and G. A. Baker, Angew. Chem., Int. Ed., 2010, 49, 6726.
25. J. H. Shen, Y. H. Zhu, X. L. Yang and C. Z. Li, Chem. Commun., 2012, 48, 3686.
26. A. Mewada, S. Pandey, S. Shinde, N. Mishra, G. Oza, M. Thakur, M. Sharon and M. Sharon, Mater. Sci. Eng., C, 2013, 33, 2914.
27. W. L. Wei, C. Xu, J. S. Ren, B. L. Xu and X. G. Qu, Chem. Commun., 2012, 48, 1284.
28. L. Cao, X. Wang, M. J. Meziani, F. Lu, H. Wang, P. G. Luo, Y. Lin, B. A. Harruff, L. M. Veca, D. Murray, S. Y. Xie and Y. P. Sun, J. Am. Chem. Soc., 2007, 129, 11318.
29. L. Zhou, Y. H. Lin, Z. Z. Huang, J. S. Ren and X. G. Qu, Chem. Commun., 2012, 48, 1147.
30. S. Pandey, A. Mewada, M. Thakur, A. Tank and M. Sharon, RSC Adv., 2013, 3, 26290.
31. D. Hanahan and R. A. Weinberg, Cell, 2011, 144, 646.
32. T. D. McKee, P. Grandi, W. Mok, G. Alexandrakis, N. Insin, J. P. Zimmer, M. G. Bawendi, Y. Boucher, X. O. Breakefield and R. K. Jain, Cancer Res. , 2006, 66, 2509.
33. R. K. Jain and T. Stylianopoulos, Nat. Rev. Clin. Oncol., 2010, 7 , 653.
34. G. Vilara, J. Tulla-Puchea, and F. Albericio, Current Drug Delivery, 2012, 9.
35. D. Bhowmik, H. Gopinath, B. Pragati Kumar, S. Duraivel and K. P. Sampath Kumar, The Pharma Innovation, 2012, 1 (10), 24.
36. H. K. Makadia and Steven J. Siegel, Ploymers, 2011, 3, 1377.

37. S. Pandey, G. Oza, A. Mewada, R. Shah, M. Thakur and M. Sharon, J. Mater. Chem. B, 2013, 1, 1361.
38. S. Pandey, R. Shah, A. Mewada, M. Thakur, G. Oza and M. Sharon, J. Mater. Sci.: Mater. Med., 2013, 24, 1671.
39. S. Parihar, M. Sharon andM. Sharon,Synthesis & Reactivity in Inorganic, Metal-Organic, & Nano-Metal Chemistry, 2006, 36(1), 107.
40. M. Khemani, M. Sharon andM. Sharon,ISRN Nanotechnology, 2012, doi:10.5402/2012/187354.
41. M. Khemani, M. Sharon andM. Sharon,Annals of Biological Research, 2012, 3 (9), 4414.
42. X. Wang, L. Cao, S.-T. Yang, F. S. Lu, M. J. Meziani, L. L. Tian, K. W. Sun, M. A. Bloodgood and Y.-P. Sun, Angew. Chem., Int. Ed., 2010, 49, 5310.
43. Y. Dong, H. Pang, H. B. Yang, C. Guo, J. Shao, Y. Chi,C. M. Li and T. Yu, Angew. Chem., Int. Ed., 2013, 52, 7800.
44. P. Anilkumar, X. Wang, L. Cao, S. Sahu, J. H. Liu, P. Wang, K. Korch, K. N. Tackett II, A. Parenzan and Y. P. Sun, Nanoscale , 2011, 3, 2023.
45. Z. Zhang, J. Hao, J. Zhang, B. Zhang and J. Tang, RSC Adv., 2012, 2 , 8599.
46. B. Kong, A. Zhu, C. Ding, X. Zhao, B. Li and Y. Tian, Adv. Mater., 2012, 24, 5844.
47. S. Sahu, B. Behera, T. K. Maiti and S. Mohapatra, Chem. Commun., 2012, 48, 8835.
48. X. Zhang, S. Wang, L. Xu, Y. Ji, L. Feng, L. Tao, S. Li and Y. Wei, Nanoscale , 2012, 4, 5581.
49. B. Han, W. Wang, H. Wu, F. Fang, N. Wang, X. Zhang andS. Xu, Colloids Surf. B , 2012, 100, 209.
50. H. Yan, M. Tan, D. Zhang, F. Cheng, H. Wu, M. Fan, X. Ma and J. Wang, Talanta , 2013, 108, 59.
51. A. Sachdev, I. Matai, S. U. Kumar, B. Bhushan, P. Dubey and P. Gopinath, RSC Adv., 2013, 3, 16958.
52. B. Chen, F. Li, S. Li, W. Weng, H. Guo, T. Guo, X. Zhang, Y. Chen, T. Huang, X. Hong, S. You, Y. Lin, K. Zeng and S. Chen, Nanoscale, 2013, 5, 1967.
53. M. Saxena and S. Sabyasachi, Mater. Express, 2013, 3, 201.

54. S. K. Bhunia, A. Saha, A. R. Maity, S. C. Ray and N. R. Jana, Sci. Rep., 2013, 3, 1473.
55. J. Wei, J. Shen, X. Zhang, S. Guo, J. Pan, X. Hou, H. Zhang, L. Wang and B. Feng, RSC Adv., 2013, 3, 13119.
56. X. Zhang, S. Wang, C. Zhu, M. Liu, Y. Ji, L. Feng, L. Tao and Y. Wei, J. Colloid Interface Sci. , 2013, 397, 39.
57. H. Ding, L.-W. Cheng, Y.-Y. Ma, J.-L. Kong and H.-M. Xiong, New J. Chem., 2013, 37, 2515.
58. M. Saxena, S. K. Sonkar and S. Sarkar, RSC Adv., 2013, 3, 22504.
59. Y. Xu, M. Wu, Y. Liu, X.-Z. Feng, X.-B. Yin, X.-W. He and Y.-K. Zhang, Chem. Eur. J., 2013, 19, 2276.
60. K. Qu, J. Wang, J. Ren and X. Qu, Chem. Eur. J. , 2013, 19, 7243.
61. C. H. Lee, R. Rajendran, M.-S. Jeong, H. Y. Ko, J. Y. Joo, S. Cho, Y. W. Chang and S. Kim, Chem. Commun., 2013, 49, 6543.
62. L. Shen, L. Zhang, M. Chen, X. Chen and J. Wang, Carbon, 2013, 55, 343.
63. P. Huang, J. Lin, X. Wang, Z. Wang, C. Zhang, M. He, K. Wang, F. Chen, Z. Li, G. Shen, D. Cui and X. Chen, Adv. Mater. , 2012, 24, 5104.
64. L. Cao, S.-T. Yang, X. Wang, P. G. Luo, H. H. Liu, S. Sahu, Y. Liu and Y. P. Sun, Theranostics , 2012, , 295.
65. H. Tao, K. Yang, Z. Ma, J. Wan, Y. Zhang, Z. Kang and Z. Liu, Small, 2012, 8, 281.
66. L. Wu, M. Luderer, X. Yang, C. Swain, H. Zhang, K. Nelson, A. J. Stacy, B. Shen, G. M. Lanza and D. Pan, Theranostics, 2013, 3, 677.
67. X. Huang, F. Zhang, L. Zhu, K. Y. Choi, N. Guo, J. Guo, K. N. Tackett II, P. Anilkumar, G. Liu, Q. Quan, H. S. Choi, G. Niu, Y.-P. Sun, S. Lee and X. Chen, ACS Nano, 2013, 7, 5684.
68. C. W. Lai, Y.-H. Hsiao, Y. K. Peng and P. T. Chou, J. Mater. Chem., 2012, 22, 14403.
69. Q. He, M. Ma, C. Wei and J. Shi, Biomaterials, 2012, 33, 4392.
70. S. Mitra, S. Chandra, D. Laha, P. Patra, N. Debnath, A. Pramanik, P. Pramanik and A. Goswami, Mater. Res. Bull. , 2012, 47, 586.
71. Q. Wang, X. Huang, Y. Long, X. Wang, H. Zhang, R. Zhu, L. Liang, P. Teng and H. Zheng, Carbon, 2013, 59, 192.
72. J. Kim, J. Park, H. Kin, K. Singha and W. J. Kim, Biomaterials, 2013, 34, 7168.

73. S. Pandey, M. Thakur, A. Mewada, D. Anjarlekar, N. Mishra and M. Sharon, J. Mater. Chem. B, 2013, 1, 4972.
74. A. Mewada, S. Pandey, M. Thakur, D. Jadhav& M. Sharon, J. Mater. Chem. B, 2014, 698.
75. P. G. Luo, S. Sahu, S.-T. Yang, S. K. Sonkar, J. Wang, H. Wang, G. E. LeCroy, L. Cao and Y. P. Sun, J. Mater. Chem. B, 2013, 1, 2116.
76. N. Li, X. Liang, L. Wang, Z. Li, P. Li, Y. Zhu and J. Song, J. Nanopart. Res., 2012, 14, 1177.
77. S. Srivastava, R. Awasthi, D. Tripathi, M. K. Rai, V. Agarwal, V. Agrawal, N. S. Gajbhiye and R. K. Gupta, Small , 2012, 8, 1099.

CHAPTER II

Synthesis and Purification of C-dots and C-dots Conjugates

2.1 INTRODUCTION

"The edifice of science not only requires material, but also a plan. Without the material, the plan alone is but a castle in the air- a mere possibility; whilst the material without a plan is but useless matter"

-Dmitery Ivanovich Mendeleev

There are a variety of protocols for synthesis of C-dots. The various established methods can be mainly divided into two categories i.e. chemical synthesis and physical synthesis. A typical synthesis procedure involves 3 steps to get C-dots that can be used for various applications:

1. Synthesis of raw C-dots
2. Purification and passivation of C-dots &
3. Functionalisation of C-dots

Figure 2.1displays the schematic diagram of various methodologies for synthesis of C-dots **[1].**

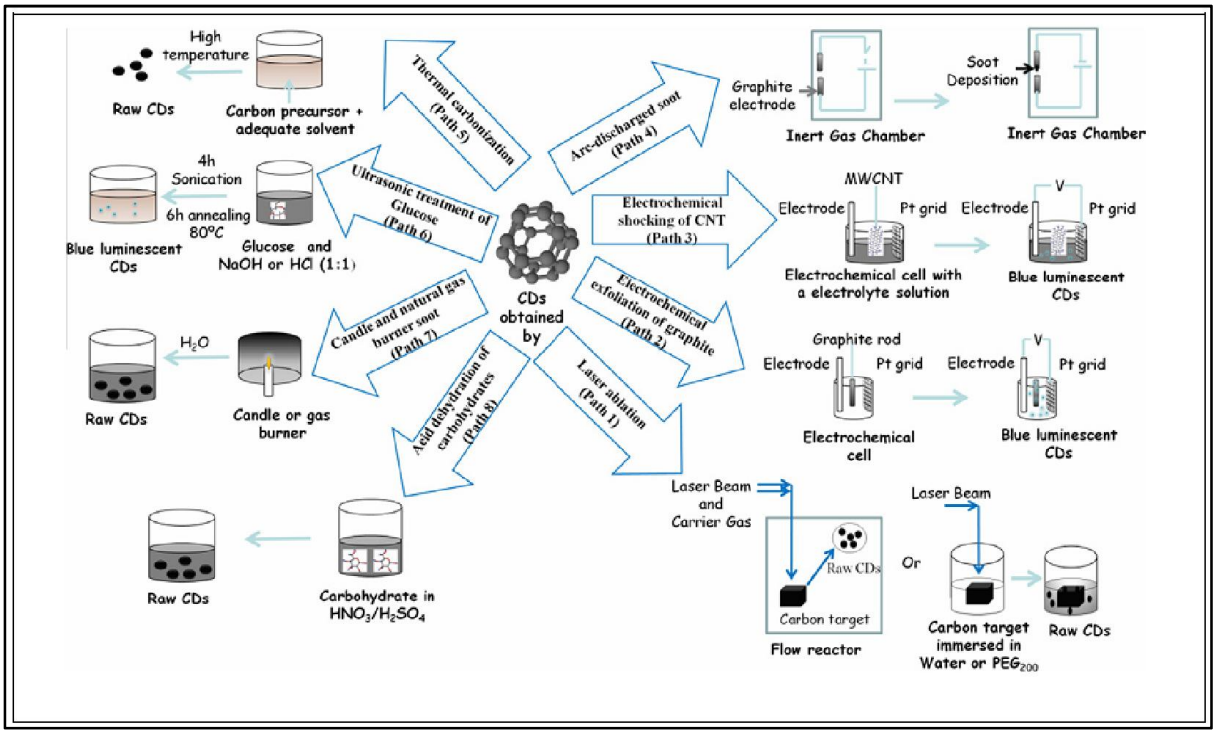

Figure 2.1: Schematic representation for methods of synthesis of C-dots (adapted from Ref no. 1)

Purification becomes an important step to get relieved from unwanted impurities and carbonaceous materials in the C-dot solution and also obtain homogenous suspension of the same for further biological applications. For biological applications like Drug delivery and Bio-imaging, C-dots need to be highly stable in the physiological environment. Purification step also enhances the fluorescence property of C-dots.

2.2 MATERIALS AND METHODS

Synthesis of C-dots was attempted from different precursors which included both natural as well as of chemical origin. The precursors were selected on the basis of their high carbon content and the ratio of H, C and O in their sugar moieties.

Trapabispinosa peel (Water chestnut peel) **[2]**, *Azadirachtaindica* gum (Neem gum) **[3]** and *Sachharumofficinarum* juice (Sugarcane juice) **[4]**and *Acacia Arabica* gum (Gum Arabic) **[5]**were selected as natural precursors, whereas Sorbitol **[6]** and Phenylalanine **[7]** were selected as chemical precursors for the synthesis of C-dots. Three methods namely refluxing at high temperature, microwave assisted heating and synthesis at room temperature was employed for different precursors.

Two widely used methodologies in nanoparticle separation and purification like Dialysis and Sucrose Density Gradient Centrifugation (SDGC) were used in the present work.

Trapabispinosa(water chestnut) and Sugarcane juice were procured from the local market. Neem gum was removed from the *Azadiractaindica* tree in the nsnRccampus. Sorbitol and Phenyl alanine were procured from Sigma Aldrich, USA. Sodium Hydroxide (Merck) and Ethanol (HangsuHuaxi Int. ltd) were used as surface passivating agent. Sucrose (HiMedia) and Dialysis membrane (Mol. Wtcutoff 12-14 kD, HiMedia) were used for purification of C-dots. All the chemicals used in the experiments were of analytical grade. The reagents were prepared in double distilled water (18 MΩ). Glasswares were pre-washed with chromic acid, (2% solution of Potassium dichromate in conc. H_2SO_4 and the diluted upto 10 times using distilled water for washing purpose) to remove all the metal contaminants and later washed 3 times with double distilled water. The glasswares were dried in hot air oven at 100ºC prior to use.

2.2.1 Synthesis of C-dots by Reflux method

2.2.1.1 Synthesis and Purification of C-dots synthesized from peels of Water chestnut

Water chestnut peel was soaked in cold water for 30 min to soften the peel. 50 grams of the peel was crushed in 500 ml of distilled water and centrifuged to obtain clear light pink extract. For synthesis of C-dots, 100 ml of *Water chestnut* peel extract was refluxed for 2 h at 90 °C till the solution becomes pinkish brown (Fig. 2.2).

Resulting solution was centrifuged at 5000 rpm for 20 min and suspended in 5 ml 1 M NaOH to solubilize C-dots and enhance the fluorescence ability. In order to purify C-dots, 3 ml of the above solution was dialysed in pre-activated Dialysis bag against nanopure water for 24 h. A Clear yellowish suspension of C-dot was obtained which exhibited intense green fluorescence under UV-light.

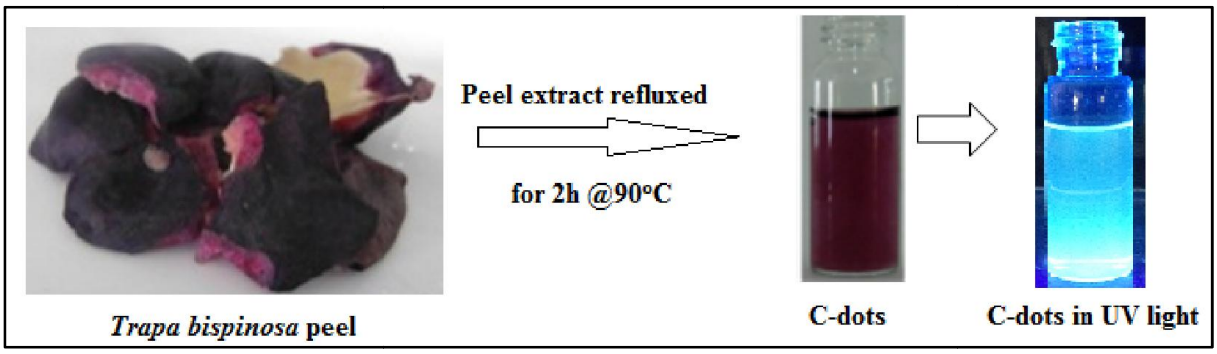

Figure 2.2: Synthesis of Water chestnut peel C-dots and appearance of green fluorescence under UV light

2.2.2 Synthesis of C-dots at Room Temperature

2.2.2.1 Synthesis and purification of C-dots synthesized from Sugarcane juice

Sugarcane juice contains high amount of sucrose which acts as an excellent precursor for C-dots synthesis at room temperature. Alkali induced degradation of Sugar by sonication and other unknown components present in the juice lead to the formation of C-dots as per earlier speculations. Sugarcane juice was purified by repeated centrifugation till a clear supernatant was obtained. In a typical procedure, 3 ml of 5 M NaOH and abs. Ethanol mixture was added drop wise in 50 ml purified juice under stirring. Solution was subjected to sonication for 30 minutes under similar conditions till it becomes reddish brown in color (Fig. 2.3). After centrifugation for 15 minutes at 5000 rpm, solution was observed under UV-light

(365 nm). Dark green fluorescence was observed as comparison to feeble green fluorescence of sugarcane juice.

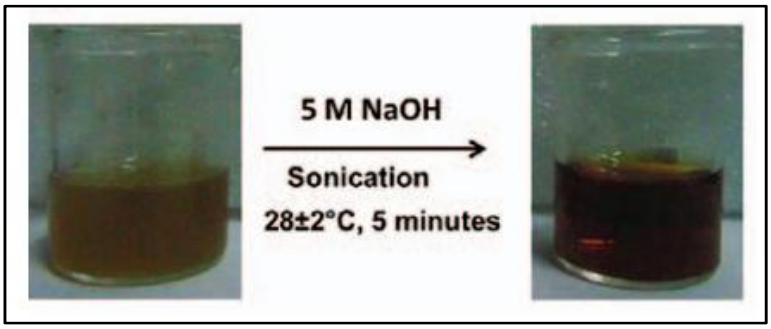

Figure 2.3: Synthesis of sugarcane juice C-dots at room temperature

To separate C-dot from this mixture, a lucid technique widely used in biology for the separation of materials based on their size and shape called Sucrose Density Gradient Centrifugation (SDGC) was performed. Gradient was made by overlaying 50–100% of pure sucrose in test tube starting from highest concentration at the bottom. 2 ml of the sample to be fractionated was top layered and spun for 30 minutes at 6000 rpm (Fig. 2.4).

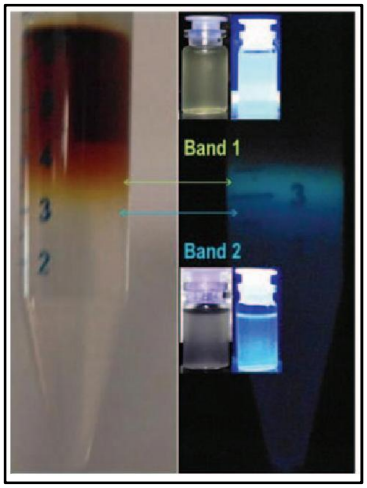

Figure 2.4: Separation of C-dots using SDGC and the fluorescent image of bands in UV light

Due to limitations like low reproducibility, contamination of C-dots with sucrose and less yield; SDGC was further not used for separation. C-dots were purified using Dialysis membrane.

2.2.2.2 Synthesis and Purification of C-dots synthesized from Neem Gum

Owing to the chemical components of Neem gum which is rich in various carbohydrates, it was selected as a potential precursor for synthesis of C-dots at Room

temperature. 1g of Neem gum was dissolved in 20 ml of nanopure water. This solution was incubated without heating in presence of 20 ml of 1M NaOH and abs. ethanol in ratio 1:1. After incubation at RT, dark yellow colored solution was observed under UV-light (λ=388nm) (Fig. 2.5).

Purification of CDs was achieved by conventional dialysis method. For this pre-activated dialysis membrane was used and crude C-dot solution was dialysed against nanopure water with constant mild stirring for 3 hours. Further the solution was observed under UV light which showed light green fluorescence.

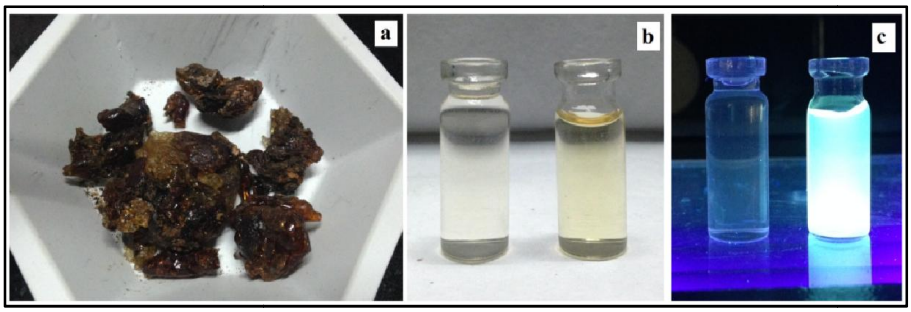

Figure 2.5: (a) Neem gum, (b) Neem gum solution and C-dots in ambient light and (c) in UV light.

2.2.3 Synthesis of C-dots by microwave assisted heating

2.2.3.1 Synthesis and Purification of C-dots synthesized from Gum Arabic (GA)

1g of GA was dissolved in 10mL of cold distilled water to obtain light yellow colored solution. To this mixture, 3 ml 1 M NaOH and abs. Ethanol mixture(1:1 ratio) were added and subjected to microwave assisted pyrolysis for 5 min till color of the mixture turned to wine red (Fig. 2.6).

C-dots were purified using Dialysis membrane against nanopure water under mild stirring.

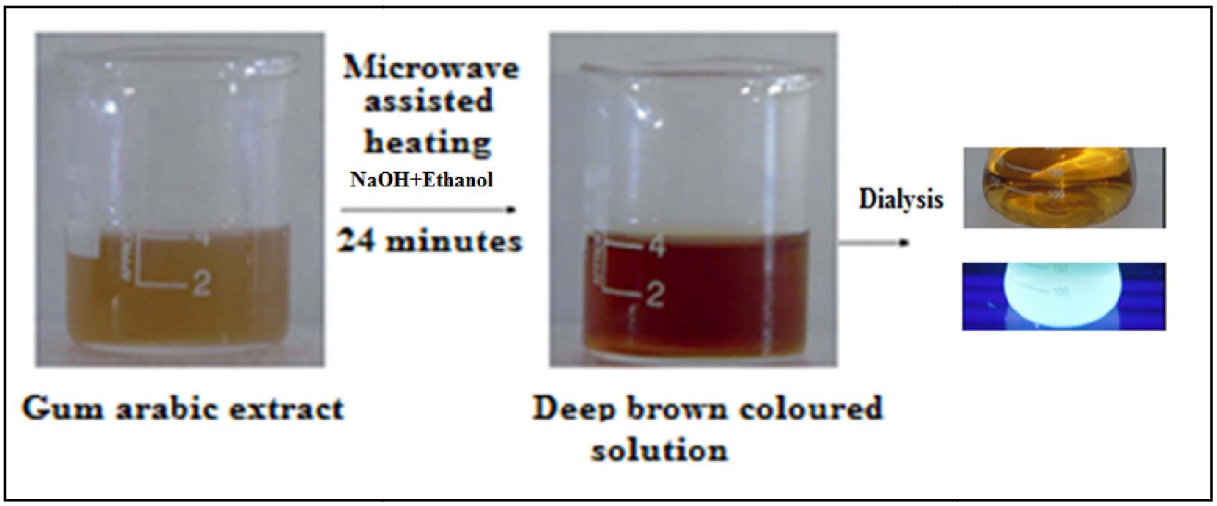

Figure 2.6: Synthesis of C-dots using GA solution &purified using Dialysis (upper panel in ambient light and lower panel in UV light)

2.2.3.2 Synthesis and purification of C-dots synthesized from Phenylalanine

2 g of phenylalanine was subjected to microwave-assisted heating for 30 s. To the precipitate, 3 ml of 1 M NaOH and abs. ethanol mixture (1:1 ratio) were added and further subjected to microwave heating for 30s. The resulting solution was cooled and its fluorescence under UV light (365 nm) was observed after addition of 1 ml of 1 M NaOH (Fig. 2.7).

In order to get pure C-dots from a mixture of other carbonaceous materials, the obtained solution was transferred to a pre-activated dialysis bag and dialysed against nanopure water for2-4 h under mild stirring conditions. The sample was analyzed spectrophotometrically.

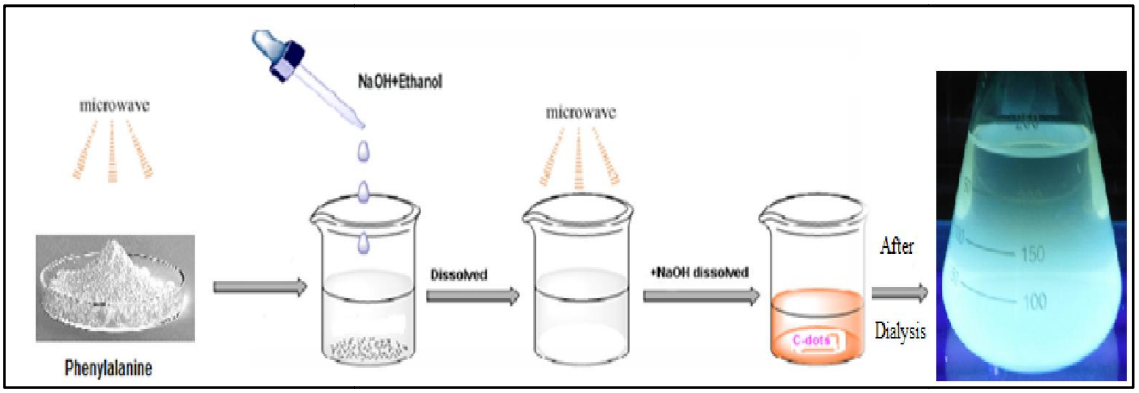

Figure 2.7: Schematic presentation of synthesis and purification of C-dots synthesized from Phenylalanine

2.2.3.3 Synthesis and purification of C-dots synthesized from Sorbitol

For synthesis of C-dots 15 ml of 1 M NaOH was added to 5 ml of Sorbitol and subjected to microwave assisted heating in a domestic microwave power output 900 W, 2450 MHz for 2 min. A black precipitate was obtained, which was re-dissolved in a15 ml mixture of 1 M NaOH and abs. ethanol (1:1 ratio). The resulting solution was observed under UV light (365 nm) for fluorescence (Fig. 2.8).

To get pure C-dots from the dark mixture containing other carbonaceous materials and impurities, the solution obtained was transferred to a pre-activated dialysis bag and dialysed against nanopure water for4 h under stirring conditions. The sample was analyzed spectrophotometrically.

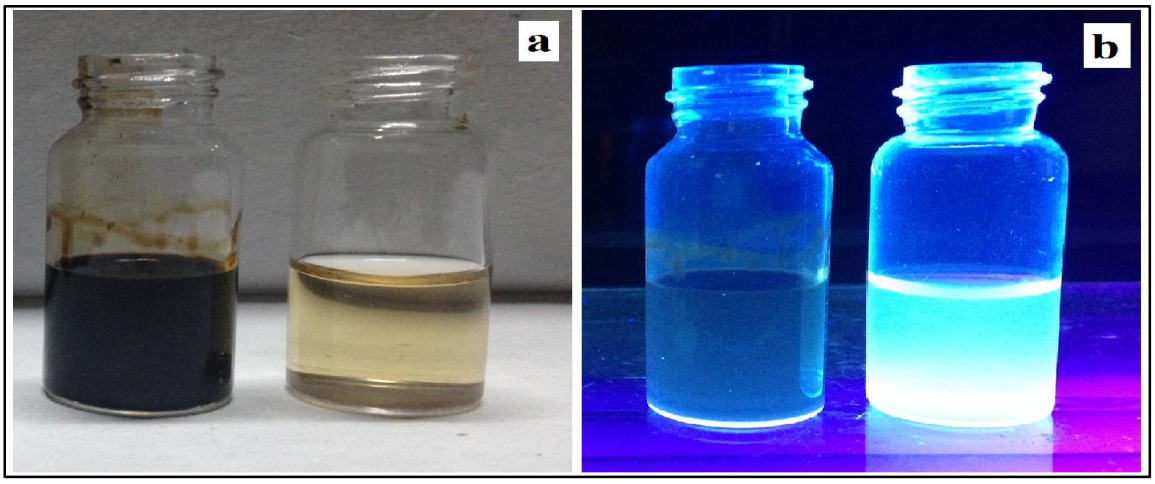

Figure 2.8: (a) Crude C-dots synthesised by microwave assisted method and purified C-dots as seen in ambient light & (b) in UV light

2.2.4 Synthesis of Mesoporous silica oxide- C-dot conjugate (meso-SiO_2/C-dots)

The main advantage of synthesizing Mesoporous silica oxide along with C-dots is that it can act as versatile potential drug delivery vehicle with high drug loading capacity. In an earlier attempt by other research group; to synthesize C-dots entrapped in meso-SiO_2in order to enhance the homogeneous size distribution, silica oxide nanoparticles were prepared separately followed by their attachment to synthesized C-dots and surface protection using polyethylene glycol **[9]**. In the present work, to prepare meso-SiO_2 capped C-dots, we selected rice husk (RH) as an ideal precursor because of the very high content of silica

present in it (>67%). We also developed a hot injection method for the preparation of the above complex at 80ºC using a three neck flask.

Rice husk was purchased from a local shop and washed several times with double distilled water to remove impurities. In a typical procedure, 20 g of washed rice husk (RH) was pyrolyzed for 3 h at 250ºC.Pyrolyzed RH was crushed to make a fine powder and used as the precursor for the synthesis of C-dots. 2 g of the above RH powder was mixed with 2 g of Cetyl Trimethyl Ammonium Bromide (CTAB) and was refluxed with 50 ml of ethyl acetate for 20 min in a three neck flask. At ~70ºC, a mixture containing 1 ml of Cysteamine hydrochloride (Cys-HCl) (3000 ppm), 3 ml 5N NaOH and 3 ml abs. Ethanol was injected with the help of a syringe. The reaction was allowed to continue for 4 h (Fig. 2.9).

The yellowish colored solution obtained was filtered and dialyzed against distilled water for 12 h under mild stirring. After dialysis, the resultant yellow colored solution exhibited very intense green fluorescence under UV light (365 nm), which is preliminary confirmation of the formation of C-dots. Before performing any biological studies, the meso-SiO_2/C- dot solution was centrifuged at 6000 rpm for 20 min and re-suspended in double distilled.

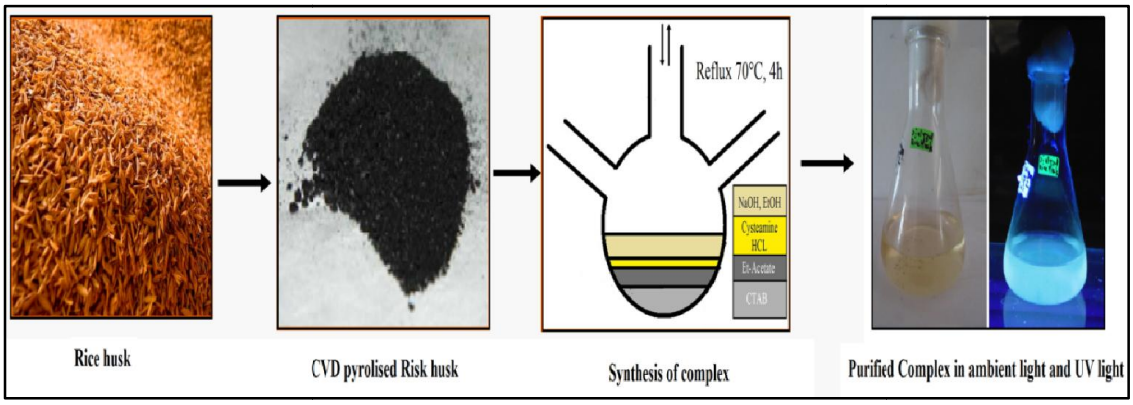

Figure 2.9: Schematic diagram of synthesis of meso-SiO_2/C-dot conjugate

2.2.5 Synthesis of Gold Nanorod- C-dot conjugate (C-dots@GNR)

Gold Nanorods (GNR) are metal nanoparticles explored for a broad spectrum of bio-medical applications such as drug/gene delivery, photothermal therapy, computational tomography, optical imaging etc**[10]**. GNRs with suitable aspect ratios can absorb and scatter electromagnetic radiation intensely in the NIR region, which can be used for improved optical imaging and photothermal cancer therapy. There are comparatively few reports of GNRs for drug delivery**[10,11],** mainly because of the potential toxicity due to the presence

of CTAB**[12]** on the surface. To eliminate detrimental effects of CTAB, we created a modified protocol for the attachment of exceptionally biocompatible C-dots on the surface of GNRs via weak interactions.

C-dots were synthesized from Gum Arabic and purified by the method as stated above in this same chapter. To obtain the C-dots@GNR conjugate, Bare GNRs were synthesized using a seed mediated method **[13]**. In short, to make primary seed solution, 2.5 ml of 1 mM of $HAuCl_4$ was added to 5 ml of 0.2 M CTAB. After addition of CTAB, the solution turned orange, which was further reduced by adding 600µl of pre-chilled 10 mM $NaBH_4$ under stirring for 5 min. To initiate formation of rods, the experiment was performed at 20°C.There was a slight modification in the preparation of growth solution for synthesizing C-dots@GNR conjugate. 2.5 ml of 1 mM$HAuCl_4$was added in 2.5 ml of 0.2 M CTAB. 113mlof4mM$AgNO_3$and 35ml of 78.8 mM ascorbic acid were added to this solution under gentle agitation forming a transparent growth solution. While stirring, 200µl of purified C-dots were added in clear growth solution. This mixture was vigorously agitated for 5 min before adding 4ml of seed solution. The reaction was allowed to take place for 2 h during which the solution turned royal blue.

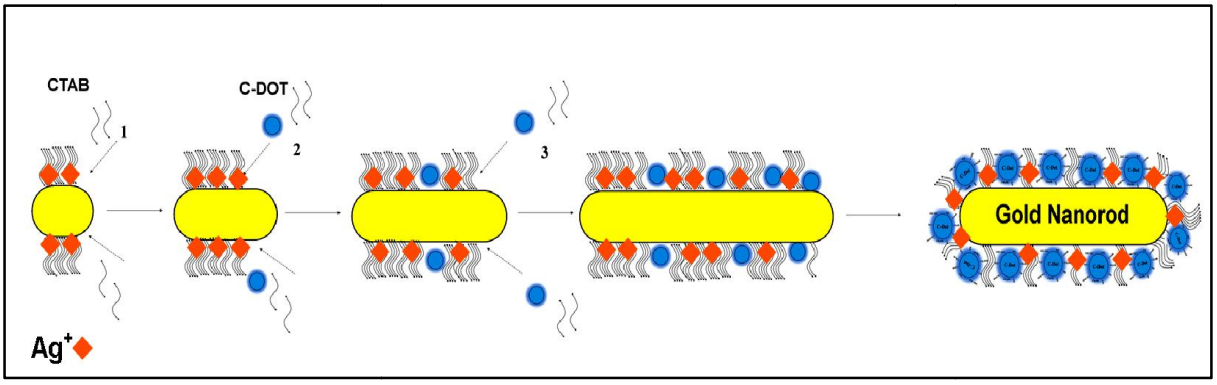

Figure 2.10: Schematic diagram of synthesis of C-dots@GNR conjugate

2.2.5.1 Drug Delivery and Cytotoxicity studies

DOX (0.0625mM) was attached on C-dot@GNR conjugate by a modified protocol as per our earlier work **[14]**. The solution was purified and attachment was confirmed using FTIR analysis. The drug loading Efficiency was calculated **[14]**. For drug release studies, samples were sealed in dialysis bag and placed in Phosphate buffer solution (pH 5.8 and 7.2) under mild stirring conditions. Samples were collected at regular time intervals and analysed

spectrophotometrically for concentration release using standard calibration curve of DOX at 485 nm.

Cytotoxicity analysis was performed using MMT assay on Vero (normal) cells and MCF 7(Cancerous) cells. Cells were seeded ($5x10^5$ per ml) in 96-well plates and incubated at 37°C under 5% CO_2 for 24 h. After sufficient growth of the cells, the medium was replaced with samples under consideration (bare GNRs, C-dots@GNR, C-dots@GNR–DOX and bare DOX) and incubated for 48 h. All the samples were replaced with MTT (200µg/ml). Cells were incubated for 2 h at 28±2°C to initiate formation of formazan. After development of the color, medium was replaced with 200 µl of DMSO. This complex was agitated moderately to dissolve formazan crystals. Formazan in DMSO was transferred to fresh 96-well plates and read on a microplate reader (Thermo, USA) at 570 nm.

2.3 REFERENCES

1. J. C.G. Esteves da Silva, H. M.R. Goncalves, Trends in Analytical Chemistry, 2011, 30 (8), 1189.
2. A. Mewada, S. Pandey, S. Shinde, N. Mishra, G. Oza, M. Thakur, M. Sharon and M. Sharon, Mater. Sci. Eng., C, 2013, 33, 2914.
3. C. Phadke, A. Mewada, R. Dharmatti, M. Thakur, S. Pandey and M. Sharon, J. Fluorsce, 2015, 25(4), 1103.
4. S. Pandey, A. Mewada, G. Oza, M. Thakur, N. Mishra, M. Sharon and M. Sharon, Nanosci. Nanotechnol. Lett., 2013, 5, 775.
5. M. Thakur, S. Pandey, A. Mewada, V. Patil, M. Khade, E. Ghoshi and M. Sharon, Journal of Drug Delivery, 2014, 1.
6. A. Mewada, S. Pandey, M. Thakur, D. Jadhav and M. Sharon, J. Mater. Chem. B,2014, 2, 698.
7. S. Pandey, A. Mewada, M. Thakur, A. Tank and M. Sharon, RSC Adv., 2013, 3, 26290.
8. W.H. Melhuish, J. Phys. Chem., 1961, 65, 229.
9. C. W. Lai, Y. H. Hsiao, Y. K. Peng and P. T. Chou, J. Mater. Chem., 2012, 22, 14403.
10. J. Siepmann and A. Gopferich,Adv. Drug Delivery Rev., 2001, 48, 229.
11. Barua,etal.,Proc. Natl. Acad. Sci. U. S. A., 2013, DOI: 10.1073/pnas.121689311, published ahead of print.
12. L. Vigderman, P. Manna and E. R. Zubarev,Angew. Chem., Int. Ed., 2012, 51, 636.
13. H. M. Courrier, N. Butz and T. F. Vandamme,Crit. Rev. Ther. Drug Carrier Syst., 2002, 19, 425.
14. S. Pandey, G. Oza, A. Mewada, R. Shah, M. Thakur and M. Sharon, J. Mater. Chem. B., 2013, 1, 1361.

CHAPTER III

Characterisation of C-dots and C-dot conjugates

3.1 INTRODUCTION

"Scientific principles and laws do not lie on the surface of nature. They are hidden, and must be wrested from nature by an active and elaborate technique of inquiry"

- John Dewey

In this Chapter characterization study of (i) Biogenically and Chemically synthesized C-dots and (ii) C-dot Conjugate is presented.

C-dots were purified as per the methods stated in Chapter 2, and solution was used for their characterization. Initial confirmation that the material synthesized is C-dots was assumed by checking the characteristic non-blinking fluorescence under UV light (λ=365nm).Further characterisation was done as follows:

1. Spectral properties of C-dots were studied by UV-Vis Spectroscopy (Lambda-25, Perkin Elmer) and Fluorescence Spectroscopy (Perkin Elmer, USA) using a standard quartz cuvette having path length 1 cm.

2. Morphological analysis and size of the synthesized C-dots and conjugates was done by Field Emission Scanning Electron Microscopy (FE-SEM) (Zeiss Microimaging GmbH, Germany) and Transmission Electron Microscopy (TEM) (Zeiss Microimaging GmbH, Germany) and High Resolution Transmission electron Microscopy (HRTEM) (Carl Zeiss MicroImaging, GmbH, Germany).Purified C-dots were concentrated in a vacuum oven at 60ºC for 3 h. Later, the concentrate was loaded on silicon substrate and formvar coated copper grid for FE-SEM and TEM/HRTEM analysis respectively.

3. To determine the elemental composition of the C-dots, Energy Dispersive X-ray Analysis (EDAX) was performed (Carl Zeiss Micro-Imaging, GmbH, Germany).

4. Presence of Carbon in C-dots was studied using X-ray Diffraction (XRD) (Phillips, The Nederland) and Raman spectroscopy (Jobin–Yvon Labram spectrometer). The samples were concentrated and then used for respective analysis.

5. Finally, to assess the functional groups associated with the surface of C-dots Fourier Transform Infrared (FTIR) spectroscopy (Brücker) studies were performed within the spectral window 500 to 4000 cm^{-1}.

3.2 RESULTS AND DISCUSSIONS OF C-DOT CHARACTERIZATION

3.2.1 UV-Vis Spectroscopy of C-dots

C-dots generally show absorbance in UV region with an extending tail in the visible region. Surface functionalisation may increase its absorbance to longer wavelengths **[1]**. Most of the times C-dots display two characteristic peaks in the UV range mainly because of the $\pi \rightarrow \pi^*$ electronic transitions of C=C and $n \rightarrow \pi^*$ transition of electrons associated with the carbonyl groups **[2]**. As per several hypotheses proposed by earlier researchers, the inception of fluorescence in C-dots is due to defects in the organization of their structures, mainly due to the presence of sp^2 and sp^3carbon clusters in definite ratios**[3]**.Moreover, decoration of the edges of C-dots by functional groups containing epoxides, hydroxyl groups and carboxylic acids also plays a central role in destroying energy traps (thereby generating electron–hole pairs) leading to fluorescence under UV light of a suitable wavelength**[4, 5]**.

Figure 3.1 displays UV-Vis spectra of all the C-dots synthesized using different precursors.

UV-Vis spectra of C-dots synthesized from Water chestnut peel extract show a broad hump at 536 nm (Fig. 3.1.a). To study the optical changes during formation, spectra were recorded at an interval of 30 min till 120 min when the color change was observed confirming the presence of C-dots. The sample was checked for fluorescence under UV light and displayed a deep green color (Fig. 2.2-Chp 2). Initially, a broad peak and a shoulder at 538 and875.61 nm were observed indicating the slow formation of C-dot as per previous studies. After 60 min, there was a slight narrowing and red shift (from 538 to 541 nm) indicating formation of fairly mono-dispersed C-dots. Finally after 120 min, a peak and shoulder at536 and 907 nm respectively were observed. There was a blue shift of2 nm after 120 min explaining the stabilization of the nanoparticles and/or decrease in the size of the C-dots. The peak at longer wavelength signifies functionalisation of C-dots with natural moieties which lead to a red shift in the spectra. PL spectrum was observed at 473 nm when C-dots were excited at 350 nm. Such narrow range emission spectra may be due to the clusters of nanoparticles and impurities of other carbonaceous materials (Inset of Fig. 3.1a).

On the other hand C-dots synthesized at Room temperature using Sugarcane juice and Neem gum showed Absorbance in the UV region. C-dots synthesized using sugarcane juice showed dark green hazy fluorescence which is possibly due to the presence of other carbonaceous materials in the solution. The solution was purified using dialysis which displayed bright

green fluorescence. The UV-Vis spectra of C-dots showed peaks centered at 237 nm and 380 nm due to the C=C stacking and the presence of carbonyl/hydroxyl groups respectively (Fig. 3.1b). Neem gum C-dots displays peaks at 216 nm and 275 nm which signifies that the structure of the nanoparticles may be more compact and not much functional groups could be exposed on the surface (Fig. 3.1c). It can also be seen that the background absorbance for neem gum C-dots was found to be less in comparison to sugarcane C-dots clearly showing presence of impurities in C-dots obtained from Sugarcane juice due to other carbonaceous materials which absorb at longer wavelengths **[6]**. Also, C-dots synthesized using natural precursors tend to contain a plethora of biological compounds which would hinder in the process to obtain pure nanoparticles solution.PL intensity was observed at 592 nm for sugarcane C-dots and a comparatively narrow PL of less intensity was found in case of Neem gum C-dots. The inception of PL is still not very clear in case of C-dots and may depend on various factors like surface functionalisation, edge effects, surface defects, size etc**[7]**.

C-dots synthesized using Gum Arabic solution show broad peak at 231 nm and 263 nm with minimised background fluorescence (Fig. 3.1d). Microwave assisted synthesis provide a controlled temperature and duration to get most optimum C-dots. The area under the peak is reduced as observed in the figure in comparison to that of Sugarcane and Neem gum derived C-dots thus showing more mono-dispersed C-dots **[8]**. PL spectra showed a sharp peak at 464 nm when excited at 250 nm which was found to be in agreement to the previous reports. C-dots absorb at shorter wavelengths and emit at longer wavelengths.

C-dots derived from phenyl alanine a sharp peak and a shoulder at 232 and 276 nm respectively (Fig. 3.1e) in the UV-Vis spectra. Almost negligible background absorbance is observed in the spectra. All the above properties are due to the specific surface functionalization and energy traps present in the C-dots. The dual peak in the UV range is a signature marker of C-dots [**7, 9]**.Another signature marker is the peak at468 nm in the PL spectra (λ_{ex}=250 nm), arising from the unique functionalization and surface properties of the C-dots **[7]**. UV-Vis spectra of Sorbitol derived C-dots highlights prominent peaks at 229 and 266 nm (Fig. 3.1f). Both the narrow peaks originate from sp^2carbon clusters present in the C-dots when functionalized by oxygen-containing functional groups. There is a blue shift in the first peak observed in Sorbitol derived C-dots indicating smaller size as well as deep UV fluorescence in comparison to all other C-dots discussed above. The inset of Figure.3.1f displays the PL spectra of the C-dots. A sharp peak at 552 nm (λ_{ex}=250 nm)indicates excitation dependent emission by C-dots; another important trait of C-dots used as a

diagnostic marker **[1]**. The origin of the PL can be speculated because of the carboxylate functional moieties on the particle surface and the oxygen-containing groups in the precursor (sorbitol in this case). Thus, we can say that C-dots synthesized using microwave assisted method showed deep UV absorbance as compared to the C-dots synthesized using other methods in our case. All the above C-dots solution were subjected to stability testing by storing the solution at room temperature. Sorbitol derived C-dots were found to be most stable and did not show any signs of agglomeration or contamination till a period of 3 months. C-dots synthesized from natural precursors showed signs of clustering and increase in turbidity possibly due to the natural moieties present on their surfaces. There was no decrease in fluorescence intensity of Sorbitol C-dots in comparison to other C-dots which displayed diminished or slightly hazy fluorescence under continuous UV light exposure. Hence, purified C-dots were selected for drug delivery applications.

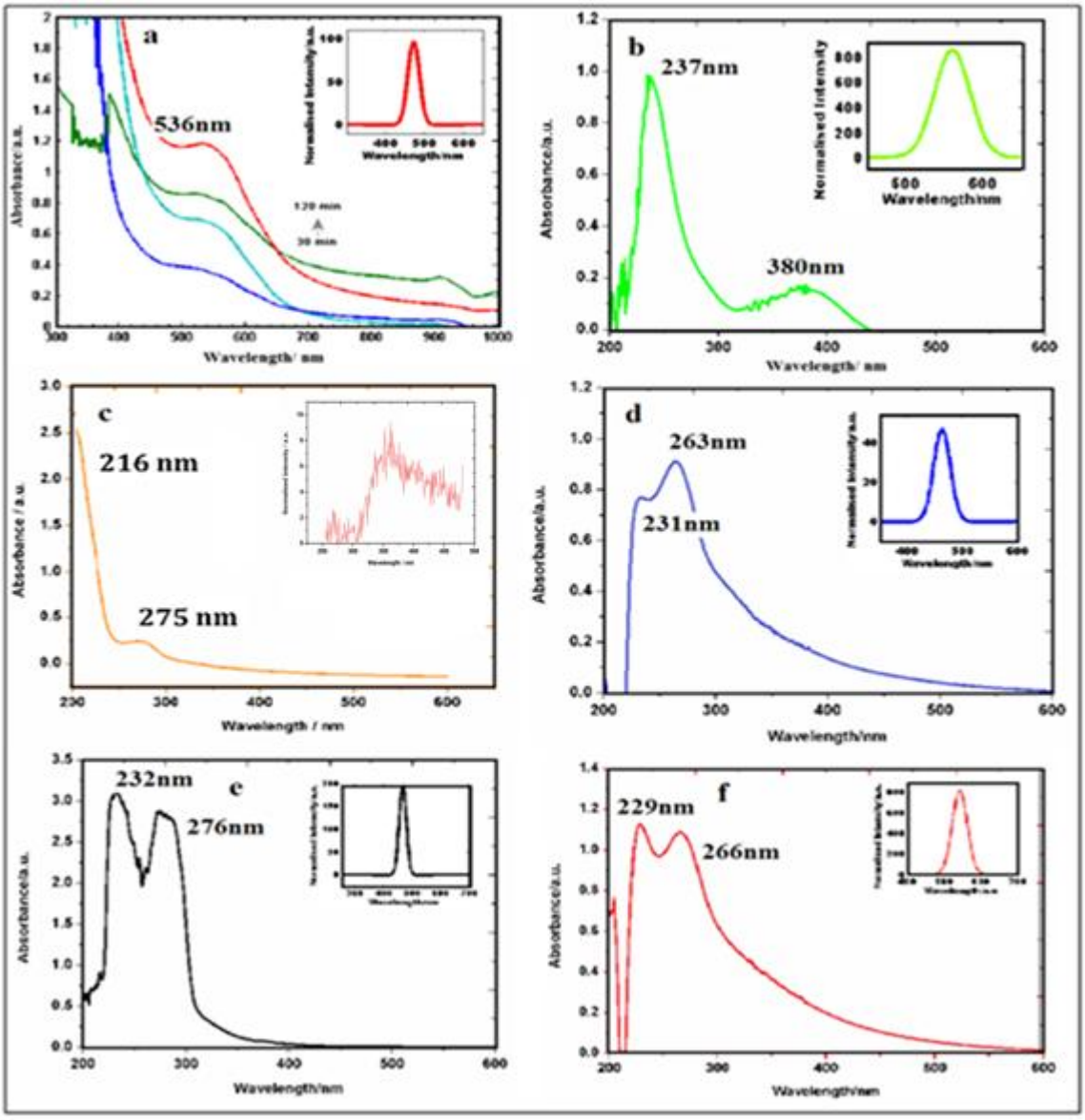

Figure 3.1: UV-Vis spectra of purified C-dots derived from (a) Water chestnut, (b) Sugarcane juice, (c) Neem gum, (d) Gum Arabic, (e) Phenyl alanine and (f) Sorbitol; inset of all the figures display PL spectra of respective C-dots

3.2.2 Morphological Analysis of C-dots

Morphological analysis have been done using FE-SEM, TEM and HRETM to study the shape size and distribution of C-dots and also to learn the difference in the different types of C-dots based on the precursors and method for synthesis. HRTEM image (Fig. 3.2a) shows the presence of spherical C-dots ranging from 5 to 10 nm synthesized using Water chestnut peel extract. It can be clearly seen that there is a range of size of the C-dots observed in the same field thus suggesting polydispersity in the solution which is in agreement with the UV-

Vis spectra of the C-dots solution which shows a broad area under the peak. Also, a thick covering or coating which could be due to the inherent proteins or polysachharides carrying a group of varied size of C-dots is seen in the image. This surface coating can be one of the reasons for the absorbance at longer wavelengths.

HRTEM image of C-dots derived from Sugarcane juice is observed in Figure 3.2b. The size of C-dots falls approximately in the range of 7-18 nm in diameter and displays a mixture of variously shaped nanoparticles. C-dots synthesized using neem gum was found to be roughly oval in shape in HRTEM image (Fig. 3.2c). The size of the C-dot can be observed as approximately 12 nm. C-dots synthesized at room temperature do not use any parameter control in the formation process and hence different shaped C-dots can be seen.

On the other hand, Microwave assisted synthesis of C-dots displayed a better control over size and shape during fabrication and mostly all spherical or roughly spherical C-dots were observed. Figure 3.2d displays TEM image of C-dots synthesized using Gum Arabic. A cluster of C-dots can be observed in the size range of 4-8 nm. The FE-SEM image (Fig. 3.2e) shows the presence of roughly spherical C-dots synthesized using Phenylalanine of size 7–12 nm. A HRTEM image showing a spherical C-dot of 7 nm is displayed in the inset of Figure. 3.2e (lattice constant=0.3 nm). The TEM image shows the presence of C-dots derived from Sorbitol is displayed in Figure 3.2f. The size of C-dots was found to be 8-10 nm. The HRTEM image of an individual C-dot is displayed in the inset of Figure. 3.2f which shows lattice constant of 0.33 nm.

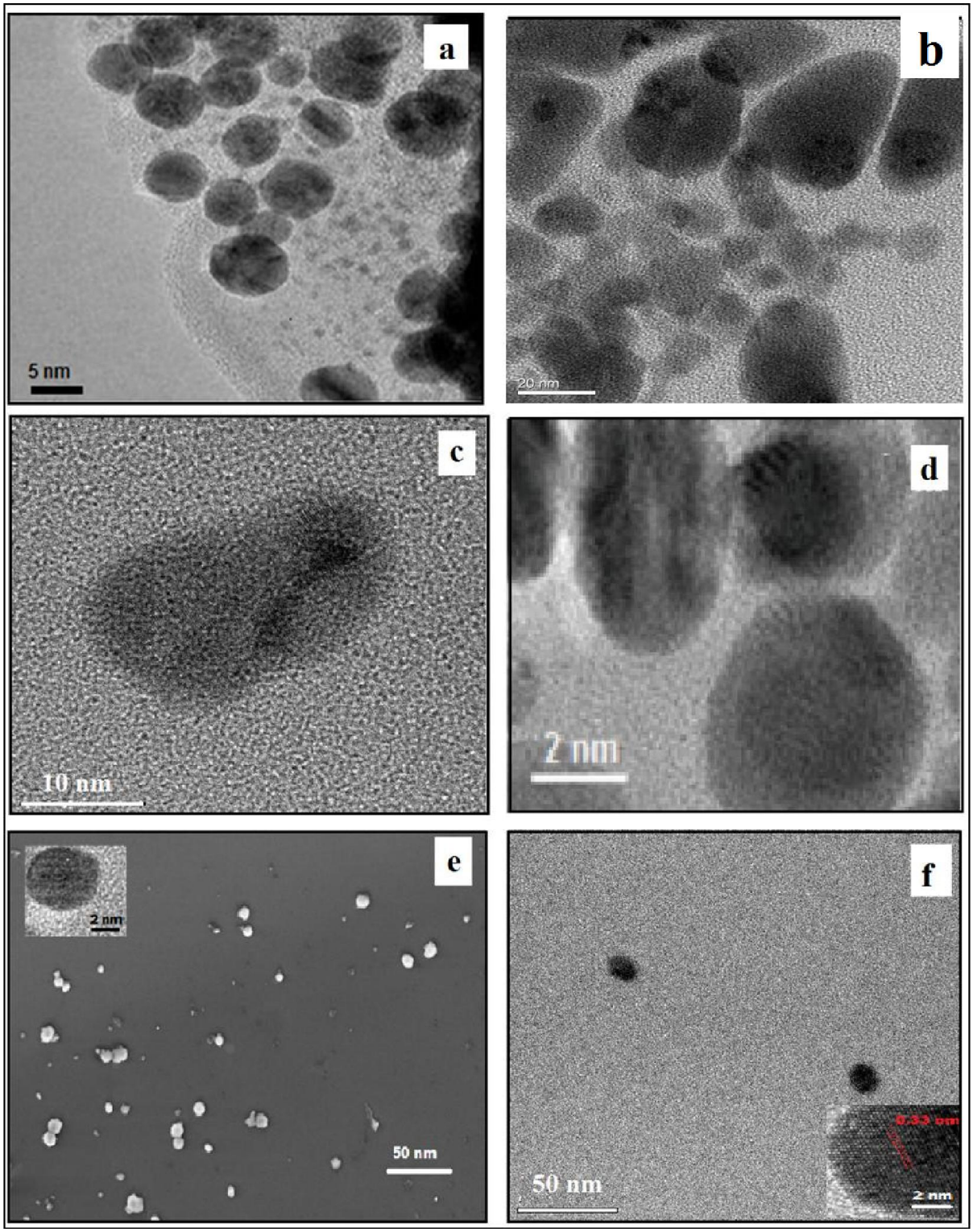

Figure 3.2: HRTEM image of (a) Water chestnut C-dots, (b) Sugarcane C-dots, (c) Neem gum C-dots, (d) TEM image of Gum Arabic C-dots, (e) FE-SEM image of Phenyl alanine C-dots; inset displays HRTEM image of single C-dot and (f) TEM image of Sorbitol C-dots; inset shows HRTEM image of a Single C-dot

3.2.3 XRD Analysis of C-dots

X-Ray Diffraction analysis is done to see the nature of crystallinity of the materials. The XRD plot shown in Figure 3.3displays sharp multiple peaks in majority of the graphs. The plot clearly shows the peaks for graphite, indicating the presence of carbon particles but the order of crystallinity is short. The characteristic XRD fingerprint for carbon is between 23-27° due to (002) plane and 41-47° due (101) plan which is seen in all of the plots, with noise present in them**[10]**.

The XRD image of C-dots synthesized using Water chestnut peel extract show the presence of intense peak at 2θ = 24.7° and a weak peak at 2θ = 43.3° that are assigned to (002) and (101) diffraction patterns of graphitic carbon respectively (Fig. 3.3a). Former peak corresponds to the interlayer spacing of ~ 3.77 Å which is slightly more than the spacing between (002)planes in bulk graphite (3.44 Å). These finding explain turbostratic carbon structures. Pan et al. explained graphitic nature of the C-dots with an inner layer spacing of ~ 4.12 Å which is in strong agreement with our result**[11]**.

The XRD plot of C-dots synthesized using Sugarcane juice is displayed in Fig. 3.3b. The broad peaks of the all the samples indicate that small grain size which is in agreement with the TEM images which shows that particles are small within few tens of nanometer(in most precursors), which is true as per Scherrer equation which shows an inverse proportionality between peak broadening and crystal thickness.

$$B = \frac{K\lambda}{Lcos\theta}$$

Where,

K = Scherrer constant

λ= Wavelength of the X ray radiation used

B = FWHM of peak after removing instrumental broadening

L = Size of the crystal (or grain)

θ= Bragg angle

Figure 3.3c displays the XRD pattern of C-dots synthesized using Neem gum extract which show multiple peaks due to noise and XRD image of C-dots synthesized using Gum Arabic (Fig. 3.3d) show a prominent peak 2θ = 25.87° and a feeble peak around 2θ = 42°, both the

peaks depicting graphitic nature of C-dots **[12]**.The multiple small peaks observed may be because of other compounds present in the solution due to the use of natural precursors.

XRD pattern of C-dots synthesized using Phenylalanine (Fig. 3.3e) displays a characteristic peak at $2\theta = 25.67°$ and at $2\theta = 42.7°$ along with several other small graphitic peaks and Figure 3.3f shows the plot for Sorbitol derived C-dots with a typical peak at $2\theta = 25.7°$ and a mild hump at $2\theta = 43.47°$ which can be assigned to the diffraction peaks of (002) and (101) planes of graphitic carbon respectively. Both the samples show an inter-layer spacing in the range of ~ 3.6-3.8 Å which is larger than the bulk graphite interlayer spacing and in accordance to the previous data on C-dots. The plot fines that the structure of C-dots is not uniformly crystalline thus proving it to be turbostratic in nature (which may be due to the surface defects and the variable arrangement of sp^2 and sp^3 carbons as well as the presence of Oxygen containing functional groups as explained in the earlier sections of the chapter).

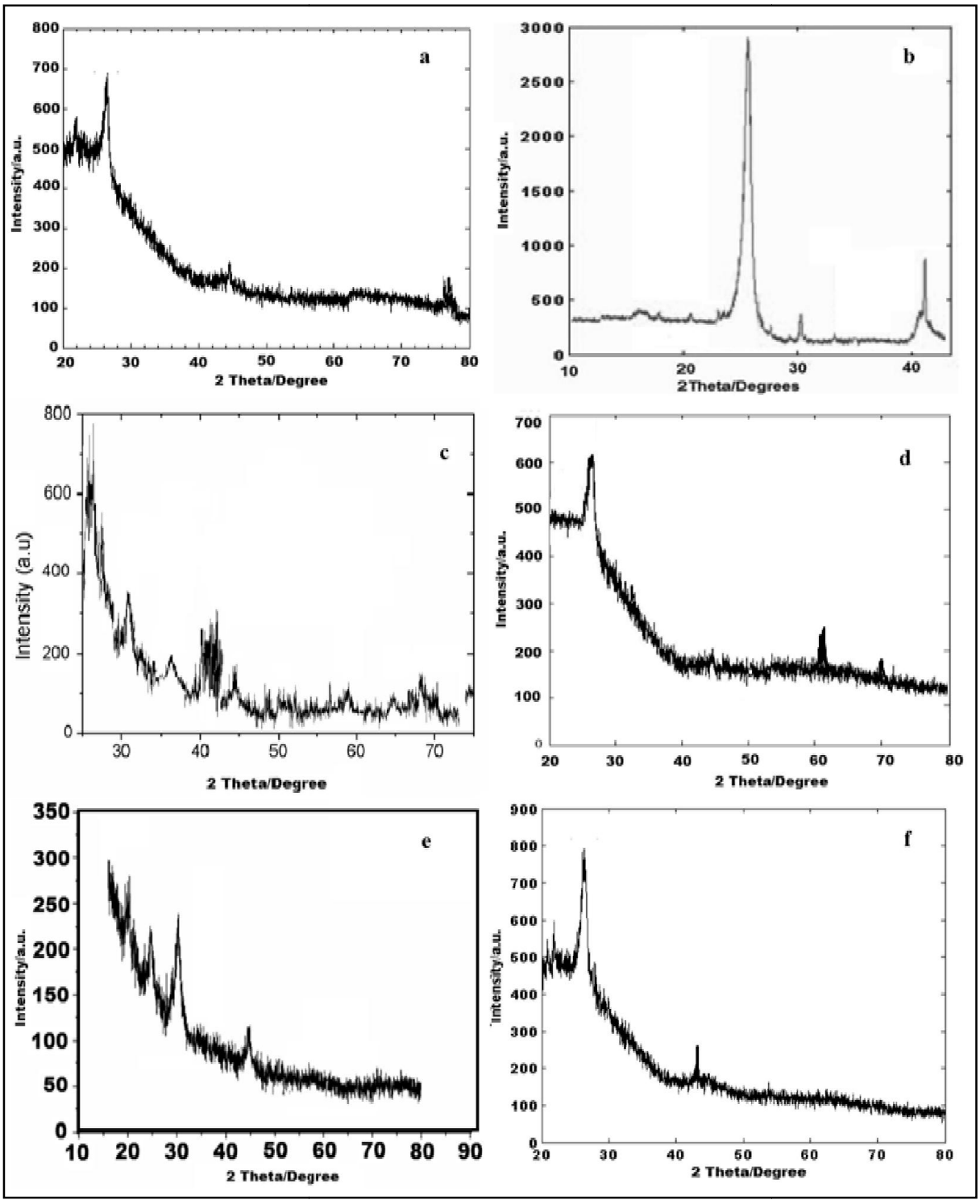

Figure 3.3: XRD pattern of (a) Water chestnut peel, (b) Sugarcane, (c) Neem gum, (d) Gum Arabic, (e) Phenylalanine and (f) Sorbitol derived C-dots

3.2.4 Raman Spectroscopy of C-dots

Raman scattering is an inelastic scattering, in which kinetic energy of the incident photon is not conserved, it gets enhanced or annihilated during interaction with phonons of the material used for study. This principle is used in Raman spectroscopy to study the vibrational and rotational excitations in the molecules; which are closely related to the chemical bond and symmetry of molecules. The intensity of photon is plotted against the energy. The intensity is measured in arbitrary units (a.u.), while energy in cm^{-1} because energy is inversely proportional to the wavelength of radiation. This gives an easier way to understand the shift (difference) in incident excitation wavelength and Raman spectrum wavelength.

The Raman spectroscopy of the C-dot confirms the presence of carbon which in support of the X-ray diffraction data and TEM characterisation.

In Figure 3.4, we can observe that C-dots synthesised using Water chestnut peel (Fig.3.4a), Sugarcane juice (Fig. 3.4b) and Phenylalanine (Fig.3.4e) shows presence of higher sp^2 carbon and having lesser hydrogen content leading to nano crystalline graphitic structure as compared to C-dots synthesized using Neem gum (Fig.3.4c), Gum Arabic (Fig.3.4d) and Sorbitol (Fig. 3.4f) which have higher sp^3 carbon and show the presence of more functional groups as they are more active than former**[13]**. The Raman spectrum is complimented by FTIR spectroscopy in the next section which suggests the similar results about C-dots derived from Neem gum, Gum Arabic and Sorbitol have higher surface energy (functional groups) as compared to other samples.

Nano-crystalline carbon forms show a typical Raman spectrum with a D-band and G-band centered around 1360 cm^{-1} and 1550 cm^{-1} respectively which are due to the presence of sp^2 carbon only **[14]**. Our results are in agreement to these findings and show the presence of graphitic carbon. The ratio of the intensity of D-band and G-band (I_D/I_G) is the measure of the disorder extent in the material and the ratio of sp^3/sp^2 carbon **[7]**. The I_D/I_G ratio of our samples was found to be in the range of 0.5-1.75 showing structure defects in C-dots due to the presence of oxygenated functional groups.

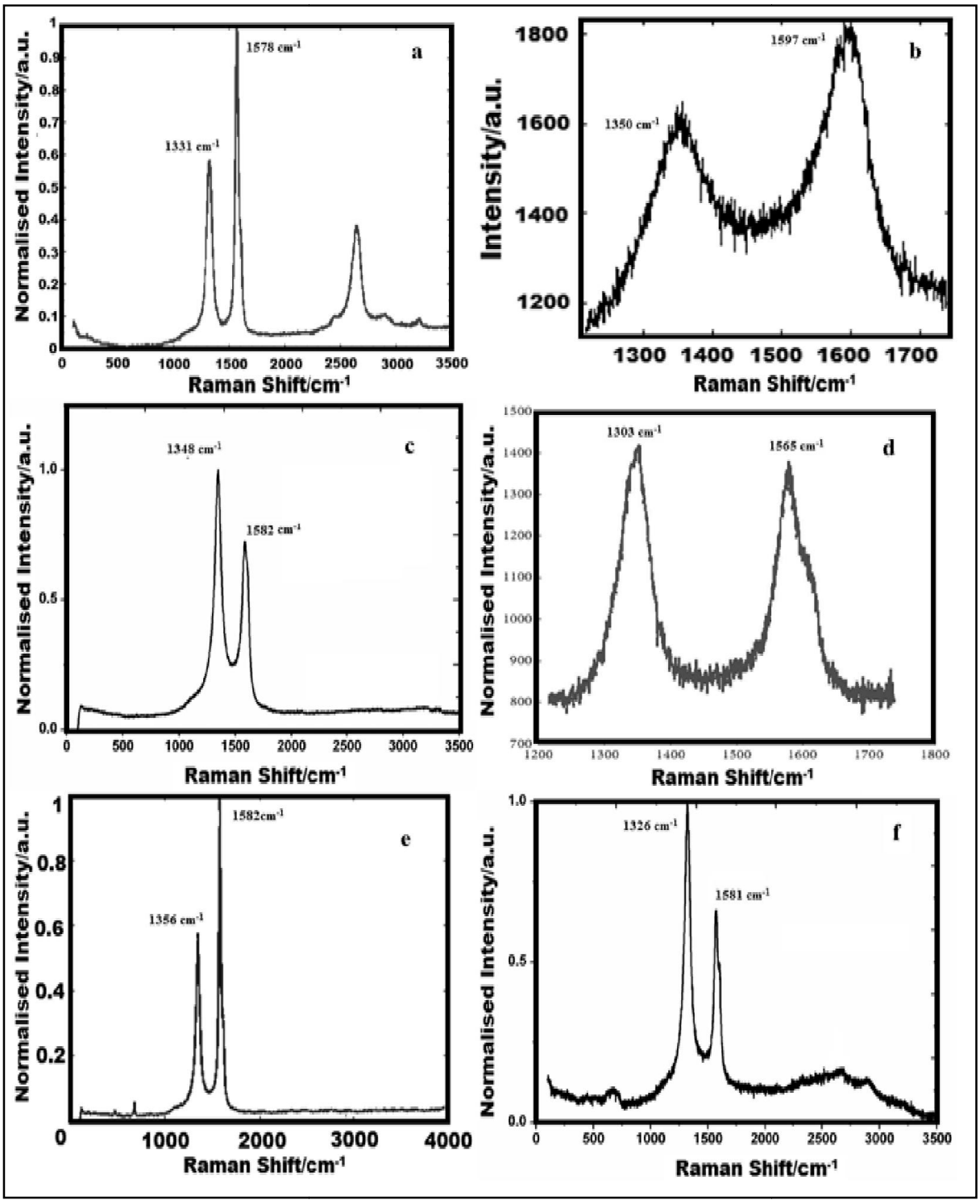

Figure 3.4: Raman spectra of C-dots derived from (a) Water chestnut peel (b) Sugarcane juice (c) Neem gum (d) Gum Arabic (e) Phenylalanine and (f) Sorbitol

3.2.5 FTIR Analysis of C-dots

FTIR is an instrument which acquires broadband Near Infra-Red (NIR) to Far Infra-Red (FIR) spectra. This spectroscopy collects all wavelengths simultaneously; the feature is called multiplex advantage. Infrared spectrum presents the footprint of sample with absorption peaks which correspond to the frequencies of vibrations between the bonds of the atoms making up the material. Energy of infrared region is not sufficient for electronic transition, rather excites the vibrational and rotational motion in molecules.

3.2.5.1 C-dots from Water chesnut peel

FTIR spectra (Fig. 3.5a) shows the functional groups associated with the surface of C-dots. A strong absorption at 2925 cm^{-1} and 2860 cm^{-1} is assigned to –C-H stretching which may arise due to methyl or methylene groups associated with the aliphatic hydrocarbons present in the extract of Water chestnut peel. A weak absorption at 3394 cm^{-1} is due to O-H stretching. An overtone at 1648 cm^{-1} is due to –C=C- stretching. The presence of such functional groups explains the functionalization of C-dots containing -CH_3 and -OH which can be used as linkers for the attachment of the therapeutic moieties such as drugs for targeted delivery to diseased cells.

3.2.5.2 C-dots from Sugarcane

FTIR studies of purified C-dots show strong peaks at 883, 1051, 1456 and 1736 cm^{-1} which are assigned to –CH bending S=O stretching, C=C stretching and –CO stretching of carboxylic acids respectively (Fig. 3.5b) Presence of Sulfur may be due to presence of proteins in sugarcane juice which must have interacted with oxygen. Peaks in the spectra are found to be sharper indicating the relative purity of the sample.

3.2.5.3 C-dots from Neem Gum

FTIR spectra (Fig. 3.5c) of C-dots from neem gum display multiple bands. A band was observed at 1028.90 cm^{-1} with fair intensity which may be due to the electrostatic interactions of alcoholic C-O stretch with other functional groups. Also appearance of band at 1365.11 cm^{-1} was observed which correspond to C-C and C-O stretch as well as CH_3 bend. All these explain the functional groups exposed on the surface of C-dots emerging after the fabrication of C-dots using neem gum.

3.2.5.4 C-dots from Gum Arabic

FTIR of C-dots (Fig. 3.5d) show IR bands at 631 cm^{-1} and 1044 cm^{-1}, representing C–H bending of acetyl groups of saturated hydrocarbons on the surface of the C-dots. Peaks at 1257 cm^{-1} and 1737 cm^{-1} represent alcoholic –OH and carboxylic $–CO_2$ stretches, which indicate surface passivation on C-dots due to NaOH treatment. Moreover, more evidence of surface passivation is seen by a few other peaks at 1534 cm^{-1}, 1626 cm^{-1} and 1680 cm^{-1}. These bands depict 1^{o} amide N–H bending, aldehyde C=O stretching, and anhydride C=O stretching from polysaccharide and residual amino acid backbones on the surface.

3.2.5.5 C-dots from Phenylalanine

The FTIR spectrum of bare C-dots (Fig. 3.5e) show bands at 582 cm^{-1} and 989 cm^{-1} for the alkene C – H bending vibrations, whereas the multiple broad bands from 1000 – 1250 cm^{-1} correspond to the C – O and C – O –C stretch vibrations on the surface of the passivated C-dots. The IR band at 1410 cm^{-1} is attributed to a few other exposed functional groups such as alkane C–H, CH_2 and CH_3 bends, and alkene C=C stretch. The band at 2897 cm^{-1} corresponds to the amine N –H bend. The strong band at 3350 cm^{-1} indicates the presence of the O –H stretch due to the NaOH mediated hydroxyl functionalization and due to the suspension of C-dots in an aqueous solution.

3.2.5.6 C-dots from Sorbitol

FTIR studies of Sorbitol derived C-dots are explained in Chapter 5 (Fig. 5.5a).

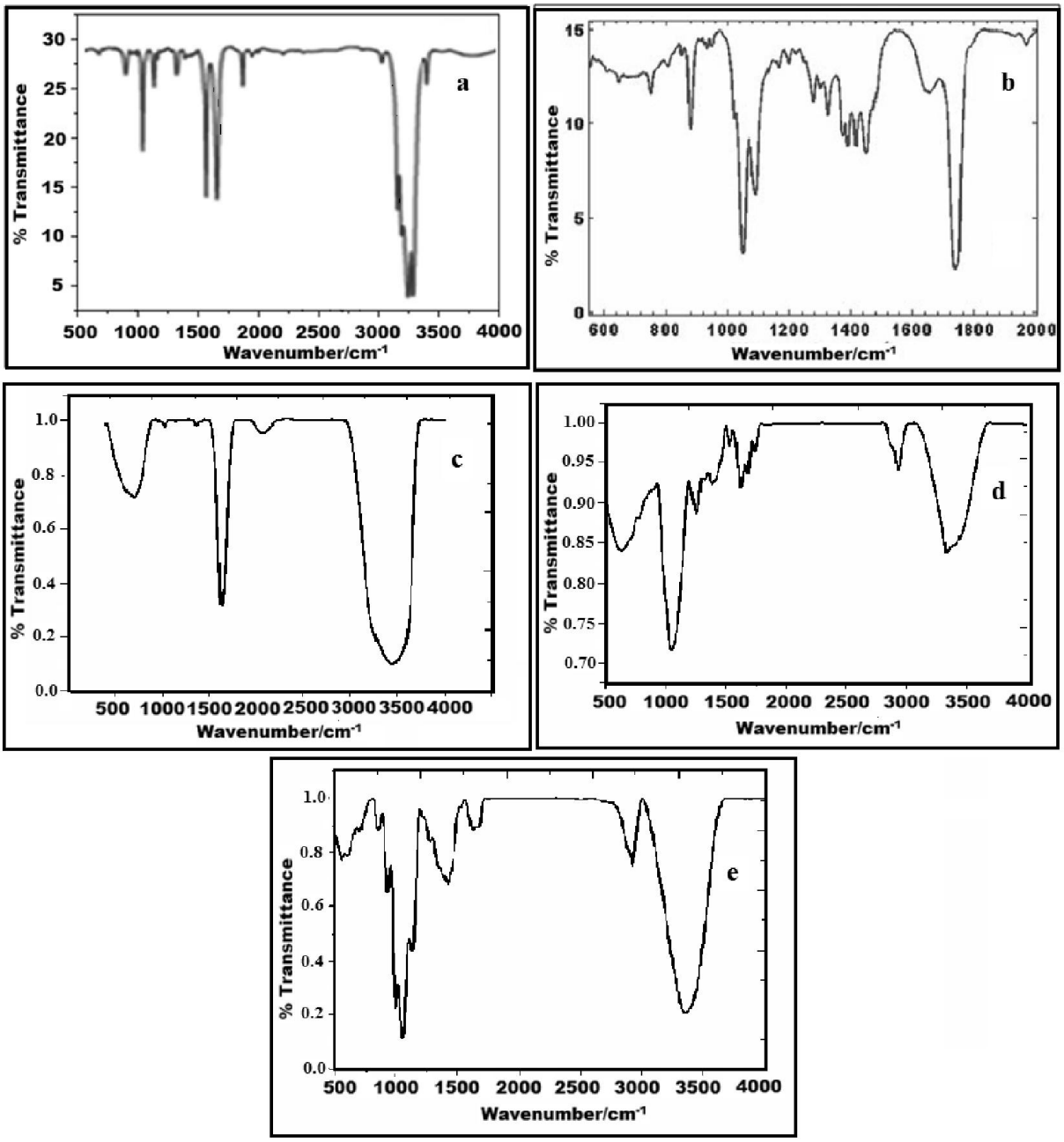

Figure 3.5: FTIR spectra of C-dots synthesized using (a) Water chestnut peel, (b) Sugarcane juice, (c) Neem gum, (d) Gum Arabic and (e) Phenylalanine

3.3 RESULTS AND DISCUSSIONS OF C-DOT CONJUGATES

3.3.1 Meso-SiO_2/C-Dot Conjugate Analysis

Rice husk ash (RHA), owing to its high content of silica has been used as a precursor for the synthesis of mesoporous silica oxide micro-particles along with highly fluorescent C-dots. Being rich in carbon and silica, rice husk can act as an ideal precursor for synthesis of C-dots as well as mesoporous silica oxide. The advantages of a one pot synthesis of meso-SiO_2/C-dots are the following:

i. Rice husk, being a natural material act as a highly biocompatible precursor for a C-dot synthesis.
ii. Involvement of toxic chemical constituents such as tetraethyl orthosilicate (TEOS) is avoided.
iii. The process is rapid hence ideal for the commercial synthesis of C-dots.
iv. Mesoporous silica oxide along with C-dots can act as a versatile drug delivery vehicle with a high drug loading capacity.

Pyrolysis of RH before the synthesis of C-dots was done to solubilise the major carbon content in ethyl acetate, and particularly, the high amount of silica present in it. During carbonization of RH the carbonaceous materials get oxygenated, which is an important prerequisite for C-dot synthesis [**15].**A major part of the silica gets separated during the reflux due to its high solubility in ethyl acetate. After injection of 5 M NaOH along with Ethanol, there was a transformation in the color from black to pale yellow, a common color marker for C-dot synthesis [**6, 9 & 16].**In the reaction vessel, due to a slightly alkaline environment (pH 6.4) and the presence of surface passivation agents such as ethanol, the synthesis of highly fluorescent C-dots was catalysed. An alkaline environment is found to be highly favourable for the synthesis of C-dots [**7].** Simultaneously, the formation of mesoporous silica oxide is helped by the cationic surfactant CTAB. Simultaneous formation of C-dots can take place, which can attach to meso-SiO_2 by adsorption, or covalent bond formation (Fig. 3.6) alternatively cysteamine hydrochloride in a lower concentration could act as a bridge between mesoporous silica and the as synthesized C-dots. Due to the above chemical reactions C-dots/meso-SiO_2 conjugate is formed. Another important observation was the presence of a silvery white suspension along with C-dots indicating the formation of meso-SiO_2 [**17].**This silvery yellow solution was first purified by dialysis against distilled water for12 h. A clear water soluble suspension was obtained after dialysis, which exhibited a

strong green color under UV light as depicted in Figure. 2.9 of Chapter 2. Aqueous solubility and bright fluorescence are two important attributes of C-dots, which are not present in other forms of carbon [**7].**

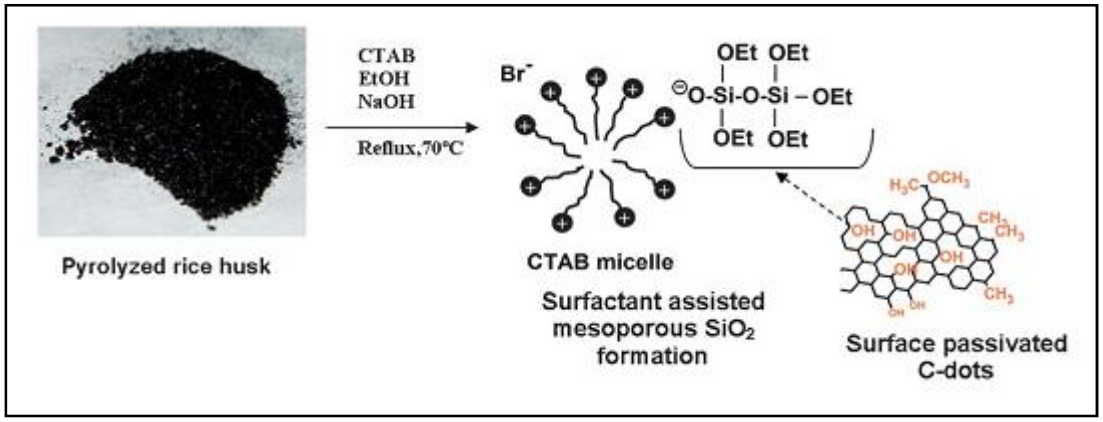

Figure 3.6: Schematic showing CTAB assisted synthesis of meso-SiO_2 and attachment of C-dots to form the meso-SiO_2/C-dot conjugate.

3.3.1.1 UV-Vis Spectroscopic analysis of meso-SiO_2/C-dots

Figure 3.7 depicts UV-Vis spectroscopy of as prepared C-dots along with meso -SiO_2. A sharp peak at 260 nm and a broad hump at 972 nm indicate the formation of C-dots in the solution. The peak at 260 nm arises due to the $\pi \rightarrow \pi^*$ electron transition of C=C associated with C-dots [**2]** and another peak at972 nm is due to the presence of silica oxide or the meso -SiO_2/C-dot conjugate. Due to significant absorption in the near infrared(NIR) region, this complex can also be used for photothermal therapy of solid tumors and/or NIR induced drug release, thus establishing a fundamental platform for chemo-photothermal therapy. Absence of background absorbance in the visible region indicates the absence of other carbonaceous materials, which usually absorb at higher wavelengths [**11, 18].**

The inset of the Figure 3.7 presents photoluminescence spectra of the meso-SiO_2/C-dot conjugate at 464, 535 and 552 nm after excitations at 250, 350and 450 nm respectively. There is a continuous red shift and enhancement in intensity of the peak with an increasing excitation wavelength. Excitation dependent emission is a signature marker of C-dots.

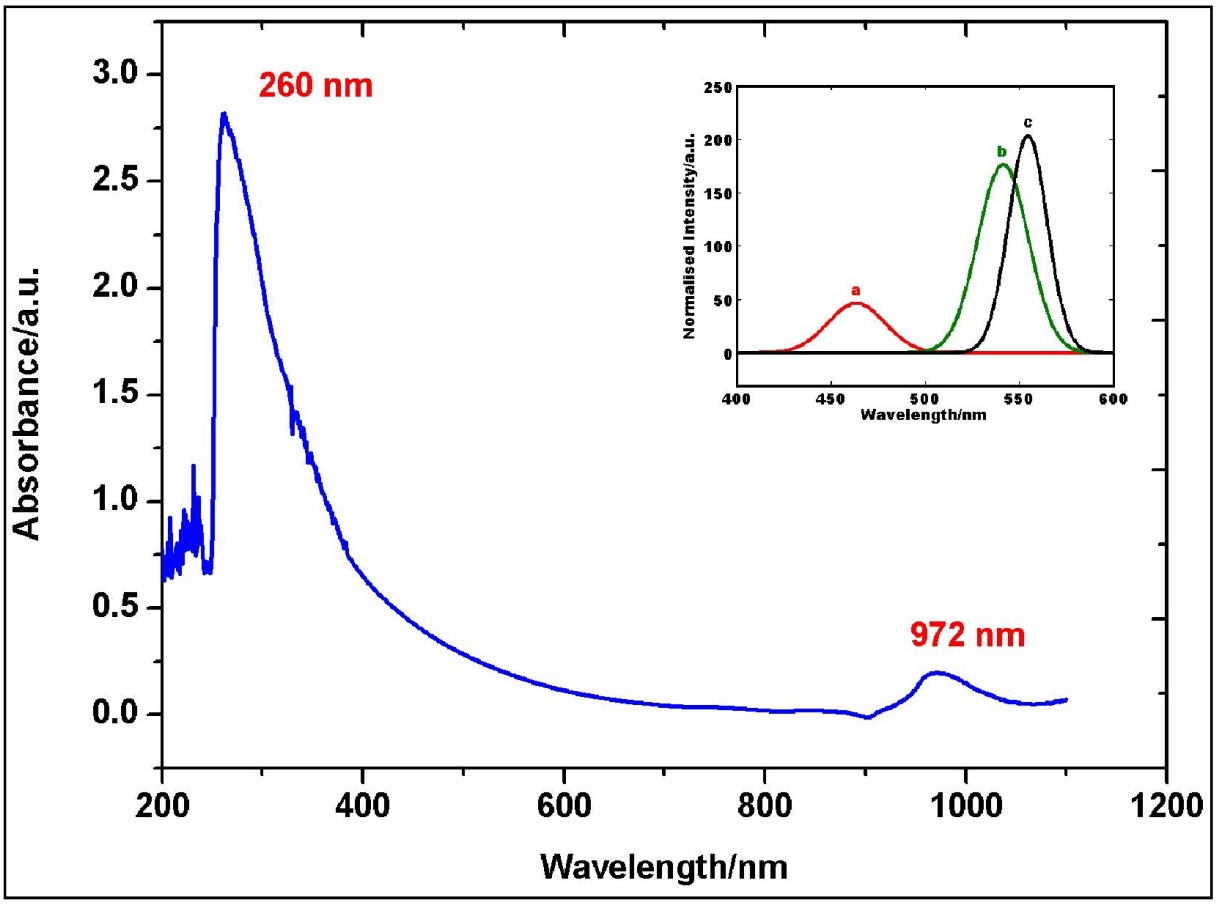

Figure 3.7: UV-Vis spectroscopy of meso-SiO2/C-dots synthesised using RH. Inset shows photoluminescence spectra excited at (a) 250 (b) 350 and (c) 450 nm.

3.3.1.2 Morphological studies of meso-SiO_2/C-dots

The most revealing feature of the present research is the synthesis of meso-SiO_2 capped on the surface by C-dots and/or that the C-dots were found to be trapped inside the meso-SiO_2. The TEM image displayed in Figure 3.8 shows meso-SiO_2/C-dots along with free C-dots and meso-SiO_2 in the background. Figure 3.8b shows mesoporous silica micro-particles along with an enlarged view showing the presence of tiny C-dots approximately 10 nm in size on the surface (Fig. 3.8c).

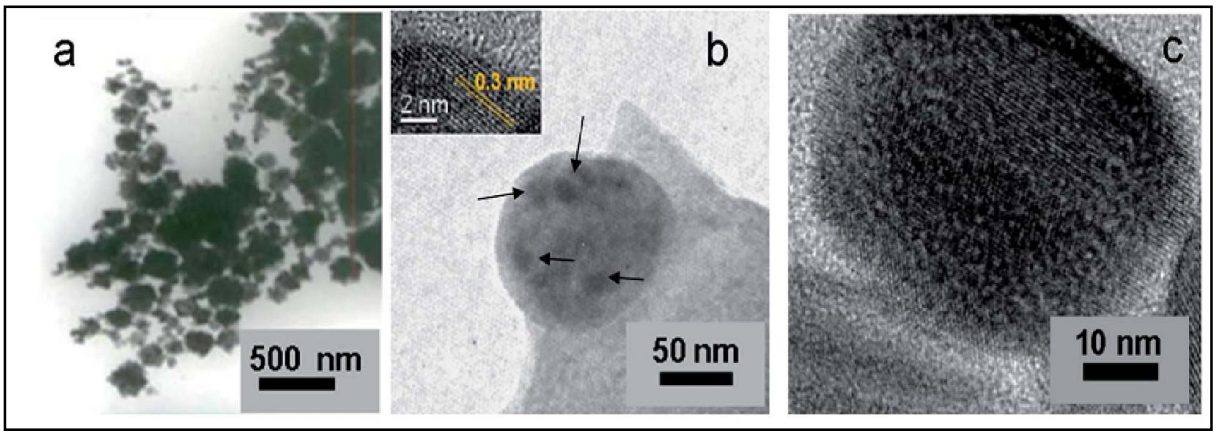

Figure 3.8: (a) TEM image of the as prepared meso-SiO_2/C-dot conjugate, (b) enlarged TEM image of selective C-dots embedded in meso-SiO_2particles where the highlighted spots being carbon-dots adhered onto meso-SiO_2 particles and the inset shows a HRTEM snapshot of a representative meso-SiO_2/C-dot particle with a fringe width of 0.3 nm, (c) HRTEM of meso-SiO_2/C-dots having porous structure with C-dots adsorbed onto them.

3.3.1.3 XRD and Raman Analysis of meso-SiO_2/C-dots

XRD (Fig. 3.9a) reveals a characteristic peak at 2θ=26.29° and a weak peak at 2θ=43.67, which are assigned to the (002) and (101) diffraction patterns of graphitic carbon respectively. The peak at 26.29º corresponds to an interlayer spacing of approximately 3.6˚A, which is higher than that between the (002) planes in bulk graphite i.e. 3.44 ˚A [**12].**

The Raman spectrum of RH derived C-dots is shown in Figure 3.9b. The G-band observed at 1594.89 cm^{-1} with respect to the more intense peak of the D-band at 1331.52 cm^{-1} indicates the presence of messy carbon nanomaterials in the form of C-dots [**19].**

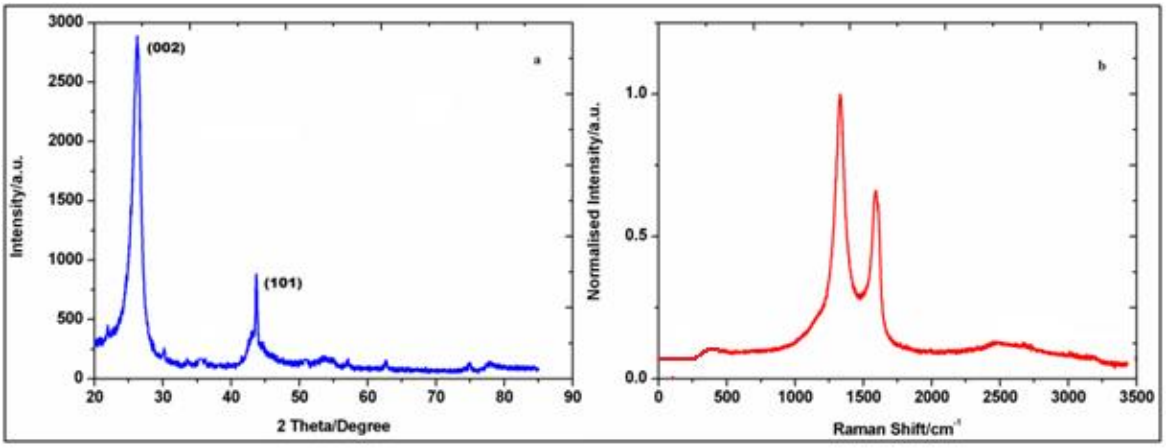

Figure 3.9: (a)XRD and (b) Raman spectra of the meso-SiO_2/C-dot conjugate

3.3.1.4 EDAX of meso-SiO_2/C-dots

Energy dispersive spectrometry (EDS) (Fig. 3.10) shows that the major components are silicon (Si) and carbon (C) in the elemental composition of the meso-SiO_2/C-dot conjugate. The prominence of silicon and carbon explains the association of C-dots and silicon oxide. Another peak corresponding to elemental oxygen (O) is present, which is particularly important for the fluorescent properties of C-dots. Sodium (Na) and bromide (Br) come from CTAB and traces of -Cl come from Cys-HCl, which are used during the synthesis procedure.

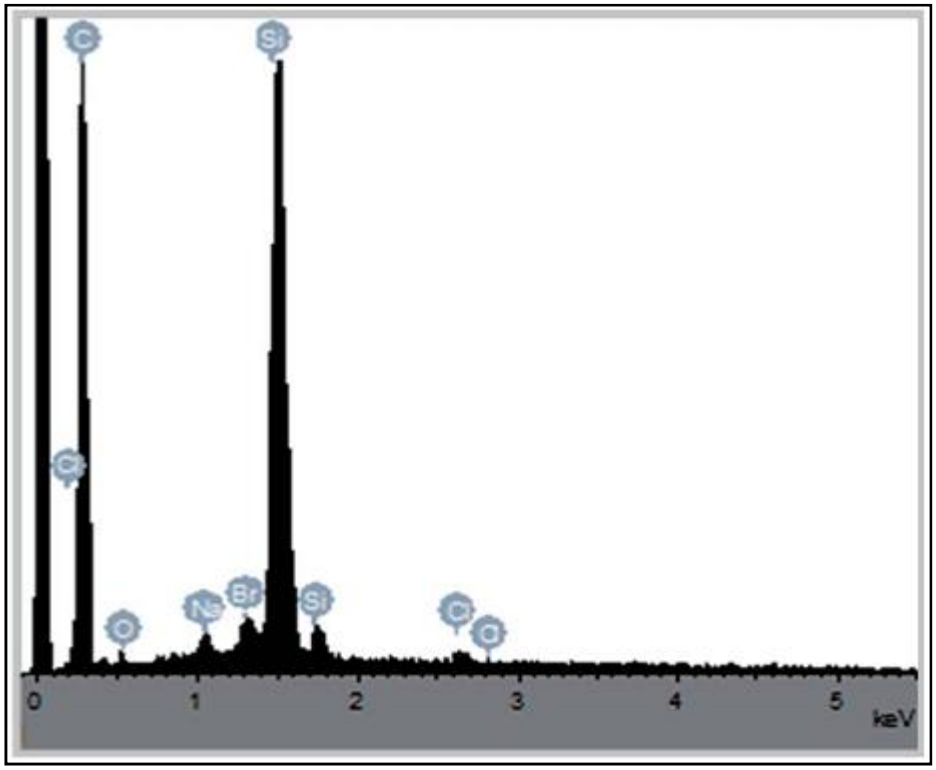

Figure 3.10: EDAX of the conjugate depicting the major elemental composition

3.3.1.5 FTIR studies of meso-SiO_2/C-dots

Surface functionalization studies were performed using FTIR. Figure 3.11 shows FTIR spectra of the meso–SiO_2/C-dot conjugate. Typical IR bands were obtained around 916 – 1094 cm^{-1}, indicating symmetric stretching vibrations of Si–O–Si at 916 cm^{-1} and asymmetric stretching vibrations at 1094 cm^{-1}. The weak band at 594 cm^{-1} was attributed to –CH_2 alkane bending. The band at 1411 cm^{-1} is possibly due to aromatic –NO_2 groups on surface passivized C-dots. Other surface passivation was observed at 1652 cm^{-1} arising from

the C=O stretching vibrations. A relatively intense IR band of a typical –CH stretching vibration from the C-dots was observed around 2952 cm^{-1}. An intense wide band was observed at 3355 cm^{-1}, which indicates typical surface passivation by –OH stretching onto C-dots and that typical silanol (Si-OH) groups were formed during the formation of the meso-SiO_2 /C-dot conjugate.

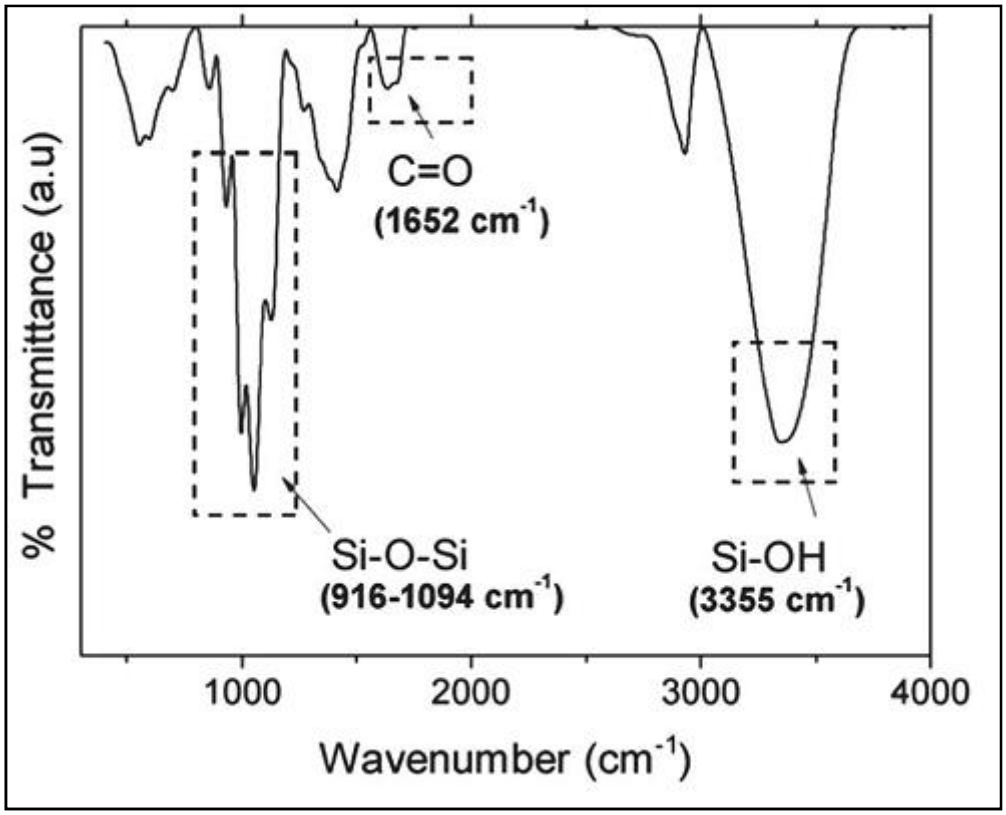

Figure 3.11: FTIR spectra of meso-SiO_2/C-dot conjugate

3.3.1.6 Cytotoxicity Analysis

Cytotoxicity was performed using standard MTT assay protocol **[9].** The cytotoxicity results (Fig.3.12) demonstrate that C-dots blended with meso-SiO_2 were non-toxic to Vero cells, thus providing an insight towards potential of C-dots in imaging over conventional Semiconductor QDs. These C-dots after administration into the body undergo rapid renal clearance and are quickly metabolised, unlike other fluorescent probes including QDs **[20]**.At all the concentration of the complex (0.1-0.5 mg/ml), the percentage viability of the cells were found to be >95% indicating exceptional bio-compatibility of the synthesised complex.

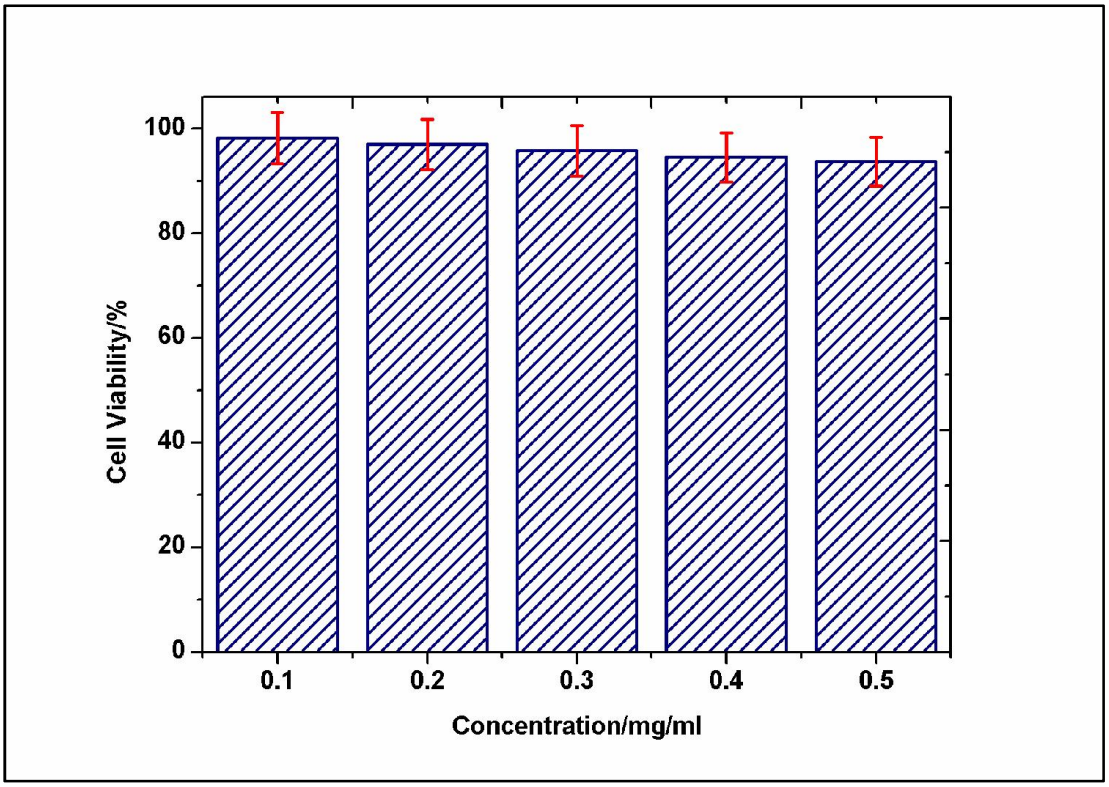

Figure 3.12: Percentage cell viability plot showing effect of mesoSiO$_2$/C-dots conjugate on Vero cell lines.

3.3.2 C-dots@GNR conjugate Analysis

3.3.2.1 UV-Vis spectroscopic analysis

GNRs synthesized using a conventional seed-mediated method displayed a characteristic purple color and two peaks at 550 and 701 nm (Fig. 3.13). These features begin to become dominant when the size of the particles enters into the nano regime. The color of GNRs is due to the interaction of light and particles, especially when the de Broglie wavelength of the valence electrons is equal to the size of the nanoparticles [**21, 22].** The two peaks correspond to Transverse Surface Plasmon Resonance (TSPR) towards lower wavelengths and Longitudinal Surface Plasmon Resonance (LSPR) towards higher wavelengths, respectively [**23, 24].**

When C-dots were added into the growth solution prior to adding seed, a strange optical behaviour of GNRs was observed. There was appreciable diminution in the intensity of TSPR followed by a blue shift from 550 to 524 nm followed by a decrease in the absorption (Fig. 3.13). A large blue shift of 59 nm was also observed in the case of

LSPR (from 701 to 642 nm). The fact that both LSPR and TSPR exhibit the above changes indicates the likelihood of complete coverage of GNRs by C-dots, an essential requirement to avoid CTAB induced toxicity. Such alterations in color as well as optical spectra may also be attributed to a change in the aspect ratio of GNRs because of the mild reducing properties of C-dots. The aspect ratios (R) of the GNRs were found to be altered to 2.95 in the case of bare GNRs and 2.33 in the C-dots@GNRs conjugate, calculated from LSPR peaks [**25]** as obtained from the same Figure.

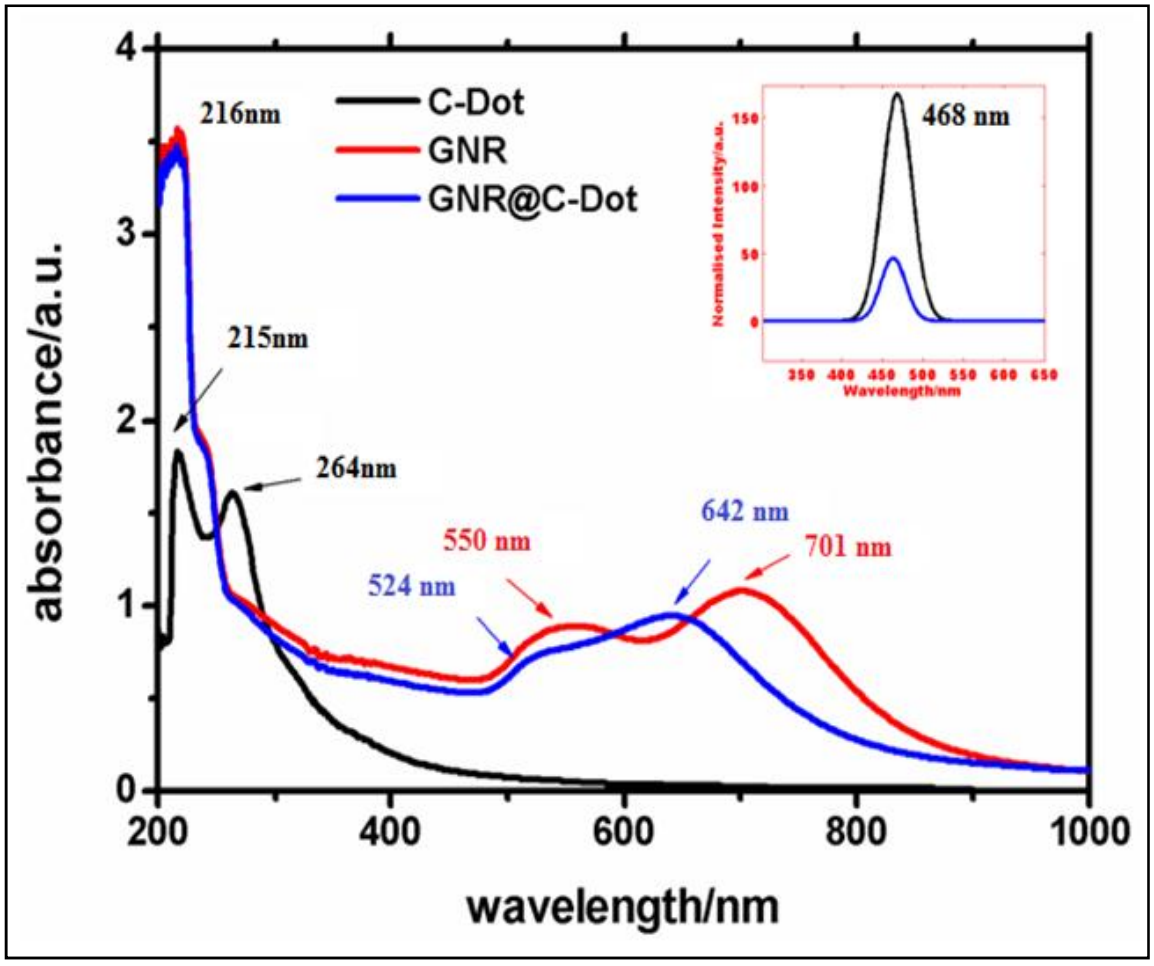

Figure 3.13: UV-Vis spectra of C-dots, GNR and C-dots@GNR conjugate; Inset shows PL spectra of bare C-dots and C-dots@GNR conjugate

Besides, shoulders at 213 and 239 nm can be seen which are assigned to C-dots. In comparison to the UV-Vis spectra of pure C-dots (Fig. 3.13) both the peaks at 215 and 264 nm were diminished after incorporation in growing GNRs solution. The inset of Fig.

3.13 shows PL spectra of C-dots and C-dots@GNR conjugate. Pure C-dots exhibited a sharp peak at 468 nm after excitation at 300 nm. The intensity of the spectrum was found to be drastically diminished after incorporation of the GNRs, possibly due to their stable complexation with each other. During the CTAB and $AgNO_3$induced zipping mechanism [**26]**, C-dots must have accommodated themselves at the advancing ends of GNRs leading to a dampening of TSPR. This is simplified in a cartoon displaying the mechanism of growth in the presence of C-dots (Fig. 3.14). Various stages (1, 2 and 3 in Fig. 3.14) explain the advancement in the growth of Nano-rods due to selective deposition of Ag^+ ions, a process called under potential deposition [**27].** During this process C-dots may become trapped at the interface along with Ag+ ions and/or also become deposited on the surface of rods. It must be noted here that in the presence of C-dots as well as ascorbic acid, Ag^+ might get reduced to Ag^0 i.e. silver nanoparticles (SNPs), however, the pH of this solution was acidic (~4.5) and for SNPs formation, basic pH is obligatory **[27]**.

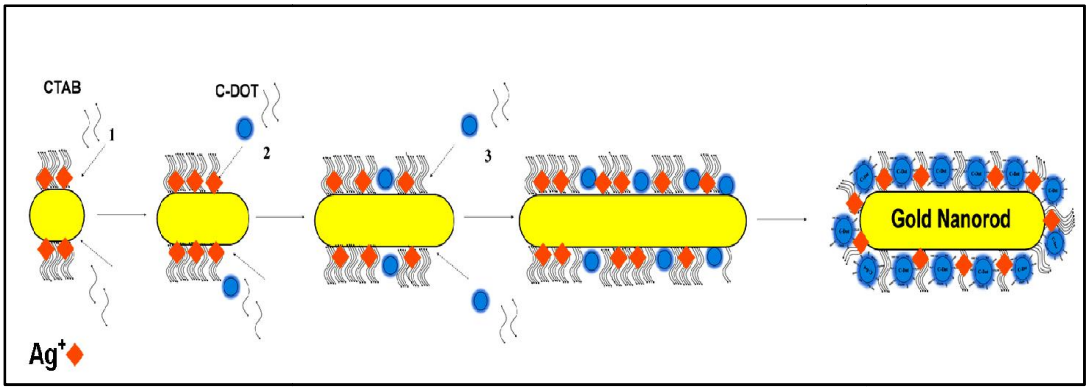

Figure 3.14: Schematic representation of possible mechanism of C-dots@GNR conjugate

Hence we could rule out SNPs formation, which is supported by EDAX displayed in the further section showing the absence of an Ag peak (Fig. 3.16a). The change in color of both bare GNRs and C-dots@GNR indicates a strong interaction between C-dots and GNRs. It must be noted here that C-dots alone could function as reducing agents [**28]** and as a consequence, there might be formation of another population of spherical GNPs and/or GNP–C-dot conjugates. This problem was dealt by separation of such spherical nanoparticles by centrifugation.

3.3.2.2 Morphological analysis

Fig. 3.15a shows TEM images of C-dots@GNRs synthesized using a modified seed mediated method. Darker regions of the GNRs display the C-dots@GNRs conjugate. Red and blue arrows show complete coating on GNRs and bridging of C-dots between GNR surfaces respectively. Selective adsorption of C-dots on the surface of GNRs is denoted by yellow arrows and white ones show the presence of irregular C-dot–nanoparticles conjugates. Fig. 3.15b shows C-dots@GNPs present in the supernatant separated during centrifugation. Fig. 3.15c shows a magnified view of a representative GNR coated with C-dots. The lattice constant of thecoat was calculated to be 1 nm, which confirms the presenceof C-dots on the surface**[9]**. Fig. 3.15d depicts spherical nanoparticles (GNPs) formed during the growth of GNRs in thesolution. Due to the mild reducing capacity of C-dots, spherical GNPs also became covered with C-dots, which is evident from darker zones (Fig. 3.15d).

.

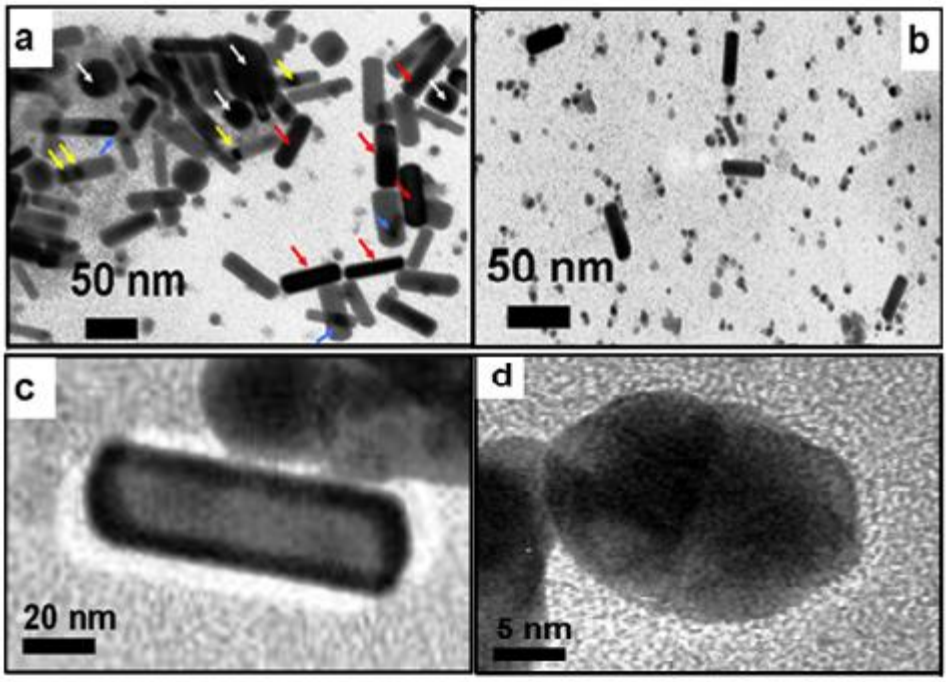

Figure 3.15: TEM images of (a) C-dots@GNR complex with various degree of coatings (Red arrows shows complete coating of C-dots onto GNR, blue arrows show bridging of C-dot between two rod surfaces, yellow arrows show selective adsorption of C-dots onto rod surface and white arrows shows presence of irregular C-dot nanoparticle conjugates) (b) TEM of post centrifugation supernatant displaying presence of C-dots with minimal amount of rods (c) representative HRTEM of single C-dots@GNR conjugate which is magnified (d) representative HRTEM of C-dots@GNP conjugate with their magnified image

3.3.2.3 EDAX of C-dots@GNR conjugate

EDAX spectra of C-dots@GNRs show the presence of carbon and gold as the major constituents of the complex (Fig. 3.16). In comparison to the EDAX spectrum of pure GNRs(Fig. 3.16b) synthesized in the absence of C-dots, the intensity of the peaks showing the presence of Br, a major constituent of CTAB, is decreased by a significant amount in the case of the EDAX spectrum of C-dots@GNRs (Fig. 3.16a). This addresses our claim of a depleted amount of CTAB covering, after association of C-dots onto GNRs to form a C-dots@GNRs conjugate. Such work has also been performed earlier using silica as a protecting agent in order to reduce the detrimental effects of CTAB **[29]**.

Moreover, the higher concentration of carbon in C-dots@GNRs also supports the surface decoration by C-dots.

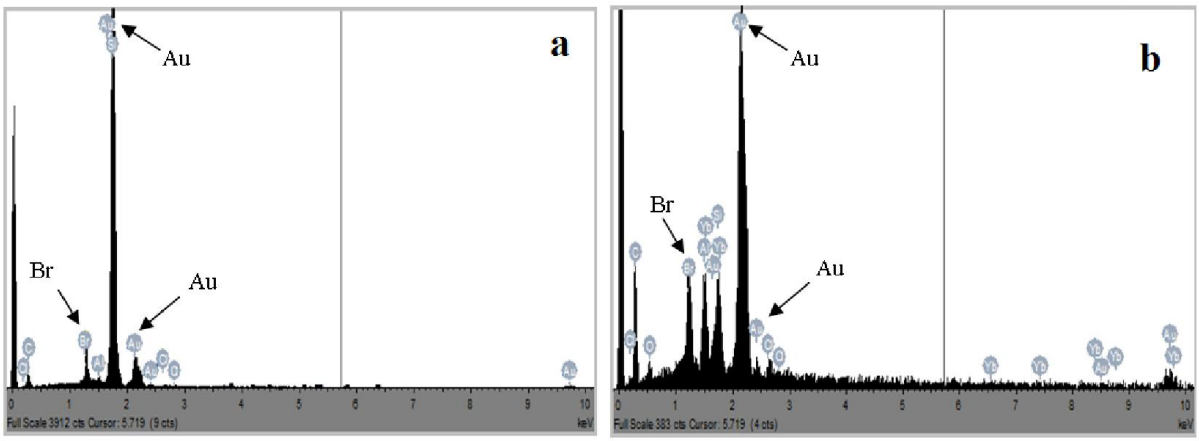

Figure 3.16: EDAX spectrum of (c) C-dots@GNR-DOX (d) bare GNRs

3.3.2.4 FTIR Analysis

Fig. 3.17 displays FTIR spectra of C-dots, C-dots@GNR conjugate and C-dots@GNR-DOX complex. FTIR of C-dots (Fig. 3.17a) show IR bands at 631 cm^{-1} and 1044 cm^{-1} represent C-H bending of acetyl groups of saturated hydrocarbons on the surface of the C-dots. Peaks at 1257 cm^{-1} and 1737 cm^{-1} represent alcoholic –OH and carboxylic –COO stretches which dictates surface passivation on C-dots due to NaOH treatment. Moreover, more evidence of surface passivation is seen by few other peaks at 1534 cm^{-1}, 1626 cm^{-1} and 1680 cm^{-1}. These bands depict amide 1° N-H bend, aldehyde C=O stretch, anhydride C=O stretch from polysaccharide and residual amino acid backbone on the surface.

FTIR of C-dots@GNR conjugate (Fig. 3.17b) show peak at 556 cm^{-1} is a principle peak of alkyl halide (C-Br) stretch from GNRs and alkane CH_2 bend from CTAB surfactant hydrophobic chain. Multiple peaks at 1132 cm^{-1}, 1417 cm^{-1} and 1644 cm^{-1} show the alcoholic C-O stretch, ether C-O-C stretch, carboxylic acid C-O stretch which were also seen in surface passivized C-dots. This may be due to intercalated C-dots in between surfactant layers and surface decoration.

On the other hand, after interactions of the above conjugate with DOX, there were drastic changes in intensities of the peaks as well as their position. The following significant conclusions can be drawn after comparing IR spectra of the individual components involved in formation of the C-dots@GNRs–DOX complex:

New peaks at 428, 605 and 1590 cm^{-1}present in the conjugate (Fig. 3.17c) are assigned to C–Br stretching of GNRs, aromatic ‑CH bends and amide -NH stretches due to interaction with the C-dots@GNRs conjugate. A notable feature of the conjugate was found to be a significant decrease in the intensity of the peak at 428 cm^{-1}, depicting the protection of the CTAB with C-dots. There is a possibility of formation of amide linkages between the conjugates, due to the appearance of a prominent peak at 1590 cm^{-1}. Significant shifts of peaks from 1417 cm^{-1} (part of C-dots@GNRs conjugate) to 1437 cm^{-1} represent the–OH bend of the carboxylic acid of DOX, indicating the interaction between–OH and amide group which may lead to formation of amide linkages between the conjugates. A prominent peak at 2928 cm^{-1} present on the C-dots@GNRs conjugate disappeared (or rather became very weak) after interaction with DOX. This peak is assigned to–NH stretching explaining the formation of amide linkages in accordance with the previous results. In conclusion,–COOH and–NH groups were found to be involved in the formation of the C-dots@GNR–DOX conjugate. In the C-dots@GNR–DOX complex, the peak at 428 cm^{-1} shows the presence of alkyl halide (C–Br or C–Cl) as seen in the C-dots@GNR complex. IR bands at 1437 cm^{-1} and 1590 cm^{-1} depict bond formation between the C-dot surface as alkene C=C bond and/or carboxylic acid OH bends. New diminished bands at 700 cm^{-1} and 1020 cm^{-1} show alkane CH_2 bends, alkene C–H and aromatic C–H bends (meta) arising out of the DOX parent structure.

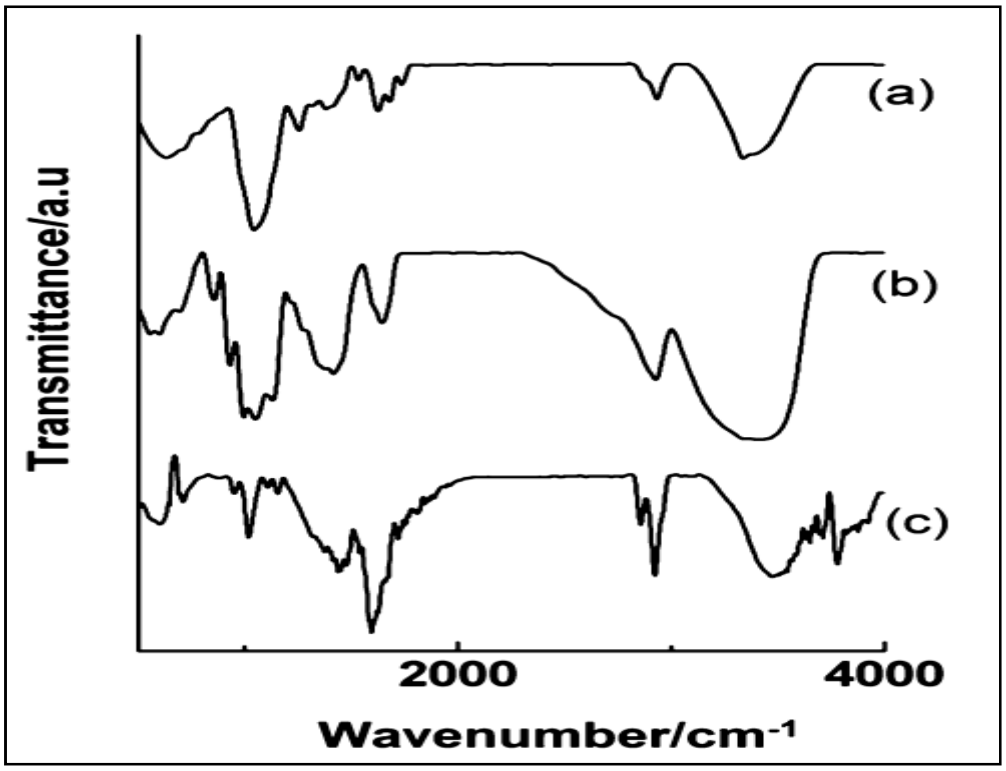

Figure 3.17: FTIR spectra of (a) Bare C-dots, (b) C-dots@GNR conjugate and (c) C-dot@GNR-DOX complex

3.3.2.5 Drug release study and Cytotoxicity Analysis

Drug loading efficiency was calculated to be 94.8% (By the same formula used in chapter 5). Figure 3.18a displays the cumulative percentage release of DOX under in-vitro conditions. Cumulative drug release was calculated to be greater than 30% in the first 5 h at both pH values (5.8 and 7.2). Complete drug release was found after 23 h. As evident from the results, there was no difference in drug release in slightly acidic (pH 5.8) or alkaline conditions (pH 7.2). Such types of delivery vehicles are of immense importance for chemotherapy of solid tumors where the pH is slightly acidic **[30]** as well as to those where the pH is not altered during cancerous transformation.

Cytotoxicity analysis was carried out on Vero and MCF 7 cells by MTT assay. Figure 3.18b shows the IC_{50}values of individual components along with the C-dots@GNRs–DOX complex. The IC_{50} values of pure GNRs capped with CTAB, C-dots@GNRs and DOX were found to be 0.04, 0.05 and 0.02 mM respectively against Vero cells. It can be clearly inferred from the above findings that the toxicity of CTAB coated GNRs is reduced after surface protection with C-dots (IC_{50} changed from 0.04 to 0.05 mM indicating the increased survival of Vero cells). The IC_{50} of C-dots@GNRs–DOX complex was found to be 0.04, much higher than that of free DOX on Vero cells,

explaining the biocompatibility of the conjugate. On the other hand, the IC_{50} values of the above components on MCF 7 cells reveal the following crucial points:

GNRs and C-dots@GNRs conjugate exhibited a similar effect on both Vero and MCF 7 having IC_{50} values of 0.04 and 0.05 mM respectively. This may be due to a lack of targeting molecules specific for cancer cells. In comparison to free DOX (IC_{50} =0.01 mM), the C-dots@GNR–DOX complex was found to have a greater impact on MCF 7 than on Vero cells, as seen by the decrease in IC_{50} value to 0.03 mM.

At a glance, the C-dots@GNRs–DOX complex was found to be biocompatible with normal cells at significantly high concentrations (0.04 mM). Also, C-dots played a role in decreasing the toxicity of GNRs by replacing the CTAB. The conjugate was found to have a high impact on killing MCF 7 cells proving its worth as an ideal drug delivery vehicle for cancer chemotherapy.

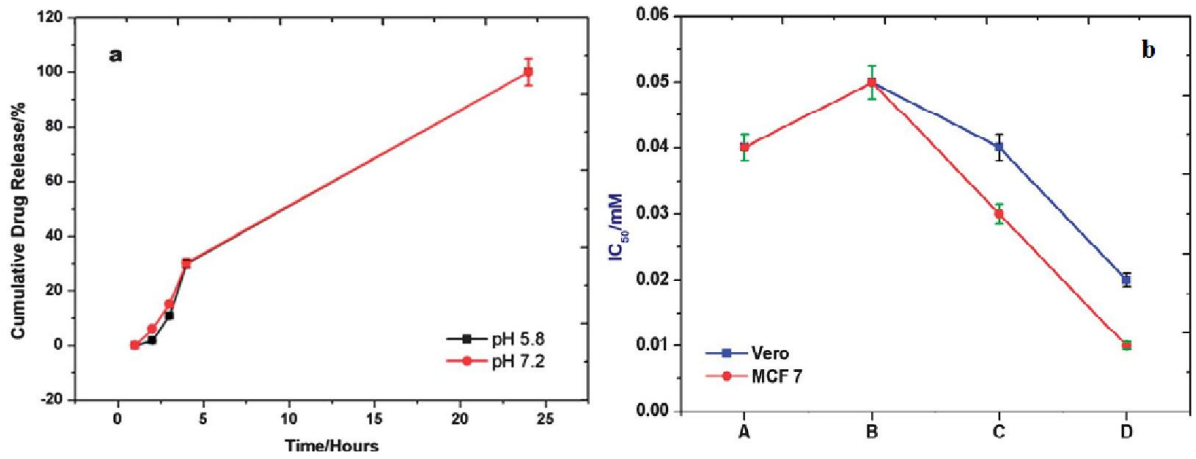

Figure 3.18: (a) Cumulative percentage of DOX release and (b) IC_{50} values on Vero and MCF 7 cells where A: Bare GNR, B: C-dots@GNR conjugate, C: C-dots@GNR-DOX complex and D: Free DOX

3.4 CONCLUSIONS

C-dots were synthesized using various natural as well chemical precursors by different methods. Based on the characterisations and after checking stability of various C-dots, it can be concluded that microwave assisted heating was found to be the best method in our case for synthesizing mono-dispersed spherical C-dots with excellent fluorescence properties. C-dots could be easily separated using Dialysis membrane in a short period of time with high yield and enhanced fluorescence. C-dots derived from Sorbitol were found to be the most stable amongst all other natural precursors which showed high amount of other carbonaceous materials.

Rice husk is found to be an excellent precursor for the synthesis of ***Meso-SiO_2/C-dots*** using a hot injection method. The nature of the nano-complex was found to be highly porous, which can be used for efficient drug loading and other biological applications. As prepared meso-SiO_2/C-dots can have an excellent bioimaging potential due to the fluorescent nature of C-dots.

Protection of GNR with biocompatible C-dots reduced the toxicity of GNRs due to the presence of surfactant CTAB. Moreover, our research has opened preliminary avenues for modifying seed mediated synthesis of GNRs and incorporation of novel functional moieties during the process of synthesis. After loading of DOX, the drug release and Cytotoxic analysis was carried out. This research could be extended by introducing targeting molecules such as Folic acid of other protein receptors to study the efficacy of the complex as a drug delivery system via targetting. ***C-dots@GNR***–drug conjugate can work as a tri-pronged molecular weapon' for drug delivery, photothermal therapy and biological imaging. This is yet can prove to be another theranostics application of hybrid nano-complex molecules combining chemotherapy and diagnosis in nanomedicine.

3.5 REFERENCES

1. S. N. Baker and G. A. Baker, Angew. Chem., Int. Ed., 2010, 49, 6726.
2. Z. Luo, Y. Lu, L. A. Somers and A. T. Charlie Johnson, J. Am. Chem. Soc., 2009, 131 , 898.
3. G. Eda, Y. Lin, C. Mattevi, H. Yamaguchi, H. Chen, I.-S. Chen, C. W. Chen and M. Chhowalla, Adv. Mater., 2010, 22, 505.
4. W. Cai, R. D. Piner, F. J. Stadermann, S. Park, M. A. Shaibat, Y. Ishii, D. Yang, A. Velamakanni, S. J. An, M. Stoller, J. An, D. Chen and R. S. Ruoff, Science, 2008, 321, 1815.
5. D. Yang, A. Velamakanni, G. Bozoklu, S. Park, M. Stoller, R. D. Piner, S. Stankovich, I. Jung, D. A. Field, C. A. Ventrice and R. S. Ruoff, Carbon , 2009, 47 , 145.
6. S. Pandey, A. Mewada, G. Oza, M. Thakur, N. Mishra, M. Sharon and M. Sharon, Nanosci. Nanotechnol. Lett. , 2013, 5, 775.
7. L. Haitao, K. Zhenhui, L. Yang and L. Shuit-Tong, J. Mater. Chem., 2012, 22, 24175.
8. S.Pandey, M.Thakur, A.Mewada, D.Anjarlekar, N. Mishra and M. Sharon, J. Mater. Chem. B., 2013, 4972.
9. A. Mewada, S. Pandey, S. Shinde, N. Mishra, G. Oza, M. Thakur, M. Sharon and M. Sharon, Mater. Sci. Eng., C, 2013, 33, 2914.
10. P. N. Vishwakarma, V. Prasad, S. V. Subramanyam and V. Ganesan, Bull. Mater. Sci., 2005, 28 (6), 609.
11. D. Y. Pan, J. C. Zhang, W. Q. Shen, Z. W. Zhang, Y. G. FangM. H. Wu, New J. Chem., 2010, 34, 591.
12. M. S. Dresselhaus, A. Jorio, M. Hofmann, G. Dresselhaus and R. Saito, Letters, 2010, 10 (3), 751.
13. P. K. Chu & L. Li, Mat. Chem. Phys., 2006, 96, 253.
14. J. Robertson, Surf. Coat. Technol., 1992, 50, 185.
15. K. P. Loh, Q. Bao, G. Eda and M. Chhowalla, Nat. Chem., 2010, 12 , 1015.
16. S. K. Palashuddin, A. Jaiswal, A. Paul, S. Ghosh and A. Chattopadhyay, Sci. Rep., 2012, 2 ,1.
17. C. W. Lai, Y. H. Hsiao, Y. K. Peng and P. T. Chou, J. Mater. Chem., 2012, 22, 14403.

18. Y. Dong, J. Shao, C. Chen, H. Li, R. Wang, Y. Chi, X. Lin and G. Chen, Carbon, 2012, 50, 4738.
19. A. M. Alkilani, S. E. Lohse and C. J. Murphy, Acc. Chem. Res., 2013, 46, 650.
20. H.S. Choi, et al., Nat Nanotechnol., 2010, 5, 42.
21. Henglein, J. Phys. Chem., 1993, 97, 5457.
22. S. Link and M. A. El-Sayed, J. Phys. Chem. B, 1999,103, 4212.
23. R. Gans, Ann. Phys., 1912, 37, 881.
24. C. Templeton, M. J. Hostelter, C. T. Kraft and R. W. Murray, J. Am. Chem. Soc., 1998, 120, 1906.
25. V. Sharma, K. Park and M. Srinivasarao, Mater. Sci. Eng., R, 2009,65,1.
26. Nikoobakht and M. A. El-Sayed, Chem. Mater., 2003, 15, 1957.
27. T. Pal, S. De, N. R. Jana, N. Pradhan, R. Mandal, A. Pal, A. E. Beezer and J. C. Mitchell, Langmuir, 1998, 14, 4724.
28. P. Luo, C. Li and G. Shi, Phys. Chem., 2012, 14, 7360.
29. P. Huang, L. Bao, C. Zhang, J. Lin, T. Luo, D. Yang, et al., Biomaterials, 2011, 32, 9796.
30. C. Song, .J. C. Lyon and Y. Luo, in *Drug resistence in oncology*, ed. B. V. Teicher, Marcel Dekker, New York, 1993, p. 25.

CHAPTER IV

Formation of Fluorescent Dendrites using C-dots

4.1 INTRODUCTION

"In a crystal we have clear evidence of a formative life principle, and although we cannot understand the life of a crystal – it is nonetheless a living being"

- ***Nicola Tesla.***

Revolutionary vicissitudes have been observed since nanotechnology has entered in. There are many nano-structures found so for. It has been conceivable now-a-days to tune and design the anticipated shape of these nanoparticles. Because of this tuning property nanoparticles have been used in many applications. Tree and flower shaped crystals have been grown in controlled manner called dendrites as shown in Figure 4.1. Tree like structures of gallium phosphide are used in biosensors to make regional ion sensitive field effect transistors **[1]**, Cadmium selenide nanocrystals (rods) give the feasibility to change band gap by changing the radius of rods and are used in hybrid solar cells for high efficiency **[2]**.Dendrites of platinum, palladium, gold and silver have been synthesized using different methods**[3-7]**.

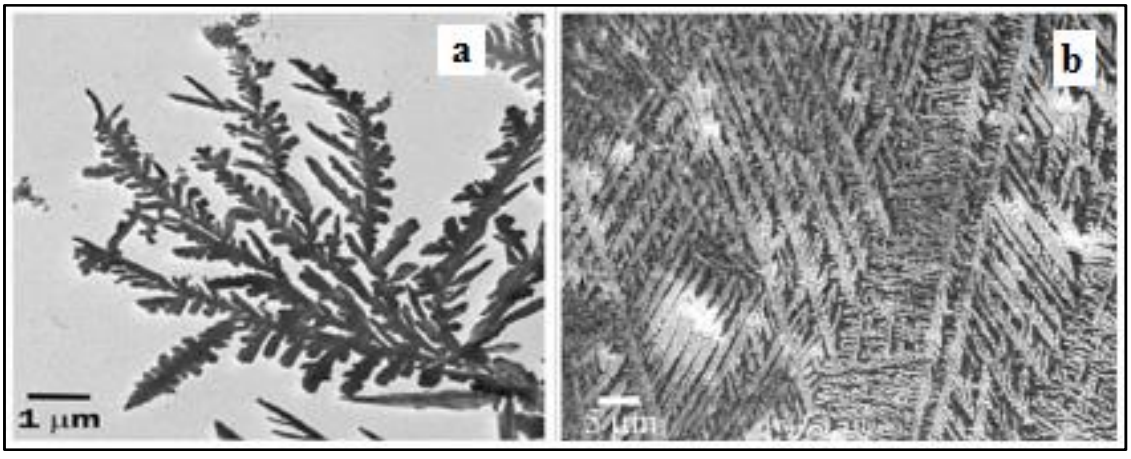

Figure 4.1: Growth of silver dendrite (a) after 17 hr (b) after 4 weeks (Adapted from ref no. 7)

Branched crystals of CdTe are grown which can have wide application from quantum information processing to artificial photosynthesis **[8]**. One of the significant contrivances in biology is fluorescence; crystals have been used for florescent biological labelling **[9]**.

Nano-forms of Carbon have been in focus because of extraordinary properties like high conductance, strength, optical and electrical properties**[7]**. Most of biological applications need water solubility, therefore Carbon dots (C-dots) which are soluble in water are used to grow the carbon dendrites.

Zero dimensional C-dots are acquainted for their size dependent fluorescence properties **[10]**, bio-compatibility and high water solubility **[11]**, chemical inertness and low toxicity **[12]**. These properties of C-dots make them apt for bio imaging, Drug delivery **[13]**, photo catalytic activity and other relevant applications**[14]**.

Rousing optical properties of C-dots entice researchers to use these tiny carbon nanoparticles as seed solution to grow fluorescent crystals. Organic nonlinear optical crystals have many applications in biological labelling **[9, 15]**. Fluorescent crystals can be used for bio sensing, optical data storage, document security, detecting forgery**[16]** and photo induced electron transfer property can be used for light harvesting**[17, 18]**. The exceptionally exciting properties of the C-dots mentioned above can be exploited to replace such metal containing semiconductor quantum dots like CdSe, CdTe and CdS that involve extremely inimical precursors **[19, 20]** as well as complex procedures for their synthesis and above all their non-biocompatibility.

In this chapter, formation of Carbon dendrites has been explained by very tranquil method using C-dots as compared to exacting conditions in chemical vapour deposition and electrochemical methods. The fluorescent studies have been performed to see the optical properties of carbon dendrites.

4.2 MATERIALS AND METHODS

C-dots were synthesized using Sorbitol as a precursor using Microwave assisted heating as mentioned in Chapter 2. C-dot solution was then purified by dialysis against nanopure water using pre activated dialysis bag (Mol. Wt. cut-off 12-14kD, pore size of 2.4 nm). Spectral properties of C-dots were studied by UV-Visible spectrophotometer (Lambda-25, Perkin Elmer, USA) and fluorescence spectroscopy (Perkin Elmer, USA) using standard quartz cuvette, path length of 1 cm. Morphological characteristics of C-dots were studied using Transmission Electron Microscopy (TEM), (Zeiss Microimaging GmbH, Germany). The sample was loaded on copper grid for TEM analysis. The purified C-dots were loaded on clean quartz plates and subjected to vacuum drying under pressure 200 mmHg for 8 hours at

60°C (Ganesh Schientific Ltd, India). The morphological studies after crystallization were studied using Inverted Optical Fluorescence Microscope (Karl Ziess-Axiovert 40).

4.3 RESULTS AND DISCUSSIONS

The light brown colored solution after dialysis exhibited deep green colored fluorescence under UV light (365 nm) as seen in inset of Figure. 4.2a. The origin of fluorescence in C-dots is speculated due to the presence of surface defects along with the appearance of hydroxyl and carboxylic acid functional groups. The optical spectra of purified C-dots displayed in Figure. 4.2a shows two distinct peaks at 229 and 266 nm which arise due to π→π* and n→n* transitions associated with C=C and carbonyl/hydroxyl groups respectively **[21]**. Photoluminescence (PL) spectra of C-dots shows sharp peak at 543 nm when excited at 350 nm (Inset of Fig. 4.2a). The appearance of PL may be attributed to the oxygen containing moieties derived from the precursor and carboxyl and hydroxyl functional groups on C-dots [**22**]. Figure.1b shows the Transmission electron micrographic image of a single C-dot of 7 nm diameter. The C-dots show lattice spacing 3.44Å (marked in Fig. 4.2b). This inter atomic spacing is equal to the (001) plane spacing of graphite which confirms the graphitic nature of C-dots and is denoted in the Surface Area Electron diffraction pattern (Inset of Fig. 4.2b).

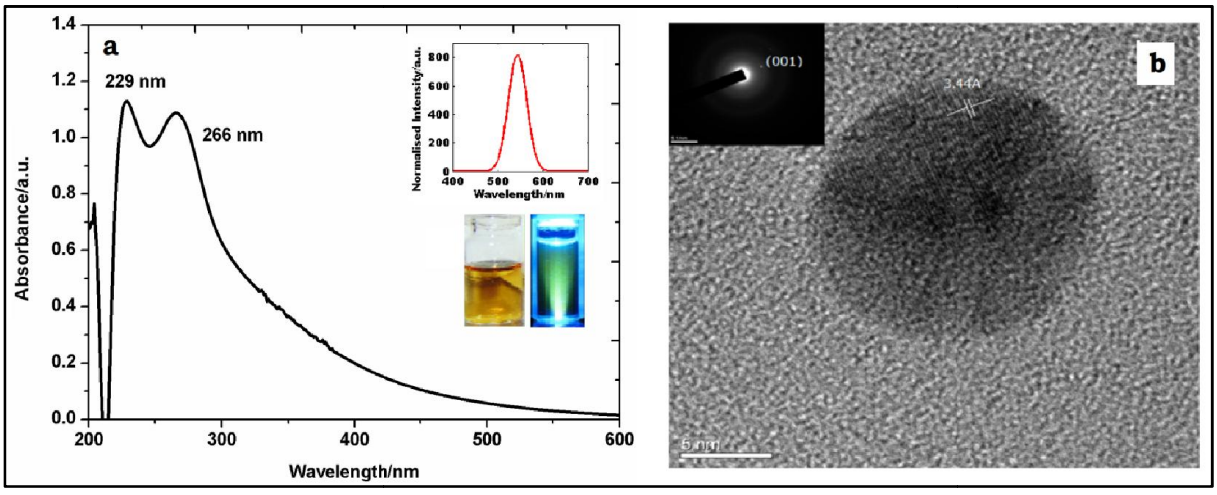

.

Figure 4.2: (a) UV-visible spectra of purified C-dots; inset shows PL spectra and C-dots solution in ambient and UV light (b) TEM image of C-dot; inset shows SAED Pattern of C-dots

After vacuum drying of C-dots solution on quartz plate, *a typical feather like pattern of C-dot crystals was observed* (Fig. 4.3a) under optical microscope which showed same green

fluorescence when exposed to UV light (Fig. 4.3b). Dialysed NaOH and ethanol solution which was used during fabrication of C-dot was also vacuum dried under same conditions mentioned in the materials and methods section. Figure 4.3c shows that the pattern of its crystallization is different and small irregularly shaped crystals are observed. Also, no fluorescence is observed under UV light (data not shown). This clearly confirms that the deep green fluorescence observed even after drying is by the virtue of C-dots.

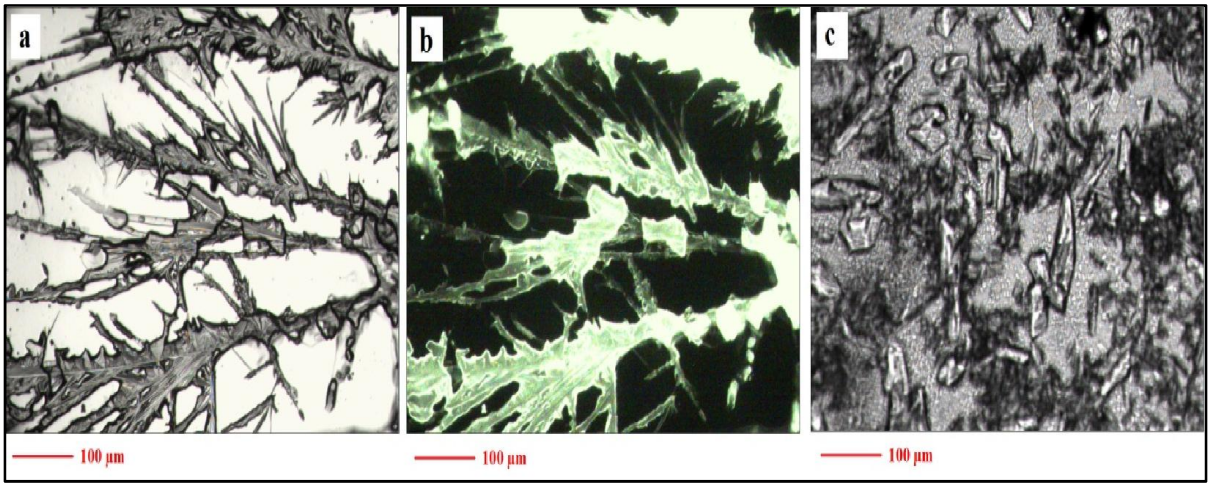

Figure 4.3: Optical microscopy image ofC-dot derived dendrites (a) in ambient light (b) under UV-light and (c) crystals of dialysed NaOH-Ethanol mixture

The arrangement of crystals is a stochastic process. The process explained below can be speculated on the basis of Classical Nucleation theory **[23]**. The solution contains smaller size C-dots, which have higher free energy with chemical potential µ as compare to supersaturated solution (chemical potential=μ_s). This C-dot solution was kept at temperature60^oC and pressure 200 mmHg under vaccum till it was completely dried. During this process, the density of C-dots in solution increases as water evaporates. At a point of critical super-saturation where $\mu>\mu_s$, crystal nucleation is initiated because supersaturated liquids are highly unstable (Fig. 4.4).As per thermodynamics, the Gibbs free energy of the solution decreases due to evaporation which initiates the nucleation of C-dots to form crystals**[24]**. The entropy of the solution decrease, hence, the fusion takes place causing disorder in the surrounding to balance the entropy of the universe**[23]**.Further research is

under progress to optimize and realize the effect of parameters such as temperature, pressure and duration etc. on the crystallization.

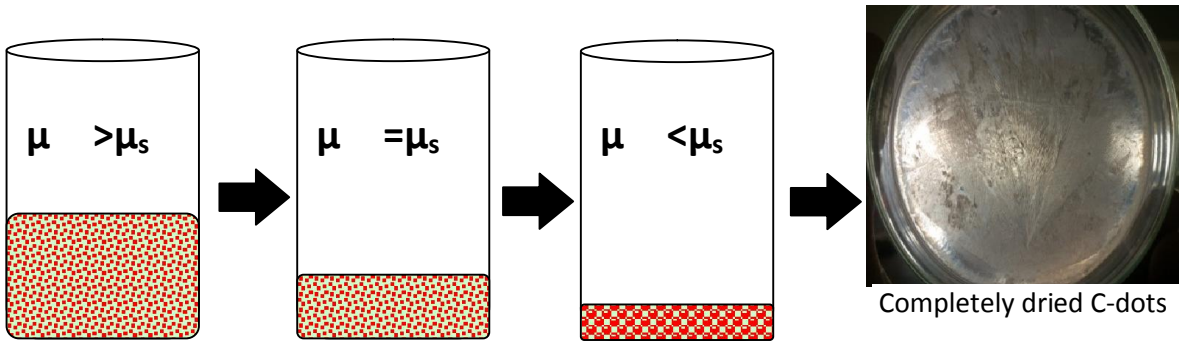

Figure 4.4: Schematic representation of formation of Fluorescent Dendritic structures

Figure 4.5 shows XRD pattern of the sample, this pattern clearly shows presence of carbon peaks at 2 theta 26° ,32.9°, 42.21°, 44.32°, 50.57° and 54.55° for planes (002), (220), (100), (101), (102) and (004) but the peaks are short because of small quantity of carbon as compared to NaOH. These peaks were compared with ICDD data for XRD with PDF no. 000230064 for carbon and 010736551 for NaOH.

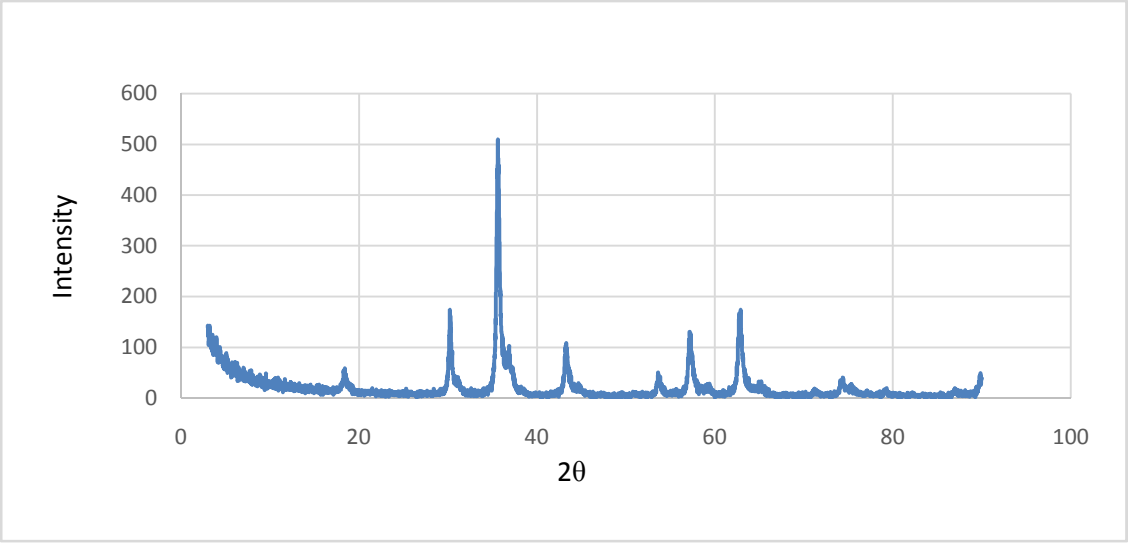

Figure 4.5: XRD of C-dots showing peaks representing carbon

Also the XPS analysis (Fig. 4.6) shows the presence of carbon, sodium and oxygen, complementing the XRD data. XPS Analysis shows presence of carbon with peak 286.3 eV indicating C-O, at 287.4 eV showing C-O-C and at 289.3 eV with O=C-OH**[25, 26].**

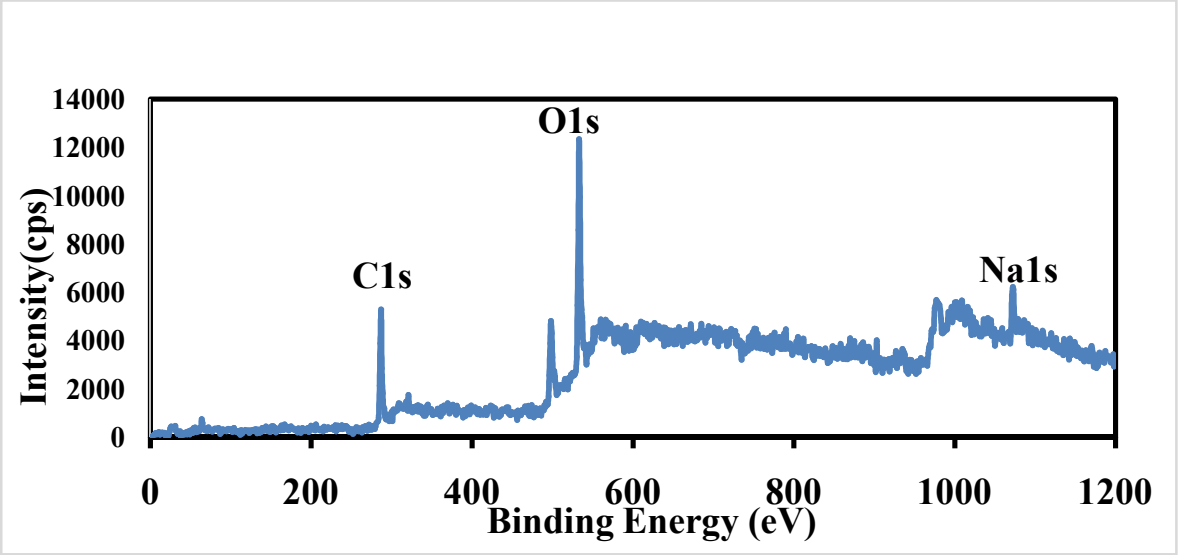

Figure 4.6: XPS of C-dot crystals

Further these re-dissolved crystals of C-dots were found to have excellent biocompatibility on Vero cells. The percentage survival of cells was found to be more than 80% at all the concentrations used (0.5-2 mg/ml). Initial concentration of 0.5 mg/ml showed negligible killing of cells whereas 88.7 % of live cells were observed at the highest concentration used i.e. 2mg/ml (Fig.4.7). Our results are in accordance with the previous reports on non-toxic nature of C-dots **[27, 28]**. These C-dots crystals hence prove to be harmless and can be used in various biological applications.

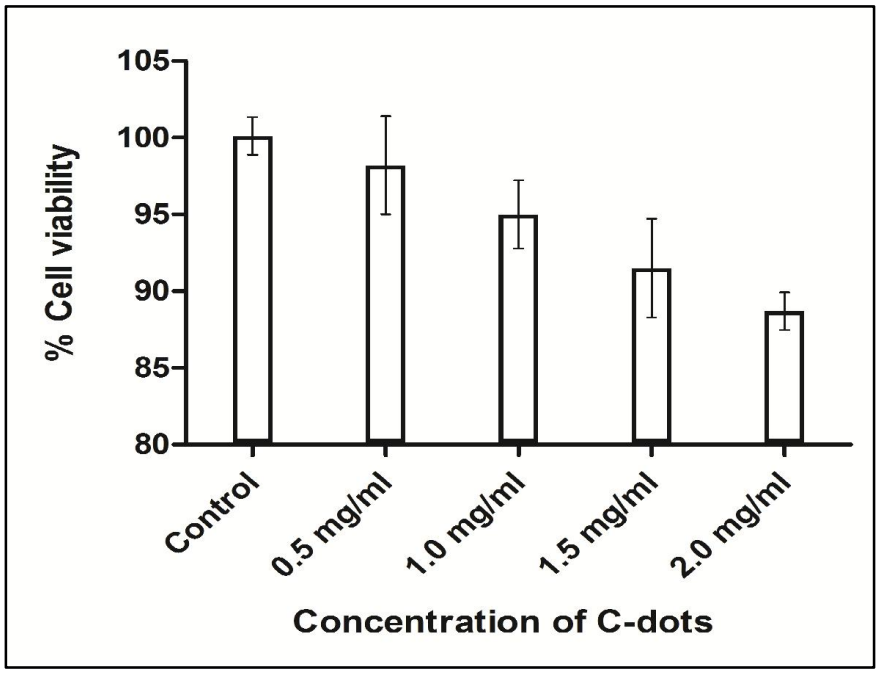

Figure 4.7: Cytotoxicity studies of C-dots on Vero cell lines

4.4 CONCLUSION

A simple hydrothermal method was used to grow the fluorescent crystals of C-dot solution at $60^{o}C$ and pressure of 200 mmHg under vacuum conditions. During evaporation of the C-dot solution fascinating structures were formed that showed consistent feather like dendritic structure. Even after the formation of crystals the C-dots retained their fluorescent property. Fluorescence property of the crystals invites to explore new research in optoelectronics.

4.5 REFERENCES

1. K. Risveden, K. A. Dick, S. Bhand, P. Rydberg, L. Samuelson and B. Danielsson, Nanotechnology, 2010, 21, 55102.
2. W. U. Huynh, J. J. Dittmer and P. Alivisatos, Science, 2002, 295, 2425.
3. T. Huang, F. Meng and L. Qi, Langmuir, 2010, 26(10), 7582.
4. F-R. Fan, A. Attia, U, Sur, J-B. Chen, Z-X. Xie, J-F. Li, B. Ren and Z-Q. Tian, Crystal Growth & Design, 2009, 9 (5), 2335.
5. Y. Song, Y. Yang, C. J. Medforth, E. Pereira, A. K. Singh,H. Xu, Y. Jiang, C. J. Brinker, F. Swol and J. Shelnutt, J. Am. Chem. Soc., 2004, 126, 635.
6. X. Wen, Y-. Xie, M.Mak, K. Cheung, X. Li, R. Renneberg and S. Yang, Langmuir, 2006, 22, 4836.
7. D. Kozak, E. Shibata, A. Iizuka and T. Nakamura, Carbon, 2014, 70, 87.
8. D. J. Milliron, S. M. Hughes, Y. Cui, L. Manna, J. Li, L-W. Wang and A. P. Alivisatos, Nature, 2004, 430, 190.
9. M. Bruchez Jr., M. Moronne, P. Gin, S. Weiss and A. P. Alivisatos, Science, 1998, 281 2013.
10. Y. Sun, B. Zhou, Y. Lin, W. Wang, K. A. S. Fernando, P. Pathak, M. J. Meziani, B. A. Harruff, X. Wang, H. Wang, P. G. Luo, H. Yang, M. E. Kose, B.Chen, L. M. Veca and S-Y. Xie, J. Am. Chem. Soc., 2006, 128, 7756.
11. A. Mewada, S. Pandey, S. Shinde, N. Mishra, G. Oza, M. Thakur, M. Sharon and M. Sharon, Mater. Sci. Eng., C, 2013, 33, 2914.
12. K. Welsher, Z. Liu, d. Darancing and H. Dai, Nano Letters, 2008, 8 (2), 586.
13. S. Pandey, A. Mewada, M. Thakur, A. Tank and M. Sharon, RSC Adv., 2013, 3, 26290.
14. H. Li, X. He, Z. Kang, H. Huang, Y. Liu, J. Liu, s. Lian, C. A. Tsang, X. Yang and S. Lee, Angew. Chem. Int. Ed., 2010, 49, 4430.
15. M. Jazbinsek, L. Mutter and P. Gunter, IEEE Journal of selected topics in Quantum electronics, 2008, 14 (5), 1298.
16. Y. Lu, J. Zhao, R. Zhang, Y. Liu, D. Liu, E. M. Goldys, X. Yang, P. Xi, A. Sunna, J. Lu, Y. Shi, R. C. Leif, Y. Huo, J. Shen, J. A. Piper, J. Paul. Robinson and D. Jin, Nat. Photonics, 2014, 8, 32.
17. F. Frascella, S. Ricciardi, P. Rivolo, V. Moi, F. Giorgis, E. Descrovi, F. Michelotti, P. Munzert, N. Danz, L. Napione, M. Alvaro and F. Bussolino, Sensors, 2013, 13, 2011.

18. X. Wang, L. Cao, F. Lu, M. J. Meziani, H. Li, G, Qi, B. Zhou,B. A. Harruff, F. Kermarrec and Y-P. Sun, Chem. Comm.., 2009, 3774.
19. S. C. Ray, A. Saha, N. R. Jana and R. Sarkar, J. Phys. Chem. C , 2009, 113 , 18546.
20. B. Bourlinos, A. Stassinopoulos, D. Anglos, R. Zboril, M. Karakassides and E. P. Giannelis, Small, 2008, 4, 455.
21. Z. Luo, Y. Lu, L. A. Somers and A. T. Charlie Johnson, J. Am. Chem. Soc., 2009, 131 , 898.
22. L. Haitao, K. Zhenhui, L. Yang and L. Shuit-Tong, J. Mater. Chem., 2012, 22, 24175.
23. S. Auer and D. Frenkel, Nature, 2011, 413, 711.
24. P. G. Vekilov, Nanoscale, 2010, 2, 2346.
25. L. Zhao, F. Di, D. Wang, L. Guo, Y. Yang, B. Wan and H. Zhang, Nanoscale, 2013, 5, 2655.
26. S. Sahu, B. Behera, T. Maiti and S. Mohapatra, Chem. Commun., 2012, 48, 8835.
27. S. N. Baker, G. A. Baker, Angew. Chem., Int. Ed., 2010, 49, 6726.
28. Y. Song, W. Shi, W. Chen, X. Li, H. Ma, J. Mater. Chem., 2012, 22, 12568.

CHAPTER V

C-dots for Folic acid mediated delivery of Doxorubicin and Bio-imaging

5.1 INTRODUCTION

"Whenever you read a cancer booklet or website or whatever, they always list depression among the side effects of cancer. But, in fact, depression is not a side effect of cancer. Depression is a side effect of dying."

- ***John Green***

Biomedical applications of nanoparticles are evident in drug delivery for synaphic and controlled release of chemotherapeutic agents to diseased sites. This property is facilitated by attaching the drugs to nanoparticles. This technique allows the use of lower doses of drugs which are less toxic with improved therapeutic efficacy **[1]**. The main advantage of drug delivery using nanoparticles is that they are target specific, avoiding unnecessary influence on healthy tissues**[2, 3]**. Nanoparticles display noteworthy conjugation capabilities due to their large surface area which allows them to bind to various chemical compounds including drugs, proteins and other molecules by covalent bonds**[4]**.

During the past few years, the potential of nanomaterials such as gold **[5]**, graphene oxides**[6]**,mesoporous silica **[7]** and polymeric nanoparticles **[8]**have been explored as vital tools to deliver drugs, as well as molecular components such as genes**[9]**. Carbon dots (C-dots) have recently emerged as the best material for biological applications due to their aqueous solubility **[10]**, exceptional biocompatibility **[11]**, tuneable optical properties **[12]**, non-toxic precursors such as carbohydrates **[13]** and unique self-passivation of surfaces. These traits make them an ideal alternative to semiconductor quantum dots such as CdTe and CdSe **[14, 15]**. C-dots have not been much explored for its potential as drug delivery vehicle, but due to all the properties stated above; they can prove to be an important candidate as efficient drug delivery vehicle.

Among many of the chemotherapeutic drugs, Doxorubicin (DOX) (Fig. 5.1) is an anthracycline which is widely used for the treatment of many types of Cancers in conventional chemotherapy.DOX intercalates at points of local uncoiling of the DNA - double helix. Although the exact mechanism is unclear, it appears that direct binding to DNA (intercalation) and inhibition of DNA repair (topoisomerase II inhibition) result in blockade of DNA and RNA synthesis and fragmentation of DNA. DOX is also a powerful iron chelator; the iron-doxorubicin complex can bind with DNA and cell membranes and produce free radicals that immediately cleave the DNA and cell membranes**[16]**.

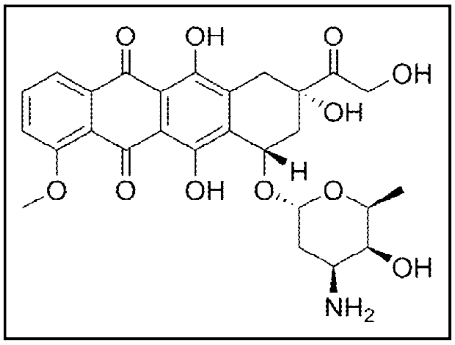

Figure 5.1: Structure of Doxorubicin

The use of folic acid (FA) as a navigational molecule **[17]**has been reported for the construction of molecular Trojan horses whereby drugs can be anchored. FA has extremely high affinity towards its receptors which are over-expressed in certain types of cancers. This unique property enables the nano-conjugate to bind robustly to the folate receptors (FRs) and get internalised via an endocytic process. There are many molecular interaction studies for delivering nano-conjugates to FR-expressing cancer cells such as delivery of radiopharmaceutical agents **[18-21]**, MRI contrast agents **[22]**,low molecular weight chemotherapeutic agents **[23, 24]**, antisense oligo-nucleotides and ribozymes **[25, 26]**, liposomes with encapsulated drugs **[27-29]**, drug-loaded nano-particles **[30]** and plasmids**[20, 31, 32]**.

Albumin-based carriers have special advantages such as low toxicity**[33]**, solubility, biodegradability and biocompatibility**[34, 35]**, feasibility in purification, availability and cost-effectiveness **[36]**. They could be utilized as a 'stealth' material for carrying therapeutic ligands into cells, since they are preferentially taken up by tumor cells **[37]**. Bovine Serum Albumin (BSA) is an acidic protein having a pH of ca. 5 – 7. This provides stability to the protein in an acidic pH environment that is a typical characteristic of the microenvironment of tumors**[38, 39]**. BSA coating in case of C-dots not only acts as a linker but also enhances the fluorescence property of the nanoparticles.

Drug release kinetics also becomes one of the important factors as constant amount of an active substance dosed within time unit provides the drug presence at a therapeutic level in human body during the long time period. In the literature, plenty of theoretical or empirical release models are described **[40–42]**. Zero order, First order, Higuchi and Hixson-Crowell are the most basic drug release models used widely in pharmaceutical industries to study the kinetic profiles of various formulations. Zero order describes system where the drug release

rate is independent of its concentration of the dissolved substance whereas in First order the release rate is dependent on its concentration. Drugs which follow Higuchi model show diffusion mechanism as a mode of release. Hixson-Crowell describes the drug release by dissolution and with changes in the surface area and diameter of the particle.

In this chapter, DOX is decorated on BSA functionalised C-dots (synthesized from Sorbitol) have been used as drug delivery vehicle. FA is used as the targeting molecule to reach Cancer cells. Release profile has also been evaluated statistically using the four mathematical models mentioned above to study the kinetics and mechanism of drug release from C-dots. Due to the excellent optical properties of C-dots and resistant to photobleaching, it acts as a dual pronged vehicle which can be used in drug delivery as well as biological imaging for diseased cells.

5.2 MATERIALS AND METHODS

5.2.1 Synthesis of C-dots

C-dots were synthesized using Sorbitol as a precursor by Microwave assisted thermal oxidation. In a typical procedure, 5 ml of Sorbitol (Sigma Aldrich, USA) and 15 ml of 1 M Sodium hydroxide were mixed and subjected to microwave assisted heating in domestic microwave (Godrej, Model GMX 30 CA1 SIM) Power Output 900 W, 2450 MHz for 2 min. Dark brown precipitate formed was re-dissolved in 15 ml mixture of NaOH and ethanol (1:1).

5.2.2 Purification of C-dots

In order to get pure C-dots from the dark mixture containing other carbonaceous materials, the solution obtained was transferred to pre activated dialysis bag (MW cut-off 12-14 kD, pore size of 2.4 nm) and dialysed against nanopure water for 24 h under stirring conditions. The resulting solution was observed under UV light (365 nm) for fluorescence (Fig.5.2).The sample was analyzed spectrophotometrically. Purified solution was subjected to continuous vacuum heating till a light coloured powder of C-dots was obtained which was weighed and re-dissolved in nanopure water and used for further experimental work.

Figure 5.2: Dialysed C-dot solution in ambient light and UV light

5.2.3 Functionalisation of C-dots with Bovine Serum Albumin (BSA)

Aqueous stock solution (3000 ppm) of BSA (Sigma Aldrich, USA) was prepared by dissolving 30 mg of same in 10 ml of nanopure water. C-dots were used at a concentration of 2mg/ml for attachment studies. Different concentrations of BSA were tried for functionalisation of C-dots in the range of 5ppm to 200 ppm. Solutions were prepared as shown in table 5.1 and incubated at room temperature (28±2ºC) for 2 h. Functionalisation was analyzed spectrophotometrically. 15 ppm of BSA gave best results and hence was used for all further preparation and studies on C-dot BSA complex (fC-dot).

Table 5.1: Optimisation of BSA functionalisation on C-dots

Tube Number	Conc. of BSA(ppm)	BSA stock solution (ml)	d/w (ml)	Volume of C-dots (ml)	Total volume(ml)
1	5	0.008	2.992	3	5
2	10	0.016	2.984	3	5
3	15	0.025	2.975	3	5
4	20	0.041	2.958	3	5
5	25	0.083	2.917	3	5
6	100	0.166	2.834	3	5
7	150	0.250	2.750	3	5
8	200	0.333	2.667	3	5

5.2.4 Activation and attachment of Folic Acid (FA) to fC-dots

Activation of the FA was carried out by dissolving 0.25 g of FA into 20 ml of DMSO (Dimethylsulfoxide) and the mixture was subjected to sonication for 45 minutes. The carboxylate group of FA was activated by addition of 0.225 gm of NHS (n –hydroxy succinamide) and 0.125 gm of DCC (Dicarboxyamino carbodiimide). The reaction was allowed to take place in an inert environment created by Argon gas at 28º±2ºC for 12 h (FA/NHS/DCC molar ratio 2 : 2 : 1). The resultant mixture was filtered through Whatman Filter paper and was used for further experiments. Attachment of FA was carried out by adding 8 ml of fC-dots to 2 ml of activated FA. The solution was subjected to purging under N_2 atmosphere for 4 h under stirring conditions. Both inlet and outlet valves were closed and the reaction was allowed to take place for 24 h. Unbound FA was removed by dialyzing the resultant solution against deionized water for 10-12 h and the samples were studied spectrophotometrically at regular intervals.

5.2.5 Attachment of Doxorubicin (DOX) tofC-dot-FA complex

Stock solution of DOX (0.5 mM) was prepared by dissolving 0.29 g of DOX (Sigma Aldrich, USA) in 10 ml of nanopure water. For attachment, 2.5 ml (0.125 mM) of DOX from the stock solution was added to 7.5 ml of fC-dots-FA and the volume was made to 20 ml using DMSO (HiMedia) as a diluent. To this solution 200 µl of Tri ethyl amine (TEA) was added and the whole mixture was subjected to purging using Argon gas for 4 h. Later the gas flow was stopped and the sealed solution was further stirred at room temperature (28±2ºC) for 12 h. The complex was purified by dialysis and characterised using UV-Vis spectrophotometer and Fourier Transform Infra Red spectroscopy (FTIR).

5.2.6 Drug loading Efficiency

5 ml of fC-dots-DOX complex was dialyzed against nanopure water for 8 h and the concentration of unbound Drug was measured spectrophotometrically at 485 nm and calculated using standard calibration curve of DOX (Linear line equation: y=6.8848x).

Drug Loading Efficiency (DLE) was calculated using the following equation-

$$DLE = \frac{\text{Theoretical amount of drug loaded - Free drug}}{\text{Theoretical amount of drug loaded}} \times 100 \quad (1)$$

5.2.7 Cell Imaging and Cytotoxicity

For cell imaging, 500 µl of purified bare C-dots (~ 1g/ml) was incubated with HeLa cells (seeded at $5x10^5$ /ml) for 2 h at 37°C. In another batch, Vero cells and HeLa cells both were treated with 500 µl of fC-dot-FA conjugate separately under the same conditions for 2 h at 37°C and subsequently, the cells were washed three times with DMSO and were observed after fixing them using 2% *para*-formaldehyde for 25 min.

Cytotoxicity effects of C-dots, fC-dots and fC-dots-FA-DOX complex were studied on Vero and HeLa cells using MTT assay. This assay is based on the conversion of pale yellow MTT to violet colored formazan crystals by mitochondrial enzyme succinate dehydrogenase. Cells were seeded ($5x10^5$ /ml) in 96 well plates and incubated at 37ºC and 5% CO_2 for 24 h. Medium was then replaced with test solutions and incubated for further 48 h. Later, these solutions were replaced with MTT (200 µg/ml) and cells were incubated for 2.5 h at 28±2ºC to initiate formation of formazan. After completion of the reaction, medium was replaced with 200 µl of DMSO. This complex was slowly agitated to dissolve formazan crystals. Finally, formazan dissolved in DMSO was transferred to fresh 96 well plates and read on micro plate reader (Thermo, USA) at 570 nm.

5.2.8 Drug Release and kinetics study of DOX

In order to elucidate drug release profile under physiological condition 3 ml of fC-dots FA DOX complex was sealed in dialysis bag (MW cut-off 12 14 kD, pore size 2.4 nm) and kept in 100 ml of PBS solution (pH 5.8) heated at 37ºC under mild intermittent stirring. Sample were collected at the interval of 30 min for 3 h and then at the interval of 24 h for 3 days. Concentration of the released drug was calculated using standard calibration curve at 485 nm wavelength. The same procedure was repeated for pH 7.2.

Precise control of the drug carrier architecture, the release of the drug can be tuned to achieve a desired kinetic profile. Four of the most common kinetic profiles are Zero Order, First Order, Higuchi & Hixson-Crowell; these are depicted below and expressed mathematically in Eq. 2,3,4,5. Various release models used for statistical computation are:

Zero order: $Q_t = Q_0 + k_0 t$ ---------- (2)

First order: $\ln Q_t = \ln Q_0 + k_1 t$---------- (3)

Higuchi: $Q_t = Q_0 = k_H t^{1/2}$---------- (4)

Hixson Crowell: $\sqrt[3]{Q0} - \sqrt[3]{Qt} = k_{H.C}\, t$---------- (5)

Where, Qt is the amount of drug released at time t, Q_0 is the initial amount of drug released, k_0 is the Zero Order release constant, k_1 is the First-Order release constant, and k_H is the Higuchi release constant.The model that fits best is selected on the co-efficient correlation (r) value in various models and the model that gives the highest r value is considered as the best fit for the drug release data.

5.2.9 Characterisation

Confirmation of C-dots in solution and its spectral and morphological studies have been characterised and explained in detail in Chapter 3. Fourier Transformed Infra red (FTIR) Spectroscopy (Brucker) studies were performed within the spectral window 500 to 4000 cm^{-1}. Thermo Gravimetric Analysis (TGA) was performed using Perkin Elmer, Diamond, USA. Typically, 20 mg of the dried sample was placed in the TGA cell and heated to 830°C at a heating rate of 20°C min^{-1} in an atmosphere of N_2 gas.

5.3 RESULTS AND DISCUSSIONS

5.3.1 Synthesis, purification and characterisation of C-dots

All the characterisation data of synthesised and purified C-dots is shown in Chapter 3.

5.3.2 Functionalisation of C-dots with BSA

To increase the efficiency of drug attachment as well as solubility of C-dots in aqueous solution, surfaces of C-dots were functionalized using BSA as a linker (fC-dots).

The presence of disulphide (S-S) linkages in BSA holds the C-dots and DOX complex (fC-dots- DOX). BSA is readily soluble in water, as it is present in all mammalians it will not cause any adverse effects to other organs in the body and efficiently used in drug delivery

application**.** 15 ppm was found to be the optimum concentration of BSA to get stable functionalised C-dots. Analysis of UV-spectra (Fig. 5.3) exhibited sharp characteristic peaks of original C-dots at 210nm and 263nm while after conjugation with C-dots peak at 210nm diminished, and slight shifting of peak observed (from 263nm to 266nm) towards red shift and the intensity of the peak also decreased. These observations showed signals for conjugation of BSA on C-dot.

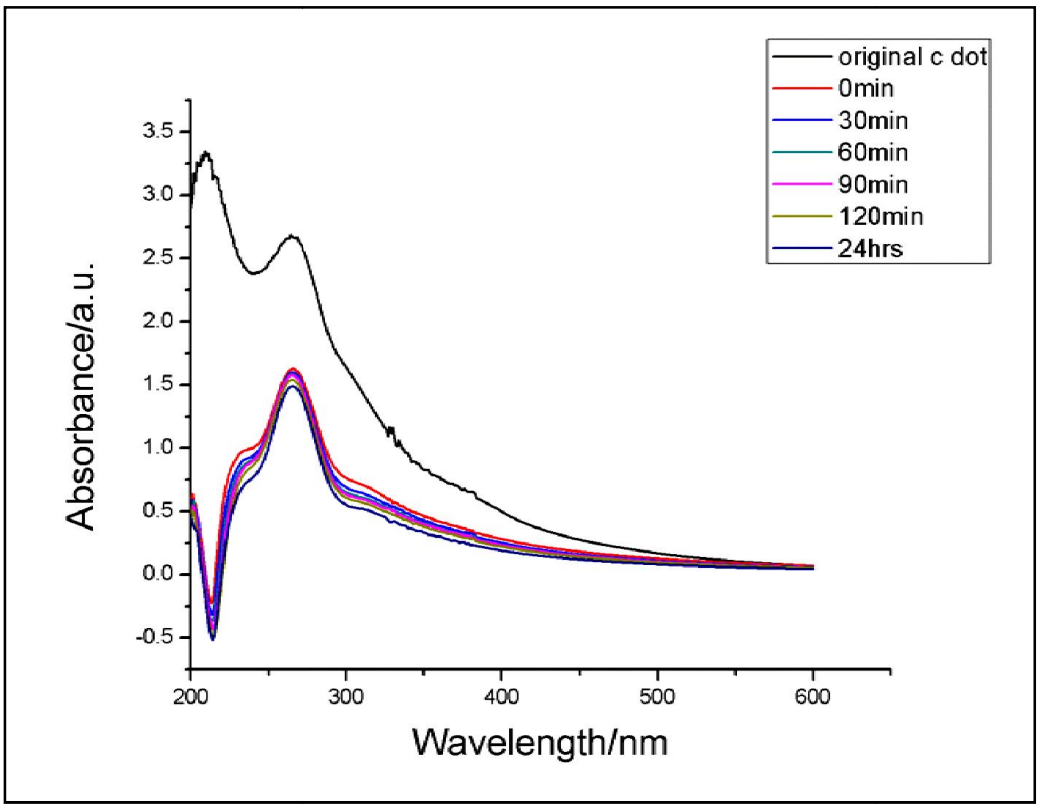

Figure 5.3: UV-spectra of C-dots and BSA linker at 15 ppm concentration taken at different time intervals.

Moreover, due to surface modification by BSA, the conjugate becomes more biocompatible as well as thermodynamically more stable under physiological milieu. After attachment of 15 ppm BSA, the peak at 212 nm in UV Vis spectra (Fig.5.4) of pure C-dots disappeared; whereas a minor red shift of 2 nm was observed in the shoulder (264 nm to 266 nm), probably due to reduction. These minor changes in the UV spectra could be the result of weak interactions between the functional groups of BSA and surface carboxylate groups of C-dots. Another crucial optical property of the fC-dots is decrease in back ground absorption in visible region and sharper peak indicating reduction of C-dots due to interaction with BSA. Also, the peak at 266 nm was found to be diminished which indicates depletion in

functional moieties containing C=C bonds, probably due to formation of bonds with BSA. Also, a blue shift in the PL spectra was observed along with decrease in the intensity which indicates surface functionalisation of C-dots (Fig.5.4 Inset).

5.3.4 Attachment of DOX on fC-dots

Further attachment of DOX resulted in a sharp peak at 213 nm and a slight hump at 308 nm (Fig.5.4). In comparison to the UV-Vis spectra of fC-dots, decrease in intensity of the peak along with red shift was observed. Intensity of deep UV peak was almost found to be diminished indicating further reduction after attachment of DOX. There was rapid increase in background absorption in higher wavelength. A blue shift in the PL spectra of the final complex was observed (from 548 to 535 nm) along with further decrease in fluorescence intensity which may be due to the involvement of the functional responsible for PL with DOX.

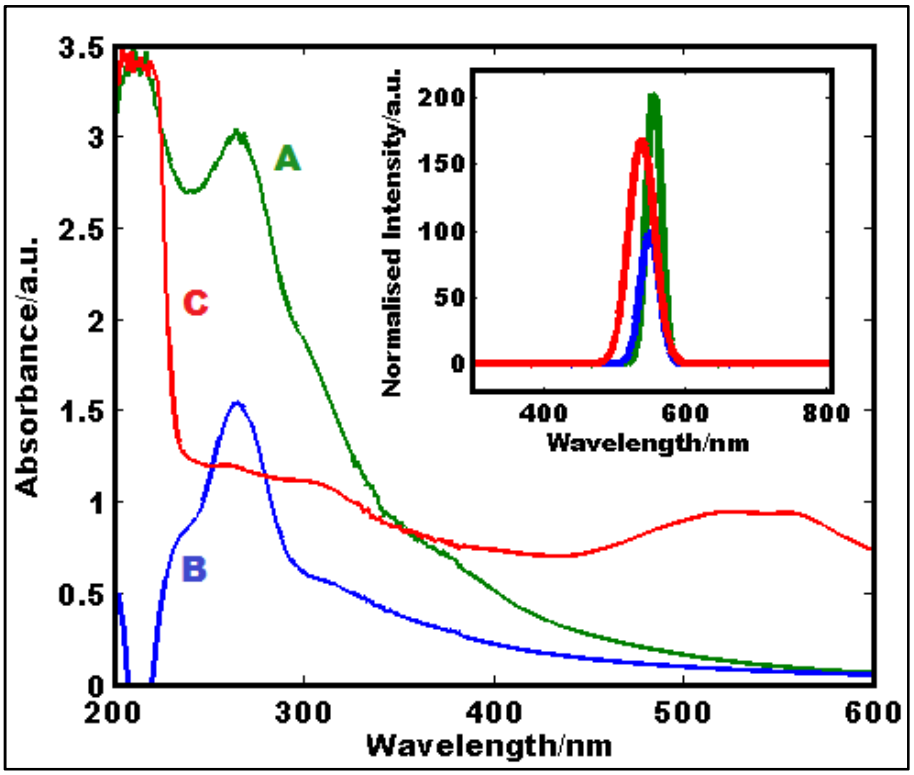

Figure 5.4: UV-Vis spectrum of C-dots and its complexes after surface modification where (A) C-dots, (B) fC-dots and (C) fC-dots + DOX complex; Inset shows PL spectra of the same (excited at 300 nm)

5.3.5 FTIR Analysis

FTIR spectra of C-dots (Fig. 5.5a-A) revealed the presence of multiple surface passivated groups.Following are some of the prominent bands:

1. IR band at 1270 cm^{-1} represent bending of alkene C-H plane and C-O-C stretching arising from reactions occurring at the sp^3 carbon atoms.
2. IR band at 1364 cm^{-1}represent carboxylic C-O stretching vibrations due to their orchestration on the surface of C-dots by NaOH treatment. However, bands at 1500 cm^{-1} and 1700 cm^{-1} are attributed to anhydride C=O stretching and carboxylic C=O stretching respectively.
3. Mild peaks at 2847 cm^{-1} and 2917 cm^{-1} are because of alkene =CH and amide N-H stretching.
4. Sharp peak at 3323 cm^{-1}represent alcoholic and carboxylic O-H stretching vibrations.

FTIR of BSA molecule (Fig.5.5a-B) exhibited a typical band at 617 cm^{-1}which signify aromatic C-H bend from hydrophobic benzene rings. Prominent bands at 1044 cm^{-1}show CH acetyl bend, alkene C-H bend (mono-substituted) of saturated hydrocarbons whereas those at 1394 cm^{-1}depict alkane CH_3 bend, aromatic C=C stretch, carboxylic acid C-O stretch and anhydrides C-O stretch. Multiple bands around 1694 cm^{-1}represent amide 1° N-H bending and aldehyde/anhydride C=O stretching. 2911 $cm^{-1}$is attributed to carboxylic acid –OH stretch and amide N-H stretch from amino acids. Peaks obtained at 3341 $cm^{-1}$and 3435 cm^{-1}represent alcoholic –OH stretching and carboxylic acid –OH stretching of the aqueous solution.

Prominent differences in the FTIR bands with respect to pure C-dots as well as BSA are as follows which confirm interaction between the above two materials (Fig.5.5a-C).

1. Widening of IR band 617 cm^{-1} is due to reactions involving formation of acetylenic C-H bends after attachment of C-dots onto BSA molecule.
2. Diminishing of band at 1023 cm^{-1}(with reference to BSA at 1044 cm^{-1}) shows surface covering of the protein with C-dots at multiple sites via weak electrostatic interactions.
3. Shift in the bands 1605 cm^{-1}(1694 $cm^{-1}$of BSA)and 1688 cm^{-1}(1700 $cm^{-1}$of C-dots) is because of reactions involving formation of aromatic C=C stretch, amide 1° N-H bend and anhydride C=O stretch between amino acids and C-dots surface moieties.

4. Fading of the bands 2858 cm^{-1} and 2917 cm^{-1} is attributed to C-dots covering of amino acids at carboxylic acid -OH stretching and amide N-H stretching.
5. Weak vibrations around 3311 cm^{-1} and 3682-3864 cm^{-1}represent hydroxyl OH stretching from aqueous part and residual amide NH stretching from amino acids.

FTIR spectrum of pure FA displays band at 617 $cm^{-1}$and 723 cm^{-1}signifies aromatic C-H bend from hydrophobic benzene rings (Fig. 5.5a-D). Band at 1023 $cm^{-1}$is due to anhydride C-O stretching whereas band at 1641cm^{-1}shows alkane CH_3 bend, aromatic C=C stretch and amine C-N stretches. Band at 3470 cm^{-1}depict alcohol O-H stretch and carboxylic acid OH stretch from aqueous suspension.

In case of typical FTIR spectra of fC-dot-FA complex (Fig.5.5a-E) narrow band at 1064 cm^{-1} is due to enhanced - CH bending of alkenes and decrease in anhydride C-O stretching of FA involved in the reaction. Absence of IR bands of C-dot-BSA complex- 1605 cm^{-1} and 1688 cm^{-1} is again due to loss of aromatic C=C stretch, amide 1° N-H bend and anhydride C=O stretching and appearance of new band at 1417 cm^{-1} is due to formation of new functional groups- alkane CH_3 bend, aromatic C=C stretch, carboxylic acid C-O stretch and amine C-N stretches. Hence, attachment of FA on fC-dot can be due to multiple bond formation between exposed FA $–NH_2$ and –OH functional groups.

FTIR spectrum of pure DOX in the Figure 5.5a-F shows a characteristic band at 614 $cm^{-1}$is attributed to aromatic C-H bend from benzene rings whereas at 717cm^{-1} and 1611 cm^{-1} depict alkane CH_2 bend, alkene C-H and aromatic C-H bend (meta). Band at 2076 $cm^{-1}$is due to Aldehyde C-H stretch, Alkenes =CH stretch, Aromatic CH stretch and wide band ranging from 3070-3647 cm^{-1}carboxylic acid OH stretch, amide NH stretch and hydroxyl –OH stretch.

In case of FTIR of fC-dots-FA-DOX complex (Fig.5.5a-G), decrease in the intensity of the band at 1471 cm^{-1} with respect to fC-dot–FA complex is due to decrease in alkane CH_3 bends and aromatic C=C stretches with respect to complete coverage of the complex by DOX molecules. New bands at 1600 $cm^{-1}$and 1711 cm^{-1}shows formation of new amide 1° N-H bonds and anhydride C=O stretches between DOX and fC-dot-FA complex at multiple sites. Intense band at 2858 cm^{-1} is due to increase in anhydride C=O and carboxylic acid OH stretches arising from DOX molecules.

Figure 5.5b displays the schematic diagram for the functionalisation of C-dots with BSA and consequent attachment of DOX to get the final complex.

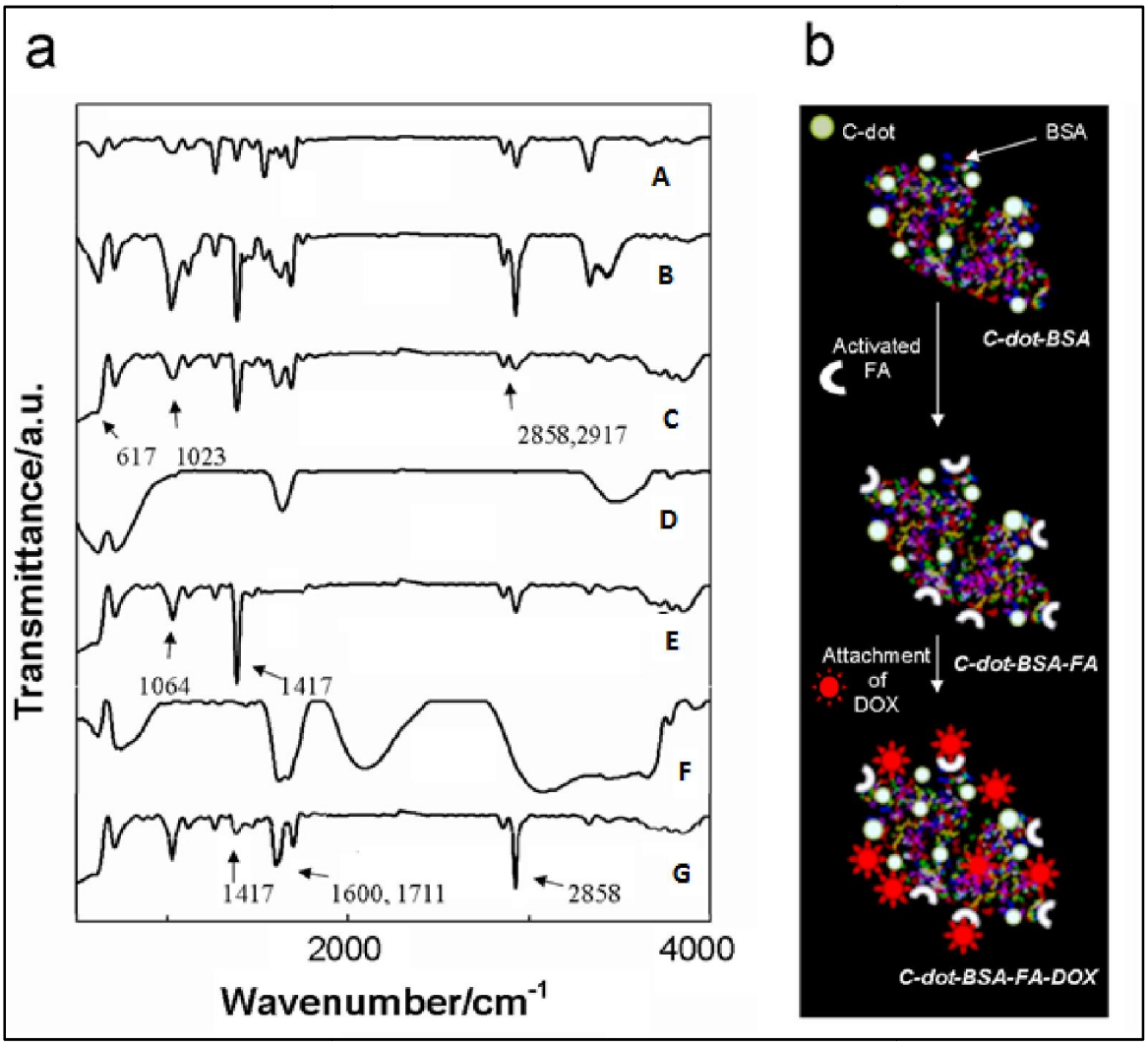

Figure 5.5: (a) FTIR spectra of bare C-dots 'A', bare BSA 'B', fC-dot 'C', bare FA 'D', fC-dot-FA complex 'E', bare DOX 'F' and fC-dots-FA-DOX complex 'G', arrows show changes in the IR bands as explained in the text and (b) A schematic representation showing formation of fC-dots-FA-DOX complex.

5.3.6 Zeta Potential measurements

Figure 5.6a displays the Zeta potential measurements of C-Dots and its complexes. C-dots showed zeta potential value as -17.8 mV. The C-dots were found to be negatively charged due to the ionized hydroxyl functional groups spread throughout the surface. After conjugation of BSA to C-Dots, there was rise in the Zeta potential value to -5.4 mV. The rise in charge was observed due to interaction of functional groups and exposure of new groups

on the resultant complex. Further the Zeta potential value of final complex was observed to be 15.7 mV due to the inherent positive charge of DOX.

5.3.7 TGA analysis

TGA of bare C-dots and the final conjugate is displayed in Figure.5.6b. The initial loss of 8-10% weight of C-dots observed between 150-200°C attributed to the water molecules and other weak hydrogen interactions present within the nanoparticles. Further, a steady weight loss was observed in C-dots till 500°C. Unlike C-dots the fC-dots-FA-DOX complex showed losses at various temperatures. Weight loss of approximately 50% was observed between 280-320°C possibly due to the interactions between BSA-functionalized C-dots as well as FA. Further more weight loss of 30% (500-600°C) may be due to detachment of DOX from the final complex.

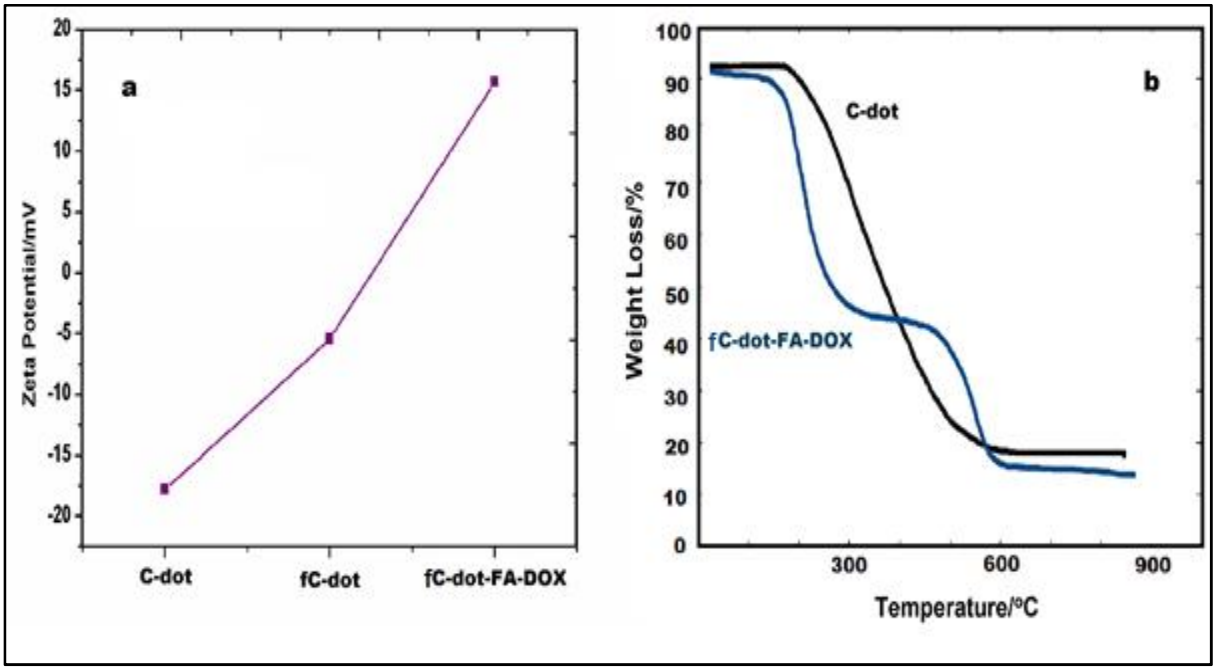

Figure 5.6: (a) Zeta potential values of C-dot, fC-dot and fC-dots-FA-DOX complex and (b) Thermo gravimetric analysis of bare C-dots and fC-dots-FA-DOX complex.

5.3.8 Drug Loading Efficiency (DLE) of C-dots

Drug loading efficiency was calculated according to equation 1 as follows-

Concentration of drug initially loaded= 0.125 mM

Concentration of unbound drug= 0.0181mM

[Concentration of drug is calculated using the standard calibration curve of DOX (Straight line equation: y=6.8848x)]

Concentration of drug finally loaded= Concentration of drug initially loaded-Concentration of drug of unbound drug

= 0.125 mM – 0.0181mM

= 0.1069mM

Drug Loading Efficiency (%) = Concentration of drug finally loaded/Concentration of drug initially loaded*100

= 0.1069/0.125*100

= **85.52**

5.3.9 Drug release kinetics

The concentration of drug released at different time intervals was calculated in similar way using the standard calibration curve of DOX with straight line equation y=6.8848x and the percentage values at pH 5.8 and physiological pH 7.2 are displayed in table 5.2.

Table 5.2: Percentage release of DOX at pH 5.8 and pH 7.2

Time/h	% release @ pH 5.8	% release @ pH 7.2
1	4.02	3.27
2	4.39	5.14
3	4.58	12.16
24	4.58	13.56
48	7.76	16.37
72	15.24	18.42

Due to certain biochemical properties of solid tumors **[43, 44]** such as fuzzy layer of distorted extracellular matrix and acidified environment, pushing drugs to tumors often becomes a daunting task. Overall outcome of these alterations is enhanced interstitial fluid pressure which obstructs the entry of most of the drugs including DOX. One of the finest solutions to tackle this situation is to fabricate smallest possible nanoparticles which can clutch high amount of drugs and unload it to solid tumors. In case of C-dots, we found an ideal drug

release profile at physiological as well as slightly acidic pH (7.2 and 5.8). There was an initial burst of drugs at both the pH values but much higher at pH 7.2. At pH 7.2, ~12%whereas at pH 5.8 ~4% DOX was found to be release under physiological condition. At the end of 60 h, > 16% DOX was found to release. At pH 5.8, there was rapid rise in the percentage DOX release after 4 h till 70 h where ~14% drug was found to be fired (Fig.5.7a). The Coefficient correlation values are listed in Table 5.3 which predicts that DOX follows first order release kinetics (Fig. 5.7b) at physiological pH. Such type of release kinetics is generally followed by drugs which are injected in the body (for example DOX).

Table 5.3: Coefficient correlation values in various models

pH / **Models**	**5.8**	**7.2**
Zero Order	0.9486	0.9530
First Order	0.9449	**0.9754**
Higuchi	0.9116	0.9660
Hixson-Crowell	0.9471	0.9743

Such type of dual sensing drug delivery flotillas can be an important asset for solid tumor chemotherapy**[45]**. In a solid tumor micro-anatomy, there are cells which maintain both acidic as well as basic pH depending upon their spatial distribution from the blood vessels**[45]**. Competence of the present drug delivery vehicle (fC-dots-FA-DOX) complex to rapidly fire drugs at both the pH values can play cardinal role in combating with most of the cell types in solid tumors.

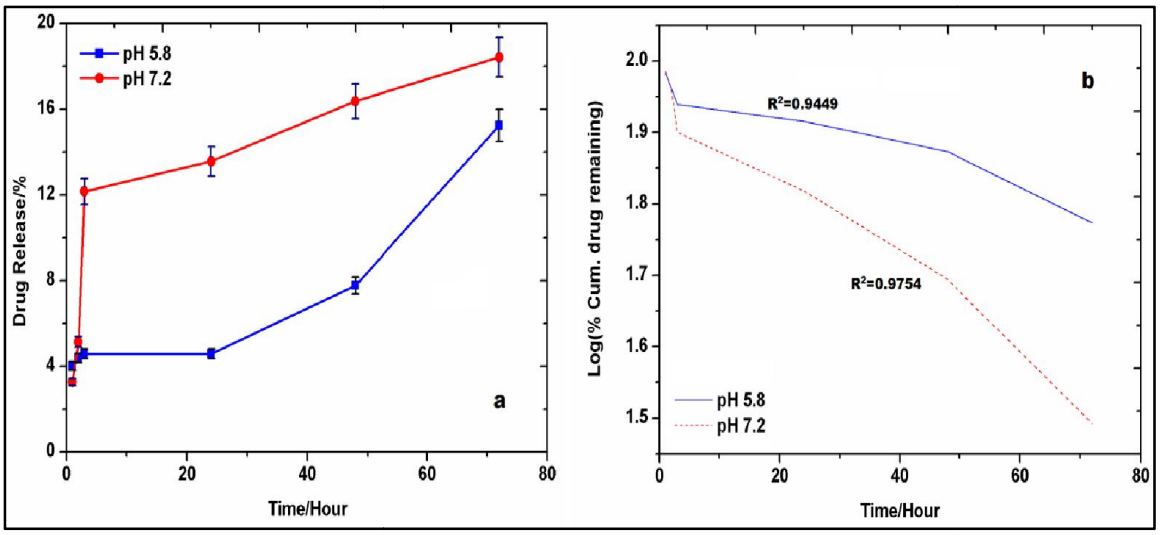

Figure 5.7: (a) Percentage release of DOX with respect to time (b) Drug release profile of DOX following first order release kinetics.

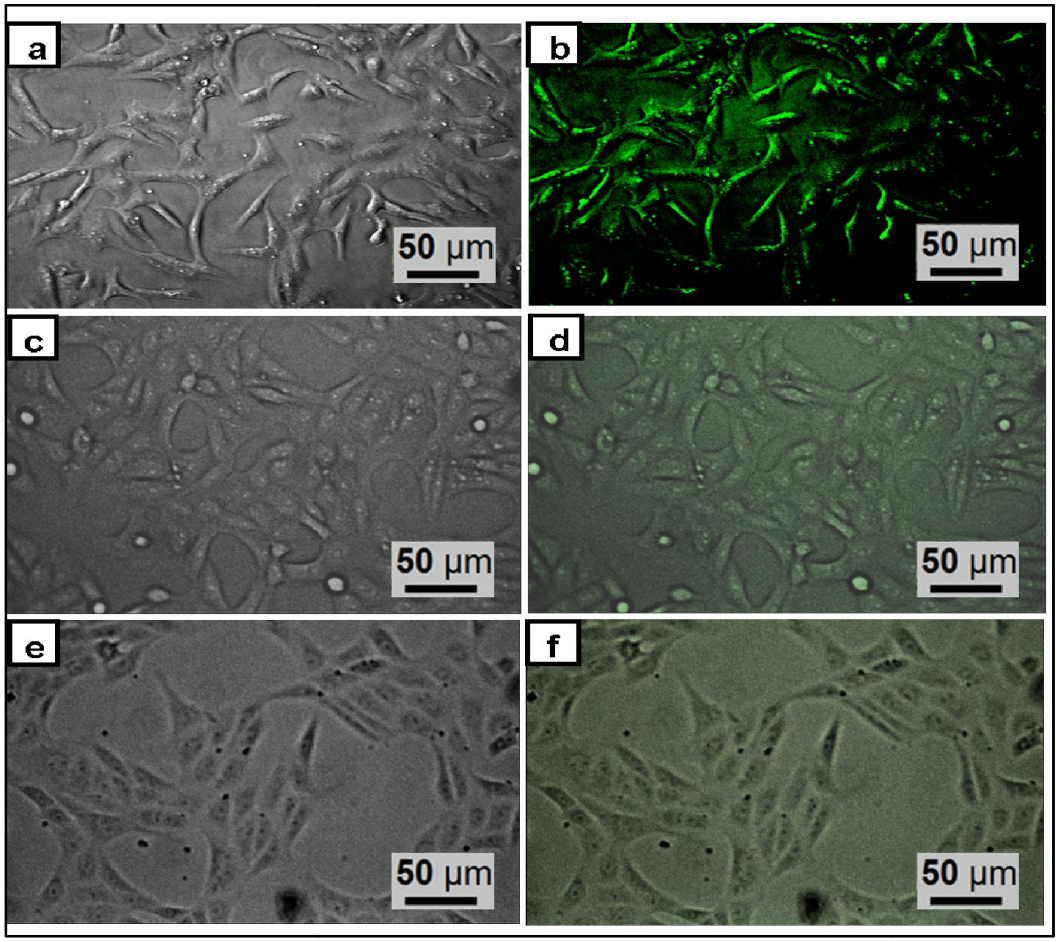

Figure 5.8: Images of cells taken in (Left panel) Bright field and (Right panel) epifluorescence microscope. (a-b) are HeLa cells treated with fC-dots-FA complex, (c-d) HeLa cells treated with only fC-dots (without FA) and (e-f) are Vero cells treated with fC-dots-FA complex.

5.3.10 Cell Imaging studies

Figure 5.8 shows cellular imaging and specific targeting of cells. Figure 5.8a-b displays the bright field and fluorescence microscopy image of HeLa cells incubated with fC-Dots-FA complex respectively. HeLa cells show clear internalization of fC-dots giving bright green fluorescence. In contrast, HeLa cells when treated with bare fC-dots (without FA), almost negligible fluorescence was observed and most of them were due to background noise (Fig.5.8c-d). As discussed earlier, HeLa cells express high concentration of FA receptors which is often used in drug targeting. Therefore, we could elucidate from this that in the absence of FA, fC-dots could not get internalized and hence role of FA was important in fC-dots-FA-DOX complex. On the other hand, when Vero cells were treated with fC-dots-FA complex (Fig. 5.8e-f), similar to (Fig.5.8d), no internalization of fC-dots was observed. Instead, faint green colour fluorescence was observed again due to background noise and non-specific binding to medium components.

5.3.11Cytotoxicity Analysis

Percentage Viability of Vero and HeLa cells against C-dots, fC-dots, fC-dots-FA-DOX complex and free DOX are listed in table 5.4.

Table 5.4: % Survival of normal and cancerous cells against various test samples

Conc (mM)	**% Survival of normal and cancerous cells treated with**							
	C-dots		**fC-dots**		**fC-dots-DOX**		**Free DOX**	
	Vero	***HeLa***	***Vero***	***HeLa***	***Vero***	***HeLa***	***Vero***	***HeLa***
0.04	97.2	97.27	98.78	97.7	70.3	40.57	55.6	54.84
0.08	96	95.36	98	96.9	65.5	35.20	50.2	49.10
0.12	95.5	94	97.6	96.16	63.3	32.11	47.1	45.58

Cytotoxicity testing revealed that C-dots were found to be highly compatible showing cell viability of 95.5 and 94 % at the highest concentration on Vero and HeLa cells respectively (Fig.5.9). Attachment of BSA to C-dots (fC-dot) showed a slight increase in biocompatibility as compared to bare C-dots on both the cell types. fC-dots-FA-DOX (DOX@C-dots) complex showed IC_{50} value on HeLa cells to be less than 0.04 mM which was much lower as

compared to free DOX (0.08 mM). IC_{50} value of free DOX on Vero cells was calculated to be 0.08 mM and that of fC-dots-FA-DOX was found to be less 0.04 mM. Targeting of cancerous cells using Folic acid leads to less damage of non-cancerous cells hence reducing the cytotoxicity of the final complex on Vero cells as compared to free DOX.

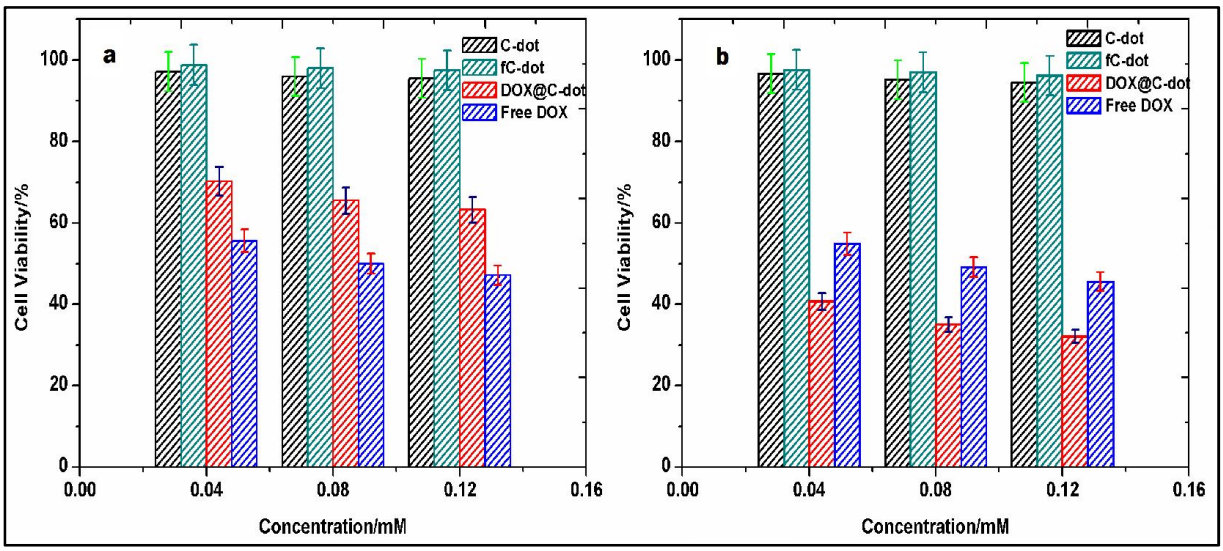

Figure 5.9: Cytotoxic effects of C-Dots, fC-dots, DOX @ C-dots and Free DOX on (a) Vero cells and (b) HeLa cells

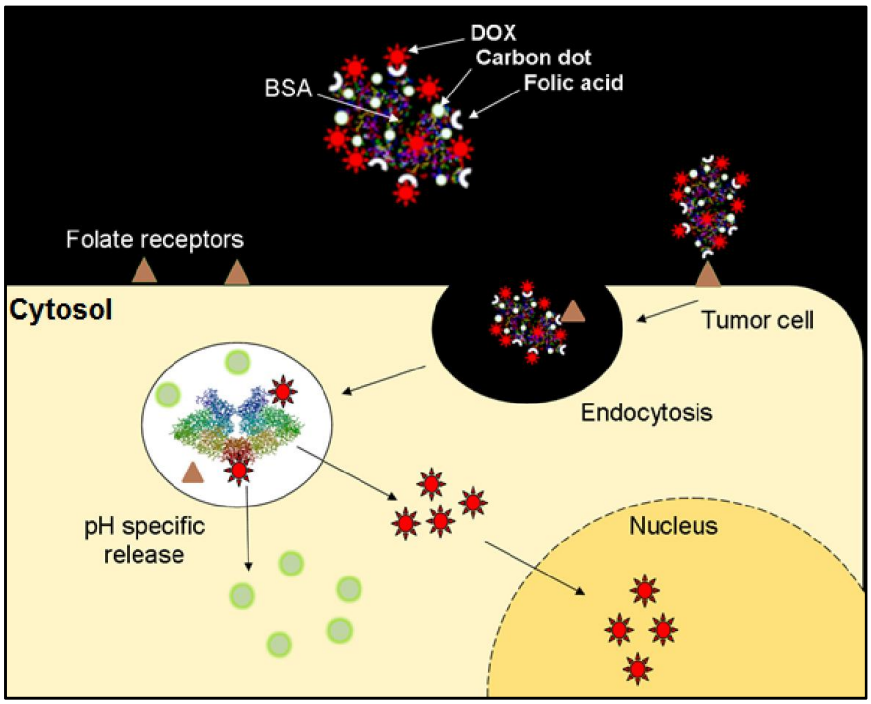

Figure 5.10: Schematic showing internalization of DOX@C-dots complex into a tumor cell and acid specific release of components.

Figure 5.10 displays the schematic representation of C-dots as delivery vehicle decorated with DOX and FA as targeting molecule. The targeting molecule follows receptor mediated endocytosis of C-dot-drug complex and pH responsive release.

5.4 CONCLUSION

C-dots were synthesized from Sorbitol using simple microwave assisted method in a short period of time and showed bright green fluorescence under UV light. DOX was successfully anchored and drug loading capacity was calculated to be very high (~86 %) thus proving efficiency of C-dots as drug delivery vehicles. C-dot-DOX complex showed ideal drug release profile at physiological as well as slightly acidic pH and was found to follow first order release kinetics based on the statistical calculations. C-dots were highly biocompatible on both the cells. C-dot-DOX complex showed higher killing rate on cancer cells than free DOX and was found to be less toxic on normal cells due to FA mediated targeting.

5.5 REFERENCES

1. I. Brigger, C. Dubernet and P. Couvreur, Adv. Drug Delivery Rev., 2002, 54, 631.
2. S. K. Sahoo, S. Parveen and J. J. Panda, Nanomed.:Nanotechnol., Biol. Med. , 2007, 3 , 20.
3. M. Prato, K. Kostarelos and A. Bianco, Acc. Chem. Res., 2008, 41, 60.
4. P. M. Heegaard, U. Boas and D. E. Otzen, Macromol. Biosci. , 2007, 7, 1047.
5. S. Shiv Shankar, A. Ahmad, R. Pasrich and M. Sastry, J. Mater. Chem., 2003, 13, 1822.
6. Y. Feng, X. Lin, Y. Wang, Y. Wang and J. Hua, Mater. Lett., 2008, 62, 4299.
7. M. Sastry, A. Ahmad, M. Khan and R. Kumar, Curr. Sci., 2003, 85, 162.
8. Y. Zhang, J. Zheng, G. Gao, Y. Kong, X. Zhi, K. Wang, X. Zhang and D. Cui, Int. J. Nanomed., 2011, 6, 2899.
9. F. Kiu, F. Ko, P. Huang, C. Wu and T. Chu, J. Chromatogr., A, 2005, 1062, 139.
10. G. Wei, F. Liu and C. R. C. Wang, Anal. Chem., 1999, 71, 2085.
11. C. Murray, D. Norris and M. Bawendi, J. Am. Chem. Soc., 1993, 115, 8706.
12. R. Whetten, et al., Adv. Mater. , 1996, 8, 428.
13. V. Sharma, K. Park and M. Srinivasarao, Proc. Natl. Acad. Sci. U. S. A., 2009, 106, 4981.
14. N. R. Jana, Chem. Commun., 2003, 1950.
15. T. Tyler, A. Henry, R. Van Duyne and M. Hersam, J. Phys. Chem. Lett., 2011, 2, 218.
16. S. Wang, E. A. Konorev, S. Kotamraju, J. Joseph, S. Kalivendi and B. Kalanaraman, J. Boil. Chem., 2004, 279, 25535.
17. B. A. Kamen and A. Capdevila, Proc. Natl. Acad. Sci. U. S. A., 1986, 83, 5983.
18. C. J. Mathias, S. Wang, R. J. Lee, D. J. Waters, P. S. Low and M. A. Green, J. Nucl. Med., 1996, 37, 1003.
19. C. P. Leamon, M. A. Parker, I. R. Vlahov, L. C. Xu, J. A. Reddy, M. Vetzel and N. Douglas, Bioconjugate Chem., 2002, 13, 1200.
20. W. Guo, G. H. Hinkle and R. J. Lee, J. Nucl. Med., 1999, 40, 1563.
21. S. Wang, R. J. Lee, C. J. Mathias, M. A. Green and P. S. Low, Bioconjugate Chem., 1996, 7, 56.
22. S. D. Konda, M. Aref, M. Brechbiel and E. C. Wiener, Invest. Radiol., 2000, 35, 50.

23. O. Aronov, A. T. Horowitz, A. Gabizon and D. Gibson, Bioconjugate Chem., 2003, 14, 563.
24. G. Steinberg and R. F. Borch, J. Med. Chem., 2001, 44, 69.
25. S. Li and L. Huang, J. Liposome Res., 1998, 8, 239.
26. L. H. Leopold, S. K. Shore, T. A. Newkirk, R. M. Reddy and E. P. Reddy, Blood, 1995, 85, 2162.
27. R. J. Lee and P. S. Low, J. Biol. Chem., 1994, 269, 3198.
28. Y. Rui, S. Wang, P. S. Low and D. H. Thompson, J. Am. Chem. Soc., 1998, 120, 11213.
29. K. Vogel, S. Wang, R. J. Lee, J. Chmielewski and P. S. Low, J. Am. Chem. Soc., 1996, 118, 1581.
30. M. O. Oyewumi and R. J. Mumper, Bioconjugate Chem., 2002, 13, 1328.
31. J. T. Douglas, B. E. Rogers, M. E. Rosenfeld, S. I. Michael, M. Feng and D. T. Curiel, Nat. Biotechnol., 1996, 14, 1574.
32. J. A. Reddy, C. Abburi, H. Ho・and, S. J. Howard, I. Vlahov, P. Wils and C. P. Leamon, Gene Ther., 2002, 9, 1542.
33. F. Wu, S. A. Wuensch, M. Azadniv, M. R. Ebrahimkhani and I. N. Crispe, Mol. Pharmaceutics, 2009, 6, 1506.
34. F. Kratz, J. Controlled Release, 2008, 132, 171.
35. E. Miele, G. P. Spinelli, E. Miele, F. Tomao and S. Tomao, Int. J. Nanomed., 2009, 4, 99.
36. H. Hequn, M. Qingming, H. Chong, H. Fen and Y. Ping, Int. J. Pharm., 2013, 444, 77.
37. R. Khandelia, A. Jaiswal, S. S. Ghosh and A. Chattopadhyay, Small, 2013, 9, 3494.
38. S. Abbasi, A. Paul, W. Shao and S. Prakash, J. Drug Delivery , 2012, 2012 , 686108.
39. Y. Kato, S. Ozawa, C. Miyamoto, Y. Maehata, A. Suzuki, T. Maeda and Y. Baba, Cancer Cell Int., 2013, 13, 89.
40. P. Costa, L. J. M. Sousa L, Eur J Pharm Sci., 2001, 13, 123.
41. J. Siepmann, A. Gopferich ,Adv Drug Deliv Rev., 2001, 48, 229.
42. S. Dash, P. N. Murthy, L. Nath, P. Chowdhury, Acta Pol Pharm., 2010, 67(3), 217.
43. S. K. Hobbs, W. L. Monsky, F. Yuan, W. G. Roberts, L. Griffith, V. P. Torchilin and R. K. Jain, Proc. Natl. Acad. Sci. U. S. A., 1998, 95, 4607.

44. T. D. McKee, P. Grandi, W. Mok, G. Alexandrakis, N. Insin, J. P. Zimmer, M. G. Bawendi, Y. Boucher, X. O. Breakefield and R. K. Jain, Cancer Res., 2006, 66, 2509.
45. R. K. Jain and T. Stylianopoulos, Nat. Rev. Clin. Oncol., 2010, 7, 653.

CHAPTER VI

General Discussions and Conclusion

Carbon is an important component of all living organisms and exists in various forms in nature. Carbon shows three different hybridisations like sp, sp^2 and sp^3 which lead to the formation of various stable forms of carbon. It has a strong tendency to form bonds with its own atom thus resulting in long networks of Carbon. All the different forms of carbon vary widely in their properties and have led to the discovery of its various allotropic forms as well as nano-forms like Diamond, Graphite, Buckminster Fullerene, Carbon Nanotubes, Graphene and the recently discovered C-dots. Due to its wide range of excellent optical and chemical properties, C-dots have been used in applications like bio-imaging and drug delivery and hold place in potential application of Catalysis, Optoelectronics and as Sensors**[1-4]**. Some of the important findings from the present work were as follows:

6.1 SYNTHESIS AND PURIFICATION

6.1.1 Precursor: selection was very important aspect of synthesis of C-dots. Synthesis of C-dots was attempted from novel natural (Water chestnut peel, Neem gum and Sugarcane juice)and *Acacia Arabica* gum (Gum Arabic) as well as chemical (Sorbitoland Phenylalanine) precursors**[4-9]**. The precursors were selected on the basis of their high carbon content and ratio of H, C and O in their sugar moieties based on the previous reports on synthesis of C-dots using various types of precursors **[7, 10-13]**.

6.1.2 Thermal impact: The outcome of the present work has emphasized that the Microwave assisted heating is an efficient, faster and reproducible method for synthesis of C-dots; rather that direct heating or refluxing. The reason could be that in microwave assisted heating the, microwave penetrates through the molecules thus giving uniform heating.

C-dots were formed at room temperature also i.e. when external surface passivating agents were used. However, this novel method was applicable for fabricating C-dots when precursors with very high sugar content (Sugarcane juice and Neem gum) were used. To the best of our knowledge, there are no reports on synthesis of C-dots at room temperature and thus can be optimised and exploited to synthesize C-dots using varieties of other precursors.

6.1.3 Purification of C-dots: Another important step after synthesis was purification of C-dots from cellular debris and other carbon components. A highly purified C-dot is a must for therapeutic applications. Both Sucrose Density Gradient Centrifugation (SDGC) and Dialysis were used for separation and purification of C-dots. SDGC has been used for separation of nanoparticles based on the difference between their sedimentation co-efficient**[14]**.

Need for Dialysis: Since, very small amount of C-dot solution was obtained after SDGC and also sucrose could not be removed completely from the fractions; further purification by dialysis was thought desirable. Therefore, dialysis membrane was used for purification of all the crude C-dot solutions. This method allows purification of large amount of C-dots along with minimal contamination of other reagents or chemicals since the process is carried out using highly pure distilled water.

6.2 CHARACTERISATION

For our initial satisfaction of being on the right path of synthesizing the C-dot; a visual observation under UV light was enough. However, further detailed morphology, crystallinity and chemical (due to surface functionalization) characterization was desirable.

Spectral properties of C-dots studied by **UV-Vis Spectroscopy** and **Fluorescence Spectroscopy**, exhibited characteristic peaks related to C-dots due to the electronic transitions based on the presence of carbonyl and hydroxyl groups on the surface**[15, 16]**. C-dots showed typical excitation dependent fluorescence spectra**[17]**.

FE-SEM, TEM and HRTEM micrographs displayed polydispersed, roughly spherical C-dots of 4-10 nm size. Polydispersity was more pronounced in C-dots synthesized from natural precursors. This is because; natural materials contain various types of bio-molecules which may lead to the synthesis of variously shaped and different sizes of nanoparticles. It must be mentioned here that the size range of synthesized C-dots were befitting the suitability for therapeutic applications. It could be even a suitable material for crossing the Blood Brain Barrier (BBB).

The **XRD** and **Raman Analysis** were used to study the Crystallinity of C-dots which displayed that the structure of C-dots was not perfectly crystalline which proves it to be turbostratic in nature**[4, 5]**. Raman spectroscopy displayed characteristic peaks of D-band and G-band. The ratio of the intensity of D-band and G-band (I_D/I_G) is the measure of the disorder extent in the material and the ratio of sp^3/sp^2 carbon **[18]**. The I_D/I_G ratio of our samples was found to be in the range of 0.5-1.75 which is higher than that of bulk graphite thus showing increased structure defects in C-dots due to the presence of oxygenated functional groups.

Functional groups assessment of C-dots was done by **FTIR**. It was found that C-dots were decorated with majority Carbon and Oxygen containing functional groups which was in agreement with the Raman data.

Based on the characterisations and after checking stability of C-dots synthesized using different precursors, purified and separated using dialysis; we can say that microwave assisted heating was the best method to get mono-dispersed spherical C-dots with excellent fluorescence properties. Moreover, C-dots derived from Sorbitol were found to be the most stable amongst all other natural precursors used. Hence, these C-dots were explored for application of drug delivery to Cancer cells in this work.

6.3 FORMATION OF FLUORESCENT DENDRITES USING C-DOTS

In order to get solid sample for characterisation and drug delivery experiment purpose, the C-dot containing solutions were dried. During the process of drying, some very interesting visual observations were made. The solutions dried forming similar patterns of dendritic crystals while continually retaining their fluorescence property.

Fluorescent crystals can be used for bio sensing, optical data storage, document security, detecting forgery **[19-21]**. All these beneficial applications have inculcated interest to grow the fluorescent crystals from non-toxic C-dot solution for biological applications; though the detailed study is yet to be done *viz.* effect of parameters such as temperature, pressure and duration *etc.* The possible mechanism for the formation of fluorescent crystals from C-dots has been explained using Classical nucleation theory **[22]**.

Using hydrothermal method the fluorescent crystals where grown from C-dots as seed solution at 60^{o}C and pressure of 200 mmHg under vaccum. During evaporation of the C-dot solution fascinating structures were formed that showed consistent feather like dendritic appearance similar to platinum, palladium, gold and silver dendrites synthesized using different methods by various research groups **[23-27]**. Fluorescence property of the dendritic crystals which was not observed in other types of dendrites invites to explore new research in optoelectronics, photo transistors and bio sensing.

6.4 C-DOTS FOR DRUG DELIVERY

Purified C-dots derived from Sorbitol were used as drug delivery vehicle to ferry Doxorubicin (DOX) to cancer cells. DOX is a potent anti-cancer drug widely used for treatment of various types of cancers studied extensively to reduce its side effects due to its high dosage.

6.4.1 Drug loading on C-dots: C-dots were initially functionalised with BSA to increase its drug loading efficiency as well as to enhance the biocompatibility and fluorescence property. BSA functionalised C-dots were loaded with DOX and its in-vitro drug release kinetics was studied. Folic acid is over expressed in many types of cancer cells**[28]**. This property can be exploited to target tumor cells and thus reduce side effects related to normal cells. Here, Folic acid was used as medium to navigate DOX loaded C-dots directly at the tumor site.

6.4.2 Drug Release Kinetics*:* The efficiency of any drug delivery vehicle lies in the pattern by which the potent molecule is released in the body at the right site and in accurate amounts. Study of in-vitro drug release kinetics using various standard statistical models gives us an insight of how the drug is getting released from the whole complex and under what specific conditions. The drug release in our case was found to be consistent at physiological pH as well as slightly acidic pH. Sustained release is one of the important facets of a drug delivery vehicle which allows small amount of drug to be delivered over a long period of time and thus overcome the side effects of repeated dosage in conventional therapy**[9]**.

DOX followed first order release kinetics at physiological pH. Such type of release kinetics is generally followed by drugs which are injected in the body (for example DOX). In first order kinetic models, the concentration of drug released in the body remains independent of the concentration of the drug remaining to be released. Such type of dual sensing drug delivery flotillas can be an important asset for solid tumor chemotherapy. In a solid tumor micro-anatomy, there are cells which maintain both acidic as well as basic pH depending upon their spatial distribution from the blood vessels. Competence of the present drug delivery vehicle (DOX loaded C-dots in our case) complex to rapidly fire drugs at both the pH values can play cardinal role in combating with most of the cell types in solid tumors. Folic acid as a targeting molecule would follow receptor mediated endocytosis of C-dot-drug complex and pH responsive release.

6.4.3 Bio-imaging & Cytotoxicity: was performed using Fluorescence microscopy which show bright green fluorescence of C-dots and also specific internalisation of Folic acid decorated complex in folate receptor expressing HeLa (Cancer) cells as compared to Vero (Normal) cells (folate receptor negative). Cytotoxicity testing revealed that C-dots do not cause toxicity to cells cultured in-vitro. The C-dot-DOX conjugate was found to be less toxic on Vero cells as compared to HeLa cells due to the use of targeting molecule. On the other hand, bare DOX poses a high level of Cytotoxicity to HeLa cells but at the same time also killing large percentage of Vero cells.

Overall we can say that C-dots can be used as an excellent drug delivery vehicle based on the following properties-

- Easy synthesis and purification
- Desired size
- Simple surface functionalisation with other bio-molecules
- High drug loading efficiency
- Sustained release at physiological and slightly acidic pH (pH of tumor micro-environment)
- Bio-compatibility to normal cells and high toxicity to cancer cells when loaded with anti-cancer drug (deu to targeting molecule)
- Offers bio-imaging at the same time acting as a dual pronged vehicle in diagnostics as well as therapeutics

6.5 C-DOTS CONJUGATES

The second part of the present work; was focussed on fabricating Composite of C-dots, so as to make them more efficient drug delivery vehicle, for which Meso-SiO_2/C-dots and C-dots@GNR were fabricated

The main advantage of synthesizing Mesoporous silica oxide along with C-dots is that it can act as versatile potential drug delivery vehicle with high drug loading capacity. In an earlier attempt to synthesize C-dots entrapped in meso-SiO_2in order to enhance the homogeneous size distribution, silica oxide nanoparticles were prepared separately followed by their attachment to synthesized C-dots and surface protection using polyethylene glycol **[29]**. In the present work, Rice Husk (RH)which acts as an ideal precursor because of the very high

content of silica present in it (>67%) to prepare meso-SiO_2 capped C-dots in a single process using hot injection method. Along with the typical absorption in the UV region, the complex also displayed a significant absorption in the near infrared (NIR) region and thus can also be used for photothermal therapy of solid tumors and/or NIR induced drug release (which has been done in chapter 3), thus establishing a fundamental platform for chemo-photothermal therapy.

TEM image shows the presence of embedded C-dots onto the synthesized silica nanoparticles and EDAX was performed to check the elemental composition of C-dots and composite. The nature of the nano-complex was found to be highly porous, which can be used for efficient drug loading and other biological applications.

GNRs are one of the most celebrated nanomaterials for photothermal therapy as well as drug delivery applications. The only hurdle in the toxic point of view of GNRs is CTAB which is used in synthesizing the rod shaped nanoparticles. An attempt is made in this work to overcome the toxicity due to CTAB by fabricating GNR-C-dot conjugate (C-dots@GNR). Highly fluorescent C-dots were synthesized using microwave assisted heating of Gum Arabic (GA) and subsequently purified using Sucrose Density Gradient Centrifugation (SDGC) as explained in Chapter 2. In a modified seed mediated protocol, purified C-dots were added into the growth solution, to make a C-dots@GNR conjugate. Synthesis of conjugate was confirmed using UV-Vis spectroscopy and HRTEM analysis. EDAX was performed to confirm the elemental analysis which confirmed that the peak for bromine had reduced in the composite sample as compared to bare GNRs thus showing C-dots taking part in the zipping mechanism. Also toxicity testing results revealed that C-dots@GNR was found to be more biocompatible than bare GNRs when tested on Vero cells.

Due to the partial porous nature of C-dots and unique optical properties of GNRs, the composite can serve as a triple action vehicle with high drug loading, decreased toxicity and photothermal behaviour for Cancer therapy.

6.6 FUTURE PROSPECTS

The potential of C-dots, synthesised at an optimised parameter, can be exploited as dual drug firing molecules. In most of the advanced Cancer chemotherapy strategies now-a-days, multiple drugs are injected in order to nullify the impact of toxic drugs e.g Camptothecin is injected along with Vitamin E to decrease the side effect generated by the former drug.

A significant novelty in current work would be grafting both i.e. the drugs and other supporting molecule on same C-dots and comprehending their release behaviours. Moreover, efforts can also be directed towards loading two drugs on the same C-dots to enhance the anticancer impact. To control the release time of both the drugs; they can be separated by a pH sensitive polymer that would degrade under appropriate conditions followed by release of the second drug.

Once the above task is culminated the pharmacokinetics for enhancing the efficacy of chemotherapy can be studied. Cytotoxic effects of C-dots as well as C-dot-drug conjugate needs be tested on Normal as well as Cancerous cell lines. To study the synergistic effect of both drugs in killing cancer cells, cytotoxic effects of individual drug can also be tested on the same cell lines. Further in vitro drug release studies can be carried out at acidic as well as physiological pH using Phosphate buffered saline. Concentration of drug released at various time intervals will be calculated using standard calibration curve of the respective drug and Drug release kinetics would be studied using various standard mathematical models.

The ultimate fate of the drugs after administration in the body could be studied using animal models and In vivo imaging strategies. Properly characterised C-dots-drug conjugate should be injected to suitable animal models and their possible trajectories can be traced along with the drug-target interaction studies. Drug conjugates that can serve as bi-functional tools for theranaustics where drug delivery can be done after extreme targeting can also be designed.

6.7 REFERENCES

1. W. L. Wei, C. Xu, J. S. Ren, B. L. Xu and X. G. Qu, Chem. Commun., 2012, 48, 1284.
2. L. Cao, X. Wang, M. J. Meziani, F. Lu, H. Wang, P. G. Luo, Y. Lin, B. A. Harruff, L. M. Veca, D. Murray, S. Y. Xie and Y. P. Sun, J. Am. Chem. Soc., 2007, 129, 11318.
3. L. Zhou, Y. H. Lin, Z. Z. Huang, J. S. Ren and X. G. Qu, Chem. Commun., 2012, 48, 1147.
4. S. Pandey, A. Mewada, M. Thakur, A. Tank and M. Sharon, RSC Adv., 2013, 3, 26290.
5. A. Mewada, S. Pandey, S. Shinde, N. Mishra, G. Oza, M. Thakur, M. Sharon and M. Sharon, Mater. Sci. Eng., C, 2013, 33, 2914.
6. C. Phadke, A. Mewada, M. Thakur, R. Dharmatti, S. Pandey and M. Sharon, Material Letters, 2014 (Submitted).
7. S. Pandey, A. Mewada, G. Oza, M. Thakur, N. Mishra,M. Sharon and M. Sharon, Nanosci. Nanotechnol. Lett.,2013, 5, 775.
8. M. Thakur, S. Pandey, A. Mewada, V. Patil, M. Khade, E. Ghoshi and M. Sharon, J. Drug Del., 2014, In Press.
9. A. Mewada, S. Pandey, M. Thakur, D. Jadhav and M. Sharon, J. Mater. Chem. B, 2014, 2, 698.
10. S. Sahu, B. Behera, T. Maiti, S. Mohapatra, Chem. Commun., 2012, 48, 8835.
11. skPalashuddin, A. Jaiswa l, A. Paul, S. Ghosh, A. Chattopadhyay, Sci. Rep., 2012, 2, 383.
12. J. Lu, J. X. Yang, J. Z. Wang, A. Lim, S. Wang, K. P. Loh, ACS Nano 2009, 3 , 2367.
13. A. Sachdev, I. Matai, S. U. Kumar, B. Bhushan, P. Dubey and P. Gopinath, RSC Adv., 2013, 3, 16958.
14. V. Sharma, K. Park and M. Srinivasarao, Proc. Natl. Acad. Sci. U. S. A., 2009, 106, 4981.
15. Z. Luo, Y. Lu, L. A. Somers and A. T. Charlie Johnson, J. Am. Chem. Soc., 2009, 131 , 898.

16. G. Eda, Y. Lin, C. Mattevi, H. Yamaguchi, H. Chen, I.-S. Chen, C. W. Chen and M. Chhowalla, Adv. Mater., 2010, 22, 505.
17. S.N. Baker, G.A. Baker, Angew. Chem. Int., 2010, 49, 6726.
18. L. Haitao, K. Zhenhui, L. Yang and L. Shuit-Tong, J. Mater. Chem., 2012, 22, 24175.
19. Y. Lu, J. Zhao, R. Zhang,Y. Liu, D. Liu, E. M. Goldys, X. Yang, P. Xi, A. Sunna, J. Lu, Y. Shi, R. C. Leif, Y. Huo, J. Shen, J. A. Piper, J. Paul. Robinson and D. Jin, Nat. Photonics, 2014, 8, 32.
20. F. Frascella, S. Ricciardi, P. Rivolo, V. Moi, F. Giorgis, E. Descrovi, F. Michelotti, P. Munzert, N. Danz, L. Napione, M. Alvaro and F. Bussolino, Sensors, 2013, 13, 2011.
21. X. Wang, L. Cao, F. Lu, M. J. Meziani, H. Li, G, Qi, B. Zhou, B. A. Harruff, F. Kermarrec and Y-P. Sun, Chem. Comm.., 2009, 3774.
22. S. Auer and D. Frenkel, Nature, 2011, 413, 711.
23. T. Huang, F. Meng and L. Qi, Langmuir, 2010, 26(10), 7582.
24. F-R. Fan, A. Attia, U. Sur, J-B. Chen, Z-X. Xie, J-F. Li, B. Ren and Z-Q. Tian, Crystal Growth & Design, 2009, 9 (5), 2335.
25. Y. Song, Y. Yang, C. J. Medforth, E. Pereira, A. K. Singh,H. Xu, Y. Jiang, C. J. Brinker, F. Swol and J. Shelnutt, J. Am. Chem. Soc., 2004, 126, 635.
26. X. Wen, Y-. Xie, M. Mak, K. Cheung, X. Li, R. Renneberg and S. Yang, Langmuir, 2006, 22, 4836.
27. D. Kozak, E. Shibata, A. Iizuka and T. Nakamura, Carbon, 2014, 70, 87.
28. B. A. Kamen and A. Capdevila, Proc. Natl. Acad. Sci. U. S. A., 1986, 83, 5983.
29. C. W. Lai, Y. H. Hsiao, Y. K. Peng and P. T. Chou, J. Mater. Chem., 2012, 22, 14403.

SUMMARY

Ever since the debut of C-dots in Carbon nano world, they have been in extreme lime light due to their exceptional optical and physical properties. These illuminating dots under UV-light falls in size range of 1-10nm and share the properties like semiconductor quantum dots and exhibit excitation dependent emission spectra. A few speculations on the origin of fluorescence in C-dots include energy emissive traps, oxygen containing functional groups, surface passivation and quantum confinement effect, turbostratic nature of Carbon or edge defects. Owing to need for treatment of Cancer with the help of Nanoparticle system to overcome the drawbacks of conventional therapy, the main aim of the present work was to Design an efficient drug delivery vehicle using C-dots for active targeting of Doxorubucin to Cancer Cells.

Chapter 1 is introduction to C-dots, their discovery and some important properties and applications of the same are discussed. A brief review of literature is stated along with the objectives of the work.

Chapter 2 describes screening of novel natural precursors (Water chestnut peel, Neem gum, Sugarcane juice, Gum Arabic) and chemical precursors (Sorbitol and Phenylalanine) on the basis of their high carbon content and the ratio of C, H and O in their sugar moieties. Three synthesis methods namely refluxing at high temperature (Water chestnut peel), microwave assisted heating (Gum arabic, Sorbitol & Phenylalanine) and synthesis at room temperature (Neem gum & Sugarcane juice) was employed. Conventional dialysis method was proven to be promising for separation and purification of C- dots. Also, synthesis of C-dot conjugates (Meso-SiO_2- C-dot and C-dot@GNR) is attempted in the present work,which hold high potential in the field of Cancer therapeutics.

Chapter 3 deals with characterisation of C-dots and C-dot composites. Spectral analysis was studied with the help of UV-Vis spectroscopy and Fluorescence spectroscopy, Morphological analysis was studied using FE-SEM, TEM and HRTEM, presence of Carbon was confirmed using XRD and Raman analysis and Surface functional group analysis was carried out using FTIR spectroscopy.

Chapter 4 explains the formation of Fluorescent C-dot dendrites whose mechanism is speculated based on Classical nucleation theory.

Chapter 5 covers the drug delivery application part of the thesis. In this chapter, the drug carrying capacity of highly fluorescent Sorbitol derived C-dots for targeted delivery of Doxorubicin (DOX) has been explored. Folic Acid (FA) has been used as navigational molecule due to high expression of Folate receptors in most of the cancer cells. Before attachment of the DOX, the surfaces of C-dots were protected with Bovine Serum Albumin (BSA) to make them more biocompatible and hold high amount of drugs. Release profile of DOX was studied using standard statistical models and confirmed to be First order at pH 7.2. Cellular imaging was performed using epifluorescence microscopy which showed bright green coloured fluorescence due to internalization of C-dots specifically targeted with FA in HeLa cells (Cancerous cells).

Chapter 6 summarises all the general discussions and conclusions of the previous chapters. Also, future prospects of the present work have been explained in brief.

LIST OF PUBLICATIONS THAT ARE PART OF THESIS

(List No 2, 4 & 6 are of equal contribution)

1. **Ashmi Mewada**[$], Sunil Pandey[$], Mukeshchand Thakur[$], Dhanashree Jadhav and Madhuri Sharon, **Swarming Carbon Dots for Folic acid Mediated Delivery of Doxorubicin and Biological Imaging,** *Journal of Material Chemistry B,* **2**, 698-705**, 2014** DOI:10.1039/C3TB21436B
2. Sunil Pandey[$], **Ashmi Mewada**[$], Mukeshchand Thakur[$], Sreenath Pillai, Roopa Dharmatti, Chinmay Phadke, Madhuri Sharon, **Synthesis of Meso-porous Silica oxide/C-dots complex (mesoSiO$_2$/C-dots) using pyrolysed Risk husk and its application in Bio-imaging,** *RSC Advances,* **4,** 1174-1179, **2013** DOI: 10.1039/C3RA45227A
3. **Ashmi Mewada**, Sunil Pandey, Sachin Shinde, Neeraj Mishra, Goldie Oza, Mukeshchand Thakur, Maheshwar Sharon and Madhuri Sharon, **Green Synthesis of Biocompatible Carbon Dots using aqueous extract of *T. bispinosa* peel,** *Material Science and Engineering C*, **33**, 2914-2917, **2013** DOI:10.1016/j.msec.2013.03.018
4. Sunil Pandey[$], Mukeshchand Thakur[$], **Ashmi Mewada**[$], Dhanashree Anjarlekar, Neeraj Mishra, Madhuri Sharon. **Carbon Dots Functionalized Gold Nanorod Mediated Delivery of Doxorubicin: Tri-functional nano-worms for Drug delivery, Photothermal therapy and Bioimaging**, *Journal of Material Chemistry B*, **1**, 4972-4982, **2013** DOI: 10.1039/C3TB20761G
5. Sunil Pandey, **Ashmi Mewada**, Goldie Oza, Mukeshchand Thakur, Neeraj Mishra, Maheshwar Sharon and Madhuri Sharon, **Synthesis and centrifugal separation of Fluorescent Carbon Dots at Room Temperature**, *Nanoscience and nanotechnology letters*, **5**, 775-779, **2013** DOI: 10.1166/nnl.2013.1617
6. Chinmay Phadke[$], **Ashmi Mewada**[$], Mukeshchand Thakur, Roopa Dharmatti, Sunil Pandey and Madhuri Sharon, **Biogenic synthesis of Fluorescent Carbon Dots at ambient temperature using *Azadiracta indica* (Neem) gum**, *Journal of Fluorescence*, **25(4)**, 1103-1107, **2015** DOI: 10.1007/s10895-015-1598-x
7. **Ashmi Mewada**[$], Ritesh Vishwakarma[$], Bhushan Patil, Chinmay Phadke, Golap Kalita, Maheshwar Sharon and Madhuri Sharon, **Non-blinking dendritic crystals from C-dot solution**, *Carbon Letters*, **16(3)**, 211-214, **2015** DOI: http://dx.doi.org/10.5714/CL.2015.16.3.1

Note: $- Authors have equal contribution in work and writing papers

ACKNOWLEDGEMENTS

I take this opportunity to express my intense gratitude to my mentor **Dr. Madhuri Sharon**, Director of Walchand Centre of Research in Nanotechnology and Bio-nanotechnology, Solapur for her perfect guidance, monitoring and invariable encouragement throughout my work. She has always been ready to impart her knowledge with or without asking and her never to stop attitude always inspires me to work hard. She has been an excellent guru (teacher) and a guide who has taught me about research which will definitely help me in my future work. I am also very thankful to **Professor Maheshwar Sharon** who has constantly supported me and has been an important critic during discussions. Their guidance has not only been important during my research but has also been helpful in personal life.

I would like to gratefully acknowledge National Institute of Technology (NIT), Nagoya, Japan for allowing me to submit my work for Doctoral degree at their prestigious institute. I am especially very thankful to **Professor Tetsuo Soga** for his valuable suggestions, constant encouragement and support during my submission. I am pleased to extend my sincere thanks to **Professor Masaki Tanemura** and **Dr. Golap Kalita** of NIT for their valuable comments and discussions during their visit to India.

I would also take this opportunity to express my immense gratitude to **Dr. Goldie Oza** and **Dr. Sunil Pandey** for their cordial support, valuable information and guidance. They have always helped in making me understand the deepness of the subject and completing my work through various stages. It would have been difficult to finish my work without their help and teachings.

I am highly obliged to **Mr. Mukeshchand Thakur** for his extreme support throughout the course of my work. He has been a great folk who always maintained a light and enjoyable atmosphere in the lab. I would also like to thank him with all the creative ideas about presenting, working and also helping me with various softwares used during my project.

I extend my sincere regards to **Dr. Bhushan Patil, Dr. Neeraj Mishra, Mr. Sachin Shinde, Dr. Arvind Gupta, Mr. Mayuresh Vishwanathan, Mr. Rohan Kesarkar** and **Dr. Bholanath Mukherjee** with whom I learned to work in a team. Their constant encouragement in my work and during thesis always helped me in achieving my targets on time with perfection. They have not only been helpful teachers but also very good friends.

A special thanks to **Roopa Dharmatti, Chinmay Phadke, Raju Gurung, Kruthi Suvarna, Krutula Nair**, **Rohit Kumar, Sailee Shroff** and **Dhanik Reshamwala** for helping me with my experiments, thesis and always keeping the atmosphere of the lab friendly and entertaining making my journey filled with wonderful memories. Also, a big thank you to **Mr. Prasad**, **Mr. Zaid** and **Ranjeet kaka** for helping me with daily lab requirements and accessories.

I feel very lucky to have friends like **Ritu Shah, Jayesh Varavadekar, Nilesh Kakadiya, Maitree Lalaji and Deepali Velankar** who have always been a constant support during the project work and helped me during my difficult times.

I would like to thank all the authorities of nsnRc for providing me funding and facilities in the laboratory during my work, especially **Shri K. M. S. Nair** and **Shri K. M. K. Nair** for their hearty support and help. I would also like to express my many thanks to **Mrs. Chalke** (TIFR, Mumbai), **Dr. Lalla** (DEA-UGC, Indore) and **Mrs. Bharti** and **Mrs. Pallavi** (IIT Bombay, Mumbai) for helping me with the analysis required during the tenure of my work.

I would also like to show my extended gratitude towards **Dr. Manikshete** and **Dr. Rao** of Walchand centre of Research in Nanotechnology and Bio-nanotechnology, Solapur for their immense help and support during thesis completion and submission.

Finally I would like to thank the almighty for giving me such wonderful **Parents**, my Fiancé **Mr. Ritesh Vishwakarma** and my loving **Family** who have seeded in me the desire to do my best and always supported me to progress and grow. Without them I would have not be where I am now.

At last, I would like to thank everybody who directly or indirectly supported me to complete my doctoral studies successfully.

Ashmi Mewada